INSTITUTE FOR SPACE STUDIES

MEASUREMENT OF THE COSMIC MICROWAVE BACKGROUND BY OPTICAL OBSERVATIONS OF INTERSTELLAR MOLECULES

John Francis Clauser

GODDARD SPACE FLIGHT CENTER
NATIONAL AERONAUTICS AND SPACE ADMINISTRATION

MEASUREMENT OF THE COSMIC MICROWAVE BACKGROUND BY OPTICAL OBSERAVTIONS OF INTERSTELLAR MOLECULES

John Francis Clauser

Columbia University

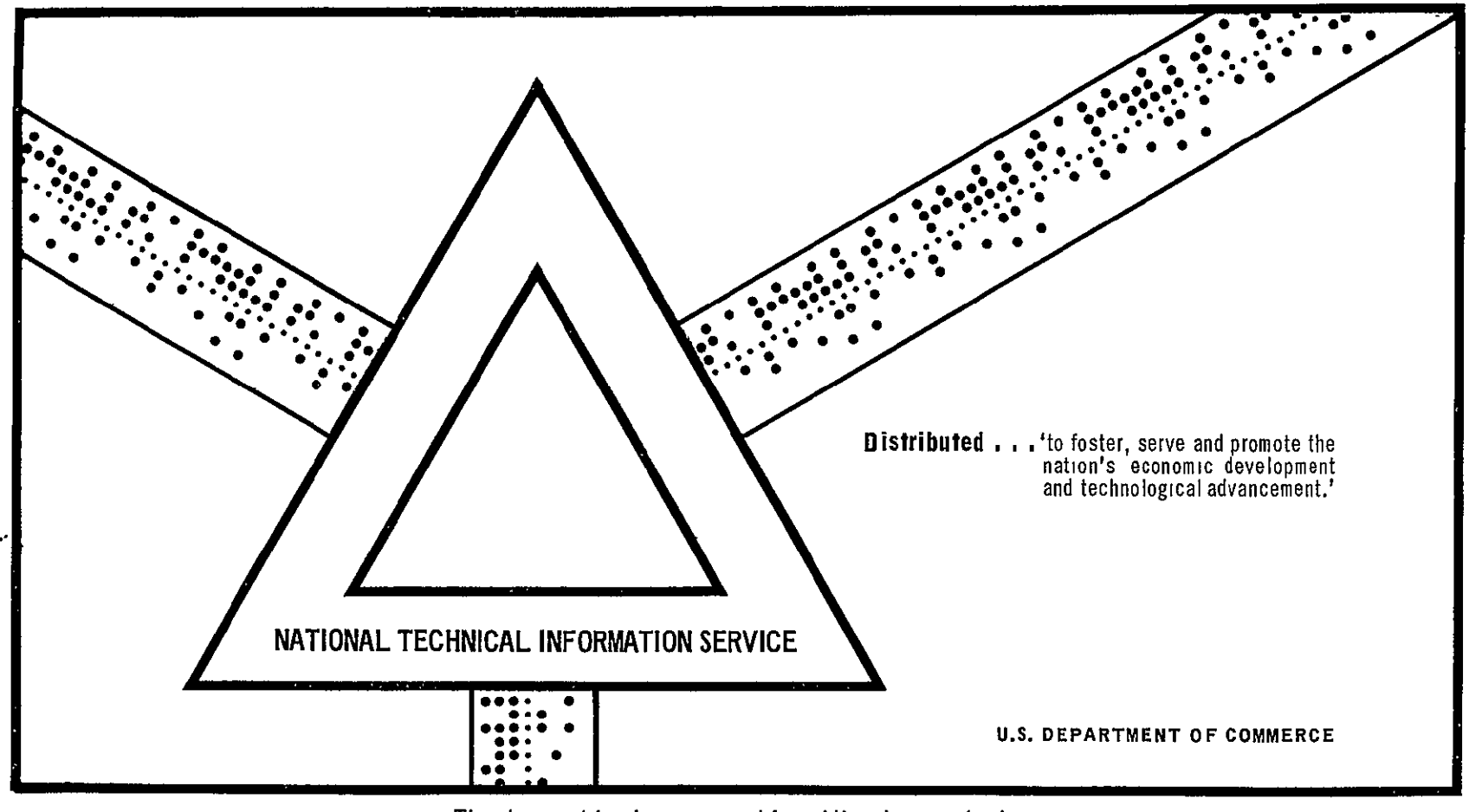

MEASUREMENT OF THE COSMIC MICROWAVE BACKGROUND BY OPTICAL OBSERVATIONS OF INTERSTELLAR MOLECULES

John Francis Clauser

Submitted in partial fulfillment
of the requirements for the degree of
Doctor of Philosophy in the Faculty of Pure Science
Columbia University

TABLE OF CONTENTS

TABLE OF SYMBOLS

a_j, a_{jn}	amplitude of state j, at transformed time w_n
"allowed"	electric dipole
A	molecular fine structure constant
A_{ij}	Einstein coefficient for spontaneous decay
b	impact parameter
b^{II}	galactic latitude
B, $B_{e'}$, B_0	molecular rotation constants
B_{ij}	Einstein coefficient for absorption and stimulated emission
c	speed of light
C_{kq}	$\sqrt{4\pi/2k+1} \cdot Y_{kq}$ Racah's normalization for spherical Harmonics
$\underset{\approx}{C}$	tensor operator with components C_{kq}
D	Debye unite of electric dipole moment = 10^{-18} esu-cm
D_1 D_2 ...	denominators used in Chapter 2
$\mathfrak{D}$ $(\alpha\beta\gamma)$	matrix elements of the finite rotation operator in terms of Euler angles $\alpha\beta\gamma$
e	electronic charge
e'', e'	electronic states
E_i	energy of level i
f, f_{ij}	oscillator strength
g_i	statistical weight of level i
$g(\lambda)$	optimal filter function for signal
$h = 2\pi\hbar$	Planck's constant
h_{slit}	slit function (rectangular peak)

$h_c(\lambda)$	optimal filter function which also removes effects of finite slit width
$\mathcal{H}$	Hamiltonian operator
$\mathcal{H}_{ij}$	matrix elements of $\mathcal{H}$
$\underset{\sim}{J}$, J	total angular momentum (excluding nuclear) operator and corresponding quantum number
J_0 J_1	Bessel functions
k	Boltzmann's constant
$\underset{\sim}{k}_i$, $\underset{\sim}{k}_f$	initial and final electron propogation vector
K	quantum number corresponding to $\underset{\sim}{K}$
$\hat{K}$	label of molecular state which reduces to state with quantum number K when molecular fine structure constant A vanishes
$\underset{\sim}{K}$	$\underset{\sim}{N} + \underset{\sim}{\Lambda}$
K_0 , K_1	modified Bessel functions
ℓ^{II}	galactic longitude (degrees)
m^*	reduced projectile mass
m	electron mass
M_i	magnetic quantum number corresponding to level i
N_e	electron number density (cm^{-3})
$n(\lambda)$	grain noise as function of wavelength
n_i	number of systems in level i
N_p	a proton number density (cm^{-3})
N_H	H I number density (cm^{-3})
$\underset{\sim}{N}$	angular momentum operator for end-over-end rotation
$\lvert \mathcal{T}^{(rot)}_{J''J'} \rvert^2$	Hönl-London factor

$\lvert \mathfrak{M}^{(vib)}_{v''v'} \rvert^2$	Franck - Condon factor
$\mathfrak{M}$ (vib-rot)	operator for vibration-rotation transitions
$p(y \mid \beta)$	conditional probability density of y given β
p_j, p_{jn}	real part of amplitude of state j, at transformed time w_n
P_{ij}	transition probability from state i to state j
$q(y)$	a posterori probability of measurement y (equation A4. 4)
q_j, q_{jn}	imaginary part of amplitude of state j, at transformed time w_n
$Q(H)$	probability that the actual value of a quantity will be in designated interval H
r	optical depth ratio (equation 2. 6)
r_{ij}, $r^{(e)}_{ij}$, $r^{(p)}_{ij}$	collisional excitation rate from level i to level j for unit flux of incident particles, electrons, protons.
$\langle r_{ij} \rangle$	thermal velocity average of r_{ij}
$\underset{\sim}{R}$	radius vector of projectile
$R_n(\lambda)$	autocorrelation function for plate grain noise (equation A4. 2)
R_{ij}	excitation rate from level i to level j by process other than direct radiation.
s	$= S_{ii'}/S_{jj'}$ (equation 2 7)
$\underset{\sim}{S}$, S	electron spin operator and corresponding quantum number
S_{ij}	transition strength (equations 2. 3 and 2. 5)
$s(\lambda)$	noise free spectrum as function of wavelength
$\underset{\approx}{S}(1)$	spin tensor operator
t	time
T	temperature
T_B	brightness temperature (equation 2. 9)

T_{ij}	excitation temperature of levels i and j (equation 2. 1)
$u(\nu)$	energy density of radiation at frequency ν per unit frequency interval in erg $cm^{-3}Hz^{-1}$
u_{ij}	$= u(\nu_{ij})$
$\hat{U}_{KK}$	transformation matrix which diagonalizes molecular Hamiltonian matrix
v	projectile velocity
v'', v'	vibrational states
$\bar{v}$	$\sqrt{8kT/\pi m^*}$ average reduced projectile velocity
v_m	$\sqrt{2kT/m^*}$ most probable reduced projectile velocity
w	$\sinh^{-1}(vt/b)/v$ (transformed time - equation 8. 23)
W	equivalent width of absorption line (area for unit base line height)
$y(\lambda)$	measured spectrum as function of wavelength
$y'(\lambda)$	densitometer measurement of $y(\lambda)$
$y''(\lambda)$	filtered $y(\lambda)$
Y_{lm}	normalized spherical harmonics
$\underset{\approx}{Y}$	spherical harmonic tensor operator
α	unspecified quantum number
$\alpha(\lambda)$	continuum height
α_{H}, α_{He}	polarizability of H, H_e
β	absorption line depth
$\hat{\beta}$	most probable value of β
β_m	see equation (A4. 8)
γ	= 0. 577 (Eulers constant)
$\delta(x)$	Dirac delta function to be taken in the sense of a generalized function (Lighthill 1959)

$\delta_{m\bar{n}}$	= 1 for m = n, = 0 for m ≠ n (Kronecker Delta)
δb	increment in b
$\delta \underset{\sim}{k}$	$= \underset{\sim}{k}_i - \underset{\sim}{k}_f$
δw	increment in w
ϵ_1 , ϵ_2	CH upper limit ratio discrepancy
η	limit to error region
θ	polar angle specifying molecular orientation in laboratory frame
θ_s	scattering angle
Θ	polar coordinate specifying projectile position in laboratory frame
λ	wavelength
Λ	electronic angular momentum quantum number, in Appendix 4 half interval for filter integration
Λ_L	wavelength of spectral line center
μ	electric dipole moment
ν	frequency (Hz)
ν_{ij}	$= (E_i - E_j)/h$ (equation 2. 2)
ξ_{ij}	$= B_{ji} u_{ij} / (A_{ij} + B_{ij} u_{ij})$ ($= n_i/n_j$ for thermal equalibrium - equation 2 11)
Π	electronic state with $\Lambda = 1$
σ	standard deviation
σ_{ij}	cross section for excitation from level i to level j
Σ	electronic state with $\Lambda = 0$
τ_{ij}	optical depth of spectral line which is due to transition from level i to level j
ϕ	azimuthal angle specifying molecular orientation in laboratory frame

Φ	polar coordinate specifying projectile position in laboratory frame
χ	angle between molecular axis and $\underset{\sim}{R}$
ψ	molecular wave function
Ψ	total wave function
ω_{ij}	$= 2\pi\nu_{ij}$
$\begin{pmatrix} J_1 & J_2 & J_3 \\ M_1 & M_2 & M_3 \end{pmatrix}$	Wigner 3j symbol
$\begin{Bmatrix} J_1 & J_2 & J_3 \\ L_1 & L_2 & L_3 \end{Bmatrix}$	Wigner 6j symbol

CHAPTER 1
INTRODUCTION

A. Cosmic Microwave Background Background

The existence of a blackbody background radiation as a permanent remnant of the flash of radiation of the "big bang" was first suggested by Gamow and his collaborators (Gamow 1948, Alpher and Herman 1958). Using Friedman's (1922, 1924) solution to the field equations of General Relativity for an expanding isotropic homogeneous universe, Gamow and his associates attempted to explain the present element abundances in terms of nuclear reactions occurring during the first few seconds or minutes of the expansion.

They showed the following (Alpher and Herman 1950, Gamow 1949, 1953, Alpher, Herman,and Gamow 1967):

1. At early epochs radiation would be in thermal equilibrium and thus would have a thermal spectrum. More important,at that time it would be the dominant component of the total energy density.

2. As the universe expanded the radiant energy decreased as the inverse fourth power of the scale factor. On the other hand, the matter rest energy density decreased only as the inverse third power of the scale factor ; hence eventually it became the dominant component of the total energy density.

3. At an epoch when the temperature was approximately 10^4 °K , the radiation decoupled from the matter. In spite of the complexities of this decoupling process the distortion of the blackbody spectrum of the radiation by this process would be small. Peebles (1968) has since treated this process in some detail and has shown this to be essentially a consequence of the fact that

the energy density of the radiation at the time of recombination of the primeval plasma ($\sim 10^9$ ev/baryon) is very much greater than the 13 ev/baryon released by hydrogen recombination.

4. Following the decoupling, the radiation would appear to an observer who was a rest with respect to local matter as Doppler shifted blackbody radiation. The well known result that Doppler shifted blackbody radiation becomes blackbody radiation with a lower temperature implies that the radiation would still have a thermal spectrum.

5. Synthesis of He^3, He^4, and H^2 is possible during the first few minutes of the expansion of the universe It is important to note here that Gamow's original aim was to account for the genesis of the majority of elements, but there now seems little doubt that elements heavier than He^4 cannot be so produced (Fermi and Turkevich 1950, Wagoner, Fowler and Hoyle 1967, Peebles 1966). They are presumably made in stars (Burbidge, Burbidge, Fowler, and Hoyle 1957).

Gamow realized that the radiation would persist to the present epoch, but unfortunately he did not suggest any attempt to detect it experimentally. It was not until the work of Dicke and his collaborators (1966) who were looking for observable consequences of an expanding universe that the background radiation was reconsidered,* and they specifically constructed a specialized radio-

* Independently Doroshkevich and Novikov (1964)examined existing observational data in an attempt to determine if there was any evidence for the existance of the radiation considered by Gamow. Unfortunately, due to a misreading of a paper by Ohm (1961) which described the results obtained at the Bell Telephone Laboratories with an absolutely calibrated corner horn reflector and a quiet receiver,

telescope for its detection. However, the radiation was first detected by Penzias and Wilson (1965), when it was pointed out to them by Dicke that the excess antenna temperature of unknown origin of their exceptionally quiet microwave radiometer might be due to the radiation which the Princeton group was seeking. The second observation of the radiation followed within a year, and was that of Dicke's co-workers Roll and Wilkinson (1966) Their measurements as well as others made subsequently, are shown in Figure 1. The best present estimates suggest $\sim 2.7°K$ for the temperature of this radiation.

One of the important predictions of the theory is that the radiation should have a spectrum corresponding to that of a blackbody. For a temperature $\sim 3°K$ this would peak at about a millimeter in wavelength. As can be seen from Figure 1, the thermal character of this radiation has been confirmed over more than two decades in frequency in the long wavelength portion of the spectrum However, since most of the energy density lies at the short wavelength portion where measurements have not yet been made, it is of great importance that observations be extended to this spectral region If the thermal character of this radiation is eventually confirmed, it will provide very compelling, and perhaps conclusive evidence in favor of the expanding universe

---

they came to the conclusion that there was no evidence for its existence. Penzias and Wilson (1965) eventually used the same instrument to first detect the radiation.

B. Observational Difficulties

Direct observations have not been made at short wavelengths because of the presence of atmospheric H_2O and O_2 absorption lines. These increase in both strength and number as one goes to shorter wavelengths. Their resulting opacity causes the atmosphere to radiate with an intensity which is large compared with that of the background. In addition, the blackbody background intensity begins to fall off exponentially with increasing frequency beyond about a millimeter in wavelength. Thus it appears that beyond $\lambda \approx 3$mm, for all practical purposes, the "radio window" is closed, and one must place radiometers above the atmosphere in order to make direct background measurements.

Fortunately, it is possible to circumvent the problem of atmospheric opacity by using observations of optical spectra which are due to absorption by the interstellar molecules CN, CH, CH+. An analysis of the absorption spectra of these molecules can be used to determine to what extent the molecules are being excited by the background radiation. A measure of this excitation can then be used to infer the intensity of the existing background.

This dissertation describes how this is done. The resulting measurements made by the use of these molecules are shown in Figure 1, where they are labeled CN, CH, CH+.

C. Interstellar Molecules

The optical interstellar absorption lines due to the interstellar molecules CN, CH, CH+, were discovered by Adams and Dunham (1937, Dunham 1941, Adams 1941, 1943, 1949). Following the suggestion of Swings and Rosen-

feld (1937) that the line at λ 4300. 3Å might be due to CH, McKellar (1940) succeeded in identifying this feature with CH as well as the line at λ 3874. 6Å with CN. At that time he predicted the presence of several other lines of CH as well as the presence of the R(1) line of CN at λ3874. 0Å. Acting on the suggestion of McKellar, Adams succeeded in observing the additional lines of CH as well as the faint CN R(1) line. Douglas and Herzberg (1941) then produced CH+ in the laboratory, and positively identified the features at λ4232. 6Å and λ 3957. 0Å as due to that molecule.

It is surprising to consider that McKellar's (1941) estimate of 2. 3°K for the rotational temperature of the interstellar CN in front of ζ Ophiuchi was probably the first measurement of the cosmic microwave background — twenty-eight years ago! His temperature measurement was made from Adams' visual estimates of the absorption line strengths, so his result was crude. At the time, though, he attributed little significance to this result stating (McKellar, 1940)

> "... the 'effective' or rotational temperature of interstellar space must be extremely low if, indeed, the concept of such a temperature in a region with so low a density of both matter and radiation has any meaning..."

His 2. 3°K measurement is also mentioned in Herzberg's (1959, p. 496) Spectra of Diatomic Molecules, suggesting that it "... has of course only a very restrictive meaning."

The starting point of our work was a crucial suggestion by N. J. Woolf based in turn on a discussion by McKellar (1940) which preceeded Adams' discovery (McKellar 1941) of CN λ 3874. 0Å. He suggested that the absence of excited state CN lines placed a severe limit on the temperature of background

radiation As we shall see, not only do these molecules set upper limits to this radiation, but in all probability they may also be used to effect an actual measurement of it

In addition to our work on this problem (Thaddeus and Clauser 1966, Clauser and Thaddeus 1969, and Bortolot, Clauser, and Thaddeus 1969) similar work has also been pursued by Field and Hitchcock (1966), while Shklovsky (1966) made an early suggestion that McKellar's (1941) observation was a consequence of the background radiation.

D. Purpose of Dissertation

The central purpose of this dissertation is to extract the largest feasible amount of information on the short wavelength spectrum of the microwave background radiation from a number of spectra of interstellar molecules that were available in the summer of 1966 The work may be divided into roughly two parts. an observational part and a theoretical part In the observational part, we first show how one calculates the background intensity from the spectra of the interstellar molecules (Chapters 2 and 3). Second, in order to utilize the existing spectrograms, we develop new techniques of spectrophotometry (Chapter 4, Appendix 4) Third, we present the results of the application of these techniques to the problem at hand, and the resulting upper limits to and measurements of the intensity of the background radiation (Chapter 5).

On the theoretical side, we first consider what assumptions concerning the location of the molecules will be necessary, such that (1) the molecules will set upper limits to the background intensity, and (2) the molecules will yield

reliable measurements of the background intensity. It will be seen that the use of the molecules to set intensity upper limits places only minor restrictions on the molecular environment, however, their use to make intensity measurements requires the absence of alternate molecular excitation mechanisms (Chapter 2).

We therefore provide an analysis which considers possible excitation schemes that are consistent with our present understanding of the conditions found in the interstellar medium We find that a necessary assumption for the molecules to yield reliable intensity measurements is that they reside in a normal H I region (Chapters 6, 7, and 8)

After a review of the existing evidence that the molecules do reside in an H I region, we proceed to present new evidence to further substantiate this contention. This will consist of (1) the observed invariance of the excitation of the interstellar molecules, and (2) the results of new 21cm H I observations in the direction of these molecular clouds (Chapter 9).

CHAPTER 2

THE USE OF INTERSTELLAR MOLECULES TO OBTAIN UPPER LIMITS AND MEASUREMENTS OF THE BACKGROUND INTENSITY

A Excitation Temperature of Interstellar Molecules

The method which we exploit to obtain information concerning the short wavelength spectrum of the background radiation is the familiar one used to find the temperature of molecules and their environment from molecular spectra (Herzberg 1959). It is a general tool widely used in astronomy to determine the temperature of planetary and stellar atmospheres, and finds considerable application in the laboratory to the study of flames, rocket exhausts, etc .

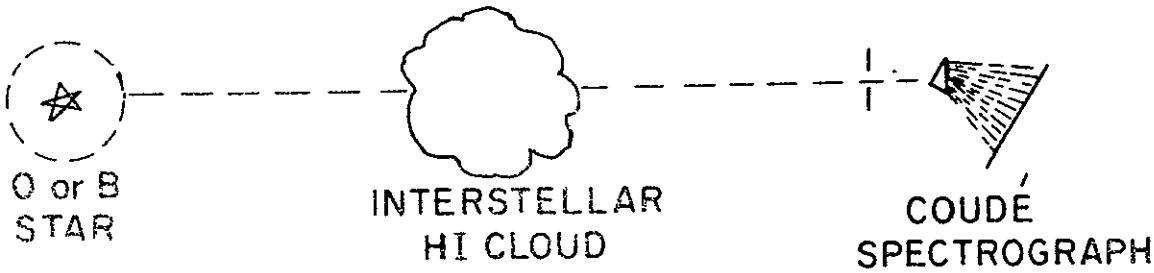

A typical observational situation is illustrated schematically above The intensity in absorption of lines in a molecular electronic band is proportional both to the square of the transition matrix element and the population of the lower level of the transition As long as the molecules are in thermal equilibrium (or at least their rotational degrees of freedom are in thermal equilibrium) the relative populations of the rotational levels are in turn given by the usual Boltzmann expression

$$\frac{n_i}{n_j} = \frac{g_i}{g_j} \exp\left[-(E_i - E_j) / kT\right] \tag{2.1}$$

where

n_i is the population of level i and

g_i is the statistical weight of that level

E_i is the energy of that level

It is now clear that the relative intensity of optical absorption lines in the band is a function of T alone, and may be used to determine T if the rotational term scheme and relative transition matrix elements of the molecule are known, as is usually the case. Even if thermal equilibrium does not hold, it should be obvious that equation (2.1) can be used to define an "excitation" or "rotational" temperature T_{ij} with respect to any two levels i and j.

Consider now possible causes of this excitation; it could be due to either radiation or collisions. If radiation which has a thermal spectrum with temperature T_B is the only (or dominant) cause of the molecular excitation, then on purely thermodynamic grounds $T_{ij} = T_B$. In this case only the emission and absorption of photons with frequencies

$$\nu_{ij} = (E_i - E_j) / \hbar = \omega_{ij} / 2\pi \tag{2.2}$$

in the molecular frame of rest are involved in the excitation; and only the portion of the radiation spectrum over the narrow Doppler width

$$\Delta\nu_{ij} / \nu_{ij} \approx 10^{-5}$$

of the transition is involved in the excitation of the molecules. Thus if the radiation does not have a thermal spectrum, but over these intervals it has the

same intensity as that of a blackbody temperature T_B, then the relation $T_B = T_{ij}$ will hold.

On the other hand if the excitation is collisional, or is due to a mixture of radiative and collisional processes, T_{ij} will generally set an upper limit to the intensity of radiation at ν_{ij}. Thus we see that a measurement of T_{ij} will yield useful information on the background radiation density.

B. Astronomical Situation

In the astronomical situation of interest to us the molecules are located in a tenuous interstellar cloud, while the source of radiation against which absorption is being observed is an O or B star at a typical distance of 100 pc. Since the interstellar lines are very sharp, and for the molecules, at least, always weak, the largest telescopes and Coudé spectrographs are required to detect the lines. In fact, virtually all the molecular observations have been made with three instruments; the Mt. Wilson 100-inch, the Mt. Palomar 200-inch, and the Lick Observatory 120-inch reflectors.

There are several reasons why interstellar lines have so far only been investigated against early stars. Perhaps the most important is the high intrinsic luminosity of these objects, which allows high resolution spectroscopy to be done in reasonable exposure times to distances of up to several hundred parsecs. For much smaller path lengths, the probability of intercepting an interstellar cloud which possesses appreciable molecular absorption is very slight. There is the additional factor that O and B stars have been so recently formed that they usually lie near the galactic plane, and thus in the vicinity (or at least the direction) of interstellar matter. Also an important technical con-

sideration is that the spectra of these stars are comparatively featureless, many of the spectral lines are due to ionized atoms and the lines are usually wide due to the high temperature and/or rotation of the star. In marked contrast to the situation with cool stars, there is therefore little likelihood that the interstellar lines will be blended or obscured by stellar features. Purely from the technical point of view we thus see that early stars are ideal objects to use as light sources for long range optical absorption spectroscopy of interstellar matter.

C. Calculation of T_{ij}

It is straight forward to calculate T_{ij} from the observed absorption intensities of lines in a molecular band. The observed optical depth $\tau_{ii'}$ of an absorption line, which is due to a transition from level i to level i', is given by

$$\tau_{ii'} = 8\pi\nu_{ii'} N_i S_{ii'} / (3hcg_i) \qquad (2.3)$$

where $S_{ii'}$ is the line strength. This is defined as the square of the electric-dipole matrix element summed over the degenerate magnetic states and polarizations of the transition (Condon and Shortley 1951, p. 98).

$$S_{ij} = \sum_{m_i m_j q} |\langle \ldots m_i | \mu C_{1q} | \ldots m_j \rangle|^2 \qquad (2.4)$$

where μ is the electric-dipole moment of the molecule and $C_{1q} = \sqrt{4\pi/3}\, Y_{1q}$, where the Y_{1q} are the normalized spherical harmonics. This summation may be expressed in terms of the reduced matrix element (Edmonds 1968, equation 5.4.7).

$$S_{ij} = \mu^2 \left| \langle i \| \underset{\approx}{C}(1) \| j \rangle \right|^2 \tag{2.5}$$

where $\underset{\approx}{C}(1) = \sqrt{4\pi/3}\ \underset{\approx}{Y}(1)$ is a spherical tensor operator of order one.

Thus for two optical absorption lines, of nearly the same wavelength, that are due to transitions to levels i' and j' from low lying levels i and j respectively,

$$r = \frac{\tau_{ii'}}{\tau_{jj'}} = s \exp -\left[\frac{h\nu_{ij}}{kT_{ij}}\right] \tag{2.6}$$

Here we have defined

$$s = \frac{S_{ii'}}{S_{jj'}} \tag{2.7}$$

The calculation of this quantity for the specific molecular systems of interest will be taken up in Chapter 3. Equation (2.6) may be rewritten to give the excitation or rotational temperature

$$T_{ij} = \frac{h\nu_{ij}}{k \ln(s/r)} \tag{2.8}$$

It should be noted in passing that since only the logarithm of the optical depth appears in equation (2.8), the rotational temperature may be well determined even though the optical depths are poorly known.

If the interstellar lines are optically thin, the optical depths are proportional to the equivalent widths of these lines (area of absorption line for unit continuum height). Fortunately, most of the interstellar lines considered in this study are weak so that the correction for saturation is small, and good approximate results may be obtained by taking r equal to the equivalent width

ratio. However, accurate temperature measurements will require a correction for saturation via a curve of-growth for the clouds which contain these molecules. A description of these corrections appears in Chapter 5.

D. Why Molecules?

We must now consider which kinds of atoms or molecules found in the interstellar medium are useful as radiant thermometers, for measurement of the background radiation. What is required to make such measurements possible is an atom or molecule which has (1) a low lying level with energy separation from the ground state $\sim kT \approx 2cm^{-1}$, for a blackbody radiation temperature $T \approx 3°K$; (2) an allowed (electric-dipole) transition connecting this level with a lower level which has an observable population and (3) allowed optical absorption transitions originating in each of these levels. Clearly these optical transitions must be mutually resolvable, and of course, to be observable from the ground they must have wavelengths $\lambda > 3000Å$. The required term diagram for such a species is shown in Figure 2.

We can see that there is nothing in principle which restricts us to use molecules. However, atomic fine-structure separations are typically much greater than $2cm^{-1}$. For example, the lowest lying fine-structure level of any interstellar atom so far observed from the ground belongs to Ti II and this is $97cm^{-1}$ above the ground state. On the other hand, hyperfine levels have separations which are too small, and are connected by magnetic-dipole transitions - the H I hyperfine separation is only $.032cm^{-1}$.

The rotational and/or fine structure energy level separations within

the electronic ground states of the three molecular species observed optically in the interstellar medium - the CN, CH, and CH+ free radicals - have energies not very much greater than 1 88cm^{-1}. The J = 0 - 1 energy level separation of the $X^2\Sigma$ (v=0) electronic ground state of CN is especially favorable with a separation of only 3. 78cm^{-1}. Partial term diagrams for these molecules are shown in Figure 3 Precise molecular data is listed in Table 1.

The R(0) absorption lines of the (0, 0) band of the $B^2\Sigma^+ - X^2\Sigma^+$ electronic system of CN at λ3874. 0Å and λ3874. 8Å arrise from the J = 1 level. All of the CN lines are easily separated with a good Coudé spectrograph It should be noted, however, that even in the best spectrographs the lines are not fully resolved. i. e. the observed line width , ~0. 02Å, is not the true Doppler line width of the interstellar cloud, but is determined instead by the resolution of the instrument, and is typically ≈ 0 05Å .

The level separations of the CH and CH+ molecules are sufficiently great that no molecules are observed to be in an excited level. However, these two molecules are still of great value to the problem of the background radiation, since the absence of the excited states lines can be used to set upper limits to the radiation intensity at very short wavelengths.

The lowest excited state in CH+ is the J = 1 level, 27. 9cm^{-1} above the J = 0 ground state, and the corresponding R(0) and R(1) transitions of the (0, 0) band of the $X^1\Sigma - A^1\Pi$ electronic system occur at λ4232. 5Å and λ4229. 3Å

The CH electronic ground state configuration is a $^2\Pi$ state, intermediate between Hund's cases (a) and (b). Accordingly, transitions are allowed from the KJ = 1 1/2 ground state to both the fine-structure level KJ = 1 3/2,

which lies at 17.8cm^{-1} above the ground state, and to the KJ = 2 3/2 excited rotational level 66.8cm^{-1} above the ground state. The strongest optical transition from these three levels are the $R_2(1)$, and $R_1(1)$, and the $R_2(2)$ lines in the (0,0) band of the $X^2\Pi - A^2\Delta$ electronic system at λ4300.3Å, λ4303 9Å and λ4296.6Å respectively. A detailed treatment of the relative intensities of the optical transitions of CH appears in Chapter 3.

The J = 2 level of the CN electronic ground state is similarly useful for setting an upper limit to the background intensity Since it is 7.6cm^{-1} above the J = 1 level, its populations will be quite small. For this reason, the R(2) line originating in this level has not yet been detected, but it is probably only about a factor of three below detection (Bortolot, Clauser, and Thaddeus 1969) and a further extension of the techniques developed in this dissertation might yield its detection.

On the other hand, without an enormous extension of present observational techniques, the CH $R_2(1)$ and the CH^+ R(1) lines are below the threshold of detectability if their temperature ~ 3°K.

E. Statistical Equilibrium of an Assembly of Multi-Level Systems Interacting with Radiation

When all its components are considered, departure from thermal equilibrium is one of the most conspicuous features of the interstellar medium It contains, for example, dilute 10^4°K starlight, H I atoms with a kinetic temperature of ~ 100°K, 10^4°K H II protons and electrons, grains which are thought to be in this vicinity of 20°K, and high energy cosmic rays. It is obvious that

in its totality, it cannot be characterized by a unique temperature.

At first glance there would, therefore, appear to be no reason to assume that interstellar CN should single out the microwave background with which to be in thermal equilibrium. However, for the rotational degrees of freedom of CN it will be shown that this is probably the case.

In order to discuss the statistical equilibrium of interstellar molecular systems, it is probably wise to be specific about a few conventions and definitions that will continually appear during the discussion.

Thermal Equilibrium: An assembly of systems is in thermal equilibrium when all of its parts are characterized by the same temperature.

Statistical Equilibrium: If an assembly of systems with energy levels E_i is in statistical equilibrium when the populations of these levels have time-independent populations

Due to the long time scale of interstellar processes (and the short time scale for observations) there are often grounds for assuming statistical equilibrium to apply, even though extreme departures from thermal equilibrium are known to exist. All of the assemblies which we will be considering i. e. clouds of interstellar molecules, will be in statistical equilibrium. This may be seen from the fact that an isolated polar molecule such as CN, CH, or CH+, interacting background radiation, will achieve statistical equilibrium with this radiation typically in less than 10^3 sec . On the other hand, it will exist in the interstellar medium for at least 10^{11} sec, before it is destroyed by radiative dissociation. Thus the assumption of a constant number of molecules in statistical equilibrium is clearly a very good one.

Excitation Temperature: Boltzmann's law states that if an assembly of systems with energy levels E_i is in thermal equilibrium, then the populations in these levels will be distributed according to Boltzmann's law - equation (2.1) - which may be used to define T_{ij} in terms of the level populations. If there is thermal equilibrium at temperature T, then all $T_{ij} = T$. Alternately if thermal equilibrium is not established, equation (2.1) may be used to define T_{ij} as the excitation temperature of the levels i, j.

Brightness Temperature: Boltzmann's law, when applied to the radiation field, yields Planck's law for the density of unpolarized isotropic thermal radiation

$$u(\nu) = \frac{8\pi h\nu^3 c^{-3}}{\exp\left(\frac{h\nu}{kT_B}\right)-1} \quad (\text{erg cm}^{-3}\ \text{Hz}^{-1}) \tag{2.9}$$

and $u_{ij} = u(\nu_{ij})$. If the spectrum of the radiation is not thermal, it is conventional to use equation (2.9) to define the brightness temperature $T_B(\nu_{ij})$. Since u_{ij} is a monatonic function of $T_B(\nu_{ij})$, the latter is frequently used in this case as a measure of the radiation density at frequency ν_{ij}.

Principle of Detailed Balance: The principle of detailed balance states that the transition rates for an elementary process and its inverse process are equal. This is just due to the invariance of transition matrix elements under time - reversal (see for example Tolman 1938, p. 521)*. Hence if the transition rate for a given process R from level i to level j is given by R_{ij}, then

---

* Although the principle of detailed balance does not strictly hold in a relativistic theory including spin (Heitler 1954, p. 412) - for our purposes it may be considered correct.

$$g_j R_{ji} = g_i R_{ij} \exp[-(E_i - E_j)/kT] \qquad (2.10)$$

where T is the kinetic temperature of the exciting agent. In the following analysis we will make the important assumption that $kT \gg E_i - E_j$, which is true for the molecular levels of interest if the kinetic temperature of the colliding particles is 125° K or higher. Then we may set the above exponential equal to one. A temperature in the vicinity of 125°K is the usual one derived for a normal H I region(Dieter and Goss 1966). The suggestion that shielding from the interstellar radiation field by grains may yield significantly lower temperatures in dense, dark H I regions does not apply to the clouds in which CN, CH, and CH^+ have been observed, since these clouds are reddened less than 1 magnitude.

The statistical weight factors arrise in (2.10) from the fact that the elementary process in question occurs from one state to another, but the labels i and j refer to levels. Following Condon and Shortley (1951) we refer to a level i as the set of g_i magnetic states with the same angular momentum and energy E.

Einstein Coefficient A_{ij} (sec^{-1}): A_{ij} is the probability per unit time that a system will spontaneously emit radiation of frequency ν_{ij} and make a transition from level i to level j. Hence the rate of such transitions for n_i molecules in level i is $n_i A_{ij}$.

Einstein Coefficient B_{ij} ($sec^{-1}\ erg^{-1}\ cm^3\ Hz$): $B_{ij} u_{ij}$ is the probability per unit time that a system will absorb radiation from a field of energy density u_{ij} at frequency ν_{ij} and make a transition from level j to level i. For n_j molecules in level j the absorption rate is then just $n_j B_{ij} u_{ij}$. For consistency with the principle of detailed balance $B_{ij} u_{ij}$ must then be the rate of stimulation of emission of radiation at frequency ν_{ij} by the radiation field u_{ij}. For n_i molecules in

level i the rate for this process is equal to $n_i B_{ij} u_{ij}$. For a two level system in equilibrium with thermal radiation then

$$\frac{n_i}{n_j} = \xi_{ij} = \frac{B_{ij} u_{ij}}{A_{ij} + B_{ij} u_{ij}} \tag{2.11}$$

if we wish to identify $T_B = T_{ij}$ then we must have

$$g_j B_{ji} = g_i B_{ij} \tag{2.12}$$

and

$$A_{ij} = \frac{8\pi h \nu_{ij}^3}{c^3} \tag{2.13}$$

F. Equations of Statistical Equilibrium:

Let us now consider an assembly of multilevel systems such as diatomic molecules in an interstellar cloud. We shall assume the molecules to be excited by background radiation and other processes as well. These might be collisions, fluorescent cycles through higher electronic state, etc., but we shall make no initial restrictions on them, at least at first, specifying them only by $R_{JJ'}$ as the rate of transitions induced by them from level J to level J'.

For statistical equilibrium of the n_J molecules in level J, we require

$$\frac{dn_J}{dt} = 0 = -n_J \sum_{J'=0}^{\infty} R_{JJ'} + \sum_{J'=0}^{\infty} n_{J'} R_{J'J} \tag{2.14}$$

$$- \sum_{J'=0}^{J'<J} \left[n_J (A_{JJ'} + B_{JJ'} u_{JJ'}) - n_{J'} B_{J'J} u_{JJ'} \right] \qquad \text{(2.14 cont'd)}$$

$$+ \sum_{J'>J}^{\infty} \left[n_{J'} (A_{J'J} + B_{J'J} u_{J'J}) - n_J B_{JJ'} u_{J'J} \right]$$

For interstellar molecules in the presence of non-thermal radiation and additional interactions T_{ij} will then be a complicated function of the various transition rates given by the solution of equations (2.14). Fortunately, we do not need to solve these equations in general, but can obtain results for three specific cases relating the molecular excitation temperature to the radiation density at the frequency of the microwave transition. The first two will apply to CN and CH+, while the third will apply to CH.

In the treatment of cases I and II, which refer to diatomic molecules with Σ electronic ground states, the levels will be denoted by their total (excluding nuclear) angular momentum J. In the treatment of case III which refers to a molecule such as CH with both spin and orbital angular momentum in its electronic ground state, we will, for simplicity of notation, refer to the levels KJ = 1 1/2, 1 3/2, and 2 3/2, as 0, 1, and 2, respectively.

G. Case I :

Let us first consider the simplest case of interest, that of a cloud of interstellar diatomic molecules which posses a Σ electronic ground state (so that the allowed rotational transitions satisfy the simple selection rule $\Delta J = \pm 1$) interacting only with background. Assuming that higher multipole transitions may be neglected, we will show that $T_{J+1,J} = T_B(\nu_{J+1,J})$.

It may be seen in this case, that different pairs of adjacent levels may have different excitation temperatures, and that these temperatures are equal to the brightness temperatures at the frequencies of the corresponding transitions. The various T_{ij} will not, however, be equal when the spectrum of the radiation is non-thermal.

The proof is straight forward. If the allowed rotational transitions satisfy the selection rule $\Delta J = \pm 1$ and all $R_{ij} = 0$, then the linear homogeneous equations (2. 14) reduce to

$$\frac{dn_J}{dt} = 0 = -n_J(A_{J,J-1}+B_{J,J-1}u_{J,J-1}) + n_{J-1}B_{J-1,J}u_{J,J-1} + n_{J+1}(A_{J+1,J}+B_{J+1,J}u_{J+1,J}) - n_J B_{J,J+1}u_{J+1,J} \tag{2 15}$$

This system of equations may be solved by inspection by noticing that the first and second lines both vanish identically if one takes

$$\frac{n_{J+1}}{n_J} = \xi_{J+1,J} = \frac{B_{J,J+1}u_{J+1,J}}{A_{J+1,J}+B_{J+1,J}u_{J+1,J}} \tag{2 16}$$

This is just a generalization of the solution (2. 11) for a two level system Thus upon combining equations (2. 9), (2. 11), (2. 12) and (2. 13), we have that

$$T_{J+1,J} = T_B(\nu_{J+1,J}) \tag{2. 17}$$

H. Case II:

Consider now the addition of other interactions (e. g collisions) to the situation of Case I. For the problem of immediate interest, we know from observation that the $J = 0$ and $J = 1$ rotational levels are the most populated levels,

and that these two populations are not inverted (or for the case of CH+, only the $J = 0$ level is observably populated).

We will show that T_{10} and T_{21} will in general set an upper limit to the brightness temperatures $T_B(\nu_{10})$ and $T_B(\nu_{21})$. Hence if the CN R(2) and the CH+ R(1) absorption lines are not detected (assuming that the corresponding CN R(1) and CH+ R(0) lines are observed) an upper limit to their optical depths will set upper limits to the radiation densities at the frequencies of the CN ($1 \rightarrow 2$) and the CH+ ($0 \rightarrow 1$) rotational transitions.

The proof for this case is somewhat more involved. If the allowed rotational transitions satisfy the selection rule $\Delta J = \pm 1$, but $R_{ij} \neq 0$ (we make no assumptions concerning the selection rules for the additional processes), then equations (2.14) specialize to

$$\frac{dn_J}{dt} = 0 = -n_J \sum_{J'=0}^{\infty} R_{JJ'} + \sum_{J'=0}^{\infty} n_{J'} R_{JJ'}$$

$$-n_J(A_{J,J-1} + B_{J,J-1}u_{J,J-1}) + n_{J-1}B_{J-1,J}u_{J,J-1} \qquad (2.18)$$

$$+n_{J+1}(A_{J+1,J} + B_{J+1,J}u_{J+1,J}) - n_J B_{J,J+1}u_{J+1,J}$$

Using equation (2.10) we can rewrite equations (2.18) for $J = 0$

$$\frac{n_1}{n_0} + \varepsilon_{10} + \frac{\sum_{J'=1}^{\infty} R_{0J'}\left(1 - \frac{g_0 n_{J'}}{g_{J'} n_0}\right)}{A_{10} + B_{10}u_{10}} \qquad (2.19)$$

and for $J = 1$

$$\frac{n_2}{n_1} = \xi_{21} + \frac{A_{10}+B_{10}u_{10} - \frac{n_0}{n_1} B_{01}u_{01} + \sum_{J'+1}^{\infty} R_{0J'}\left(1 - \frac{g_1 n_{J'}}{g_{J'} n_1}\right)}{A_{21} + B_{21}u_{21}} \quad (2.20)$$

Consider first equation (2. 20). We are given (from observation) that $n_J/n_1 < g_J/g_1$ for all $J \geq 2$. Hence the individual terms of the summation are all positive so that $n_1/n_0 \geq \xi_{10}$ and T_{10} will be an upper limit to $T_B(\nu_{10})$ Also note from equation (2. 14) that we can redefine u_{10} such that $R_{10} = R_{01} = 0$. Let us denote this by $u'_{10} \geq u_{10}$ and in the same respect define $\xi'_{10} \geq \xi_{10}$. We note that

$$\frac{n_1}{n_0} \geq \xi'_{10} \quad (2.21)$$

since we have introduced no negative terms into (2. 19) by this proceedure.

We are now in a position to consider equation (2 20). Introducing u'_{10} and ξ'_{10} into this equation we have

$$\frac{n_2}{n_1} = \xi_{21} + \frac{B_{01}u'_{10}\left(\frac{1}{\xi'_{10}} - \frac{n_0}{n_1}\right) + \sum_{J=2}^{\infty} R_{1J}\left(1 - \frac{g_1 n_J}{g_J n_1}\right)}{A_{21} + B_{21}u_{21}}$$

By our previous reasoning and by the use of inequality (2. 21) we find that $n_2/n_1 \geq \xi_{21}$, thus T'_{21} will be an upper limit to $T_B(\nu_{21})$

I. Case III:

Finally we proceed to consider the case of an interstellar cloud of CH molecules excited by both radiation and collisions. Again we appeal to observation and notice that the lowest level is by far the most populated.

CH is a diatomic molecule with both spin and orbital angular momentum in its ground state. Its coupling scheme is intermediate between Hund's case (a) and (b), hence the selection rules $\Delta J = 0, \pm 1$, $\Delta K = 0 \pm 1, \pm 2$, apply.

Since the spontaneous decay rates increase with the cube of the energy for higher levels, molecules in these levels will very rapidly decay back to the ground state. Also since the populations of these higher levels are very small, our calculation need only consider the three lowest lying rotational-fine structure levels. These are shown in Figure 3a. There are the levels KJ = 1 1/2, 1 3/2, and 2 3/2, which for brevity we will label 0, 1, and 2, respectively.

We will show that in contrast with the case of molecules with only $\Delta J = \pm 1$ transitions permitted, the fact that the transitions have a non-zero branching ratio prevents us from always using the population ratio to set an upper limit to the radiant intensity. We will find that n_1/n_0 and n_2/n_0 will not simultaneously set upper limits to the radiation density at frequencies ν_{10} and ν_{21}, but that $(1 + \varepsilon_1)\, n_1/n_0$ and $(1+ \varepsilon_2)\, n_2/n_0$ will set upper limits, i. e.

$$\xi_{10} \leq (1+\varepsilon_1)\ \frac{n_1}{n_0} \quad \text{and} \quad \xi_{20} \leq (1+\varepsilon_2)\ \frac{n_2}{n_0}$$

ε_1 and ε_2 are dependent upon the conditions of the molecules' location, and for conditions typical of the interstellar medium $\varepsilon_1 \approx 10^{-5}$ and $\varepsilon_2 \approx 10^{-12}$ Thus for all practical purposes, the level ratios themselves may be used to define the radiant intensity upper limits.

Since all these levels are connected by radiative transitions, following the proceedure used in Case II we will absorb all of the R_{ij} into $u'_{ij} \geq u_{ij}$, and in a similar fashion define $\xi'_{ij} \geq \xi_{ij}$. It will be noted that the ξ_{ij} (or ξ'_{ij})

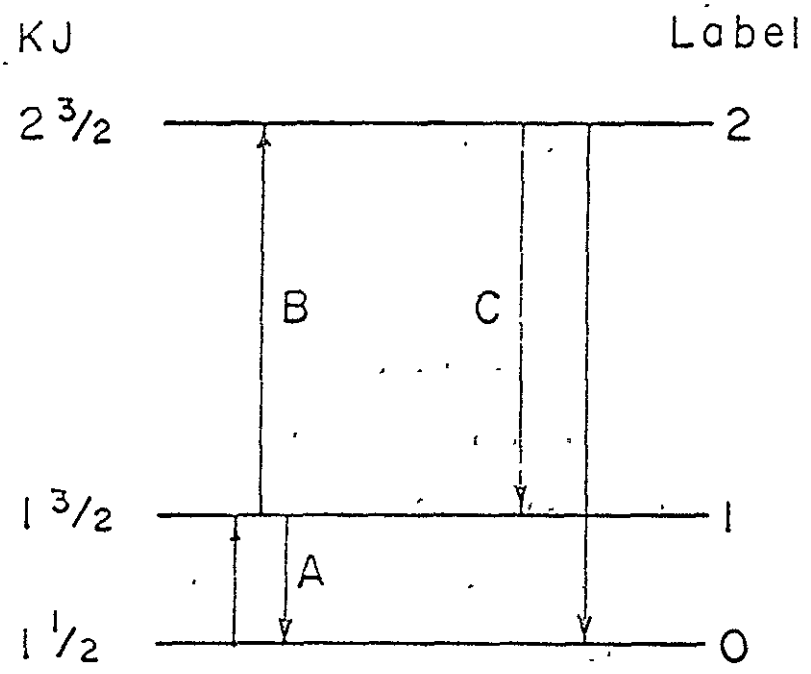

Figure 3 a. Transitions A try to keep levels 0 and 1 in thermal equilibrium. Transitions B and C depopulate level 1 and populate levels 2 and 0. The population of level 1 may become depressed if the rate of transitions B becomes very large with respect to that of transitions A.

are not necessarily related except in the case of thermal equilibrium of the whole system - then $\xi_{10}\xi_{21} = \xi_{20}$.

Specializing equations (2. 14) to this case, we can write the expression analagous to (2. 19) and (2. 20).

$$\frac{\frac{n_1}{n_0} - \xi'_{10}}{\xi'_{10}} = \frac{\frac{\xi'_{20}}{\xi'_{21}\xi'_{10}} - 1}{D_1} \tag{2. 23}$$

and

$$\frac{\frac{n_2}{n_0} - \xi'_{20}}{\xi'_{20}} = \frac{1 - \frac{\xi'_{20}}{\xi'_{21}\xi'_{10}}}{D_2} \tag{2. 24}$$

with the denominators given by

$$D_1 = \frac{B_{01}u'_{10}}{B_{02}u'_{20}} \cdot \frac{\xi'_{20}}{\xi'_{21}\xi'_{10}} + \frac{A_{10}}{B_{12}u'_{21}} + \frac{B_{10}u'_{10}}{B_{12}u'_{21}} + 1 \tag{2. 25}$$

$$D_2 = \frac{B_{02}u'_{20}}{B_{01}u'_{10}} \cdot \left(1 + \frac{A_{10}}{B_{12}u'_{21}}\right) + \frac{B_{20}u'_{20}}{B_{21}u'_{21}} + \frac{\xi'_{20}}{\xi'_{21}\xi'_{10}} \tag{2. 26}$$

Unfortunately expressions (2. 23) and (2. 24) cannot be simultaneously positive. i. e. either ξ'_{10} is bound above by n_1/n_0 or ξ'_{20} by n_2/n_0. Thus in marked contrast to the cases of CN and CH+, it is possible to depress the population of the first excited CH level by additional interactions. This can be seen from Figure 3a. If we arbitrarily increase the rate of $1 \rightarrow 2$ transitions while keeping $0 \rightarrow 1$ and $0 \rightarrow 2$ rates constant, we can effectively remove molecules from level 1 and transfer them to level 2, from which a portion will decay

to level 0. This process will effectively decrease n_1/n_0. It will occur if the $1 \rightarrow 2$ rate becomes large with respect to radiative $1 \rightarrow 0$ decay rate.

Let us consider equations (2. 23 - 2. 26) slightly further. If $A_{10}/(B_{12}u'_{21})$ is large, corresponding to a small rate $B_{12}u'_{21}$, then the denominators D_1 and D_2 will be large and n_1/n_0 and n_2/n_0 will set very good upper limits. This term is always large unless we have an enormous flux at ν_{21}. For CH $\lambda_{21} \approx 200\mu$ the strongest suggested source of radiation at this wavelength is thermal radiation from interstellar grains (Partridge and Peebles 1967). For the expected brightness of these,

$$A_{10}(B_{12}u_{21}) = 1/\epsilon_1 \approx 10^5 \tag{2. 27}$$

so ξ'_{10} is bounded by $n_1/n_0\,(1 + 10^{-5})$.

The same term also appears in the denominator D_2 multiplied by the factor $B_{02}u'_{20}/(B_{01}u'_{10})$. Since u'_{10} is now bounded, all that is required is a minimum energy density at ν_{20}, e.g. that radiated by grains, and D_2 will also be large. Taking the maximum energy density at ν_{10} allowed by observation, and the minimum at ν_{20} provided by grains, then

$$\frac{B_{02}u'_{20}}{B_{01}u'_{10}} \cdot \left(1 + \frac{A_{10}}{B_{12}u'_{21}}\right) = \frac{1}{\epsilon_2} \approx 10^{12} \tag{2. 28}$$

Hence we also are safe in using $n_2/n_0\,(1 + 10^{-12})$ to bound ξ'_{20}.

Nor can we call on collisions to significantly weaken these upper limits. In order to weaken the upper limits, we require a selective excitation rate for R_{12} with no associated increase in R_{01} and R_{02}, otherwise, the populations of at least one of the levels, 1 or 2, would have an observable population.

However, excitation of molecular rotation by collisions (of the first kind) with projectiles whose kinetic energy is very much greater than the 0 - 1 and 1 - 2 level spacing is not a selective process. Thus, collisions cannot provide the selective $1 \rightarrow 2$ excitation necessary to depress the KJ = 1 3/2 level population. In addition, even with the largest excitation cross sections due to the longest range forces (Coulomb), charged particle densities of at least 100 cm^{-3} would be required for there to be any effect at all As we will see later, there is specific evidence that the charged particle densities are nowhere near this high.

The only way to significantly weaken our upper limits is to have narrow band radiation at $\sim 200\mu$ which selectively excites the KJ = 1 3/2 - 2 3/2 transition of CH. The temperature calculated for this radiation must be at least as high as $\sim 12^{\circ}$ K. Although such "line radiation" cannot be totally ruled out by present observational work, it seems highly unlikely that such radiation might exist in the interstellar medium with an intensity this great. It must be sufficiently narrow band that it not excite the CH $\lambda 150\mu$ transition and the CH+ λ 359μ transition.

Thus it appears that we are quite safe in general in assuming that n_1/n_0 and n_2/n_0 set safe upper bounds to ξ'_{10} and ξ'_{20} and that the temperatures corresponding to these population ratios provide good upper limits to the brightness temperatures at ν_{10} and ν_{20}.

J. Sufficient Conditions for Thermal Equilibrium to Hold

From equations (2. 14) and (2. 15) it can be seen that for molecules

with a $^1\Sigma$ ground state, n_i/n_j will yield an actual measurement of $T_B(\nu_{ij})$ if all $R_{ij} \ll B_{01}\tilde{u}_{10}$ where $\tilde{u}_{10}$ is the intensity necessary to produce 2.7°K excitation. At present we need only concern ourselves with CN, since this is the only molecule in which an excited state population has been observed. *

The spontaneous decay rate may be written (Condon and Shortley 1951, p. 98) in terms of the line strength $S_{J,J-1}$ and rotation constant B as

$$A_{J,J-1} = \frac{64\pi^4\nu^3}{3hc^3(2J+1)} S_{J,J-1} = \frac{512\pi^4B^3}{3h} \cdot \frac{J^3}{2J+1} S_{J,J-1} \qquad (2.29)$$

Application of Edmonds' (1968) equation (5.4.5) to equation (2.5) yields

$$S_{J,J-1} = \mu^2(2J-1)(2J+1)\begin{pmatrix} J-1 & 1 & J \\ 0 & 0 & 0 \end{pmatrix} = \mu^2 J \qquad (2.30)$$

in terms of the Wigner 3j symbol, and hence

$$A_{J,J-1} = \frac{512\pi^4B^3}{3h} \cdot \frac{J^4}{2J+1} \mu^2 \qquad (2.31)$$

From a study of the optical stark effect of CN, Thomson and Dalby (1968) have recently determined the CN dipole moment to be 1.45 ± .08D. This agrees well with the predictions of molecular orbital calculations (Huo 1967) which indicate that the dipole moment is expected to be in the range 1.2 - 2.5D; and more or less confirms the work of Arpigney (1964) who deduced μ = 1.1D from an analysis of cometary spectra.

The rotation constant B_0 of CN has been determined to high precision by an analysis of the violet band to be $B_0 = 1.8909\text{cm}^{-1}$ (Poletto and Rigutti 1965)

---

* Expressions are derived in Appendix 2 which may be used for evaluating the corresponding Einstein coefficients for CH.

Using these values of B_0 and μ, equation (2.33) yields for CN

$$A_{10} = 1.1889 \times 10^{-5} \text{ sec}^{-1}$$

$$A_{21} = 11.413 \times 10^{-5} \text{ sec}^{-1}$$

What we must show in order to claim that the CN is in thermal equilibrium with the background radiation is that the R_{ij} are much smaller than

$$B_{01}\tilde{u}_{10} = \frac{g_1}{g_0} \cdot \frac{A_{10}}{\exp\left(\frac{h\nu_{10}}{kT}\right) - 1} = 8.69 \times 10^{-6} \qquad (2.32)$$

where $\tilde{u}_{10}$ is the intensity at ν_{10} necessary to produce an excitation temperature $T = 2.7°K$.

For most quantum mechanical processes the excitation rates fall off very rapidly with increasing ΔJ since the dipole term in the interaction potential is usually the dominant one, and has selection rules $\Delta J = 1$. Thus it will be sufficient for our purposes to simply show that for a given process, $R_{01} \ll B_{01}\tilde{u}_{10}$. We will see in Chapters 6, 7, and 8, that this is probably so if the CN is in an H I (non-ionized) region of space of reasonable density, but that it is not necessarily so if the CN resides in an H II (ionized) region.

CHAPTER 3

OPTICAL TRANSITION STRENGTH RATIO

A. CN and CH^+

In the last Chapter we saw that the rotational temperature may be calculated in terms of r, the observed optical depth ratio, and s, the theoretical transition strength ratio defined by equation (2. 8).

For lines in the same band s is independent of the electronic oscillator strength and Franck-Condon factor, and often depends upon only the angular momentum quantum numbers of the participating levels, K, K', J, and J'. The CN violet system is a good example of this. Although this transition is $^2\sum \rightarrow {}^2\sum$, the ρ-doubling produced by the electron spin is too small to be resolved in interstellar spectra, and on the grounds of spectroscopic stability (Condon and Shortley 1951, p. 20) we are justified in calculating intensities (and assigning quantum numbers in Figure 3 as our use of J for K implies) as though the transition were $^1\sum \rightarrow {}^1\sum$.

Thus when a molecule is well represented in either Hund's case (a) or (b), as are both CN and CH^+, the $S_{ii'}$ are proportional to the Hönl-London factors (Herzberg 1959, p. 208), and we have

$$s = \frac{J_i + J_{i'} + 1}{J_j + J_{j'} + 1} \tag{3.1}$$

However, for the case of CH which is intermediate between these two representations, the calculation is somewhat more involved. It requires a transformation of the matrix elements of the electric-dipole moment operator,

calculated in the pure Hund's case (b) representation, to the "mixed" representation in which the molecular Hamiltonian matrix is diagonal.

To effect this transformation, we need the matrices which diagonalize the molecular Hamiltonian matrix; hence, we also calculate this Hamiltonian matrix in the Hund's case (b) representation, and then calculate the transformation matrices which diagonalize it. As a check we notice that the resulting line strength ratio agrees with equation (3. 1) when we specialize our results to the case of a rigid rotor.

B. Matrix Elements of the Molecular Hamiltonian

Since the rotational energy of CH is large with respect to its fine structure, even for the lowest rotational levels, we calculate the molecular Hamiltonian in Hund's case (b). In this representation the appropriate coupling scheme is (Herzberg 1959, p. 221)

$$\underset{\sim}{K} = \underset{\sim}{N} + \underset{\sim}{\Lambda}, \quad \underset{\sim}{J} = \underset{\sim}{K} + \underset{\sim}{S} \tag{3. 2}$$

where in units of $\hbar$

$\underset{\sim}{\Lambda}$ is the component of electronic angular momentum along the internuclear axis,

$\underset{\sim}{N}$ is the molecular rotational angular momentum, and

$\underset{\sim}{S}$ is the spin angular momentum of the electron.

Appealing again to spectroscopic stability we ignore λ - doublets and hyperfine structure since these interactions, like ρ- doublets, are unresolved in interstellar optical spectra.

Following Van Vleck (1951), the molecular Hamiltonian is

$$\mathcal{H} = B\,(\underset{\sim}{K}^2 - \Lambda^2) + A\Lambda S_{z'} \qquad (3.3)$$

where A is the spin-orbit coupling constant, $S_{z'}$ is the spin angular momentum projected along the internuclear axis, and $B = \hbar^2/2I$, where I is the molecular moment of inertia. Ther term in $S_{z'}$ mixes together states of different K when the fine structure is appreciable with respect to the rotational energy and effects the transition away from Hund's case (b) towards case (a).

The matrix elements of this Hamiltonian for the Hund's case (b) coupling scheme are calculated in Appendix 1 to be*

$$\begin{aligned}\langle \Lambda K'SJ \,|\, \mathcal{H} \,|\, \Lambda KSJ \rangle &= B\left[\, K(K+1) - \Lambda^2 \,\right]\delta_{K'K} \\ &+ A\Lambda(-1)^{\Lambda+K'+K+S+J}\left[(2K'+1)(2K+1)\right]^{1/2} \begin{Bmatrix} J & S & K' \\ 1 & K & S \end{Bmatrix} \begin{pmatrix} K' & 1 & K \\ \Lambda & 0 & \Lambda \end{pmatrix}\end{aligned} \qquad (3.4)$$

If the 3j and 6j symbol are evaluated algebraically, this single expression yields both Van Vleck's (1951) equation (24) for the diagonal, and his equation (25) for the off-diagonal matrix elements, but with the opposite sign convention for the off-diagonal terms. **

---

* Van Vleck (1951) has calculated these matrix elements by exploiting the anomalous commutation relations of the angular momentum components referred to the molecular frame. He showed that the problem corresponds to the familiar case of spin-orbit coupling in atoms However, since his results yield the opposite sign convention from ours, and are of little value for calculating intensities, we have recalculated them here by more standard means.

** A misprint occurs in Van Vleck's equation (25). An exponent of 1/2 has been omitted from the last factor, which should read $[(K+1)^2 - \Lambda^2]^{1/2}$. The correct expression appears in the earlier paper of Hill and Van Vleck (1928).

Here selection rules may be seen implicit in the properties of the 3j and 6j symbols. The selection rule $\Delta K = 0, \pm 1$ for the molecular Hamiltonian in case (b), for example, follows from the requirement that the rwo K', 1, K of the 3j symbol in equation (3.4) satisfy the triangular rule.

For a molecule intermediate between Hund's case (a) and (b), in general, K is no longer a good quantum number in the representation where the Hamiltonian of equation (3.4) is diagonal. We may, however, label a given state with the value of K which it assumes when the molecular fine structure constant A vanishes. We will distinguish K by a carat when it is used as a label in this way The stationary state is then written as $|\Lambda \hat{K} SJ\rangle$, and the unitary matrix which transforms from case (b) to the diagonal frame as $U_{\hat{K}K}$. This unitary matrix will be used to transform the dipole moment operator into the representation in which the molecular Hamiltonian is diagonal, and may be calculated from (3.4) by a standard matrix diagonalization proceedure.

For the diagonalized molecular Hamiltonian matrix itself, we have

$$\langle \Lambda \hat{K}' SJ | \mathcal{H} | \Lambda \hat{K} SJ \rangle = \sum_{K'K} U_{\hat{K}'K} U^{*}_{\hat{K}K} \langle \Lambda K'SJ | \mathcal{H} | \Lambda KSJ \rangle \qquad (3.5)$$

Inserting into this formula the coupling constants for CH of Table 2, and diagonalizing the matrices for the upper and lower electronic states of CH, we have the partial energy level scheme shown in Figure 3.

C. Line Strengths

As before, we take the line strengths to be proportional to the absolute square of the electric dipole moment operator reduced matrix element

$$S = \mu^2 \left| \langle \Lambda \hat{K} SJ\alpha \| \underset{\approx}{C}(1) \| \Lambda \hat{K}' SJ'\alpha' \rangle \right|^2 , \qquad (3.6)$$

where α represents all other non-diagonal quantum numbers.

This reduced matrix element has been evaluated in Appendix 2 for the CH coupling scheme

$$\left| \langle \Lambda \hat{K} SJ\alpha | | \underset{\approx}{C}(1) | | \Lambda' \hat{K}' SJ'\alpha' \rangle \right|^2 = \left| \sum_{K'K} U_{\hat{K}'K'} U^{*}_{\hat{K}K} \right.$$

$$(-1)^{\Lambda+S+J'+1} \left[(2K'+1)(2K+1)(2J'+1)(2J+1) \right]^{1/2} \tag{3.7}$$

$$\left\{ \begin{matrix} K' & J' & S \\ J & K & 1 \end{matrix} \right\} \sum_{q} \langle \alpha | C_{1q} | \alpha' \rangle \begin{pmatrix} K & 1 & K' \\ -\Lambda & q & \Lambda' \end{pmatrix} \Bigg|^2$$

The usual symmetric-top selection rules for electric-dipole transitions, $\Delta K = 0, \pm 1$, $\Delta J = 0, \pm 1$, are implicit in the 3j and 6j symbols (but note that the transition to case (a) allows $\Delta \hat{K} = \pm 2$ transitions).

When both the upper and lower states are diagonal in the Hund's case (b) representation, and we let the electronic matrix elements $\langle \alpha' | Y_{1q} | \alpha \rangle$ equal one, expression (3.7) reduces to that of the Honl-London factors (Herzberg 1959, p. 208).

When equation (3.7) is specialized to the case of a rigid rotor (CN and CH+) with $K' = J'$, $K = J$, and $S = 0$, and with the electronic matrix element again equal to one, using Edmonds' (1968) equation (6.3.2) we have

$$\left| \langle \Lambda J \| \underset{\approx}{C}(1) \| \Lambda' J' \rangle \right|^2 = (2J'+1)(2J+1) \begin{pmatrix} J & 1 & J' \\ -\Lambda & q & \Lambda' \end{pmatrix}^2 , \tag{3.8}$$

where $q = \Lambda - \Lambda'$, and $|q| \leq 1$

With the molecular constants found in Table 2, the resulting values of s, calculated from equations (3.7) and (3.8)* for the coupling schemes of CN, CH,

---

* in agreement with (3.1) for CH+ and CN

and CH+, are found in Table 1.

CHAPTER 4

TECHNIQUES OF SPECTROPHOTOMETRY AND PLATE SYNTHESIS

A. Available Plates and Spectrophotometry

The optical lines of interstellar CN are characteristically sharp and weak, and occur in the spectra of only a handful of stars. The strongest line, R(0) at $\lambda 3874.6$Å, has an equivalent width which is seldom as strong as 10mÅ, while the neighboring R(1) and R(2) lines are weaker by a factor of ~ 4 and ~ 100 for an excitation temperature $\sim 3^{\circ}$K.

The state of the art in high resolution astronomical spectroscopy for the detection of weak lines has not greatly improved over the past thirty years - the weakest line which is detectable with a reasonable degree of certainty on a single spectrogram is $\sim$ 1 - 3 mÅ. Hence it was clear at the outset of this work that a new technique would have to be developed if we were to attempt to detect the CN R(2) line, as well as to measure accurately the R(1) line.

At the beginning of this work the best available spectragrams of interstellar molecular absorption lines were those of Adams and Dunham from Mt Wilson, Münch from Mt. Palomar, and Herbig from the Lick 120-inch telescope. Since long exposures are the rule for these spectrograms, and observing time on large telescopes with good Coudé spectrographs is somewhat difficult to obtain, it appeared that the most straight forward way to improve the signal-to-noise ratio was to add the many available individual plates, and to filter out the high frequency grain noise from the composite spectra.

Direct superposition of the spectrograms on the densitometer ("plate stacking") is not practical when many spectra are to be added together,

or when the spectra are dissimilar. In addition, this proceedure does not allow one to independently weight the individual spectra. The more flexible method of computer reduction of the data was felt to be best. This technique involved digitization of the spectra, and their calibration and synthesis on a digital computer. * The spectra could then be filtered of grain noise numerically in the manner suggested by Fellgett (1953) and Westphal (1965). The whole system turned out to be very flexible so that the large heterogeneous group of plates could be added without difficulty

Most of the plates were obtained from the extensive collection of high-dispersion spectrograms stored in the Mt. Wilson Observatory plate files. There were obtained primarily by Adams and Dunham with the Coudé spectrograph of the 100-inch telescope and its 114" camera, and were used by Adams (1949) in his classic study of interstellar lines. The spectra of the two ninth magnitude stars BD+66°1674 and BD+66°1675 were taken by Münch (1964) with the 200-inch telescope. The synthesis for ζ Ophiuchi includes six spectra obtained by Herbig (1968) with the Lick 120-inch telescope using the 160" camera, and were used by him in his recent study of the interstellar cloud in front of ζ Ophiuchi. (The latter were also analyzed by Field and Hitchcock [1964] in their discussion of the microwave background.) We are indebted to Drs. Munch and Herbig for the loan of these plates.

---

* Similar techniques have been used by Herbig (1966) for a small number of similar plates

Data such as the emulsion, exposure time, etc., for the individual plates were copied for the most part from the observing notebook, and are listed in Table 3. Also in this Table are the relative weights (determined from statistical analysis of grain noise as described below), which the individual spectra are given in the final synthesis.

It is evident from the Table and from the weights that they by no means represent a homogeneous collection. The weights were determined by a visual estimate of the grain noise r. m. s. level on tracings which were normalized to the same signal level. The normalized tracings were then combined with the usual prescription of weighting them inversely as the square of the noise level.

These plates were scanned at the California Institute of Technology on a Sinclair Smith microdensitometer, the output of which was fed across the Caltech campus via shielded cable to an analog-to-digital converter. This was connected to an IBM 7040 computer which wrote the digitized signal on magnetic tape, and subsequent analysis of the data was done on an IBM 360/75 computer at the Goddard Institute for Space Studies (GISS) in New York City.

Figure 4 shows the setup of equipment at Caltech The output of the densitometer was digitized at a constant rate of 100 samples per second. The lead screw was not digitized but also ran at a constant speed. The projected acceptance slit width and lead screw speed were adjusted to suit the dispersion of the plate and the width of the narrowest spectral features being studied, which were about 0.05Å. Thus for the Mt. Wilson 114" camera plates, (dispersion = 2.9Å/mm) which comprise the bulk of the data,

the plate advanced at 5. 6mm/min (16. 3Å/min). For the narrowest lines this is about five line widths per second. In other words at least 20 data points were obtained per resolution element, which is ample for our purposes.

The projected acceptance slit width was adjusted to the dispersion of the plate being scanned to approximately 1/6 of the full line width of the interstellar lines. Thus for plates from the 114" camera the projected slit width was about 2. 9μ, which leads to negligible signal distortion.

Four or more densitometer traces were usually taken in the vicinity of the three wavelength regions of interest, λ 3874Å, λ4232Å, and λ4300Å. Two were required for the comparison spectra on either side of the stellar spectrum, at least one was required for the stellar spectrum itself, while a single scan perpendicular to the dispersion of the spectrograph was necessary to record intensity calibration wedge bars.

In order to establish a reference wavelength common to the stellar and comparison spectra, a razor blade was placed across the emulsion as shown in Figure 5. A scan started on the razor blade and moved off the edge onto the spectrum as shown in the Figure, with the edge producing an initial step in the recorded spectrum. In addition to providing a wavelength fiducial mark, the step provided a measure of the response time of the electronics and the optical resolution of the system, and in the case of the intensity wedge, provided a dark-plate level.

B. Synthesis Programs:

The computer program for plate synthesis was divided into three

sub-programs, each sub-program was processed separately with the input for a given sub-program being the output tapes from the previous one. There were named Sys 3, Sys 4, and Sys 5.

Sys 3 read the 7040 tapes and data such as the transverse lead screw position, which had been punched manually onto cards, and scanned this data for errors. Preliminary plots of each vector versus index were made after it had been adjusted to start at the fiducial mark step (caused by the razor edge), so that the index of a given digitized point in the vector was proportional to its corresponding distance from the razor edge. Output of plates corresponding to different molecules were sorted onto different tapes so that processing of a tape after this point was for a single spectral region The basic purpose of Sys 3 was to pre-process as much information as possible to implement the smooth running of Sys 4.

Sys 4 took the left adjusted vectors for each plate and converted these to two (or more if there were more than one input stellar spectrum vector) parallel vectors of intensity and wavelength (shifted to the molecule's rest frame). This was done in two parts using an IBM 2250 CRT display console in conjunction with the GISS computer. The first part used the wedge vector to convert the recorded plate transmissions to intensity. The calibration density wedge bars had been put on the plate at calibrated light levels, the values of which were stored in the computer.

The wedge bars from the density wedge vector appear as rectangular peaks as shown in Figure 6. The limits of these rectangular bars were determined in Sys 4 by displaying the wedge vector on the 2250 console, and picking

out the ends of the rectangular peaks with a light pen. The computer then averaged the transmission over each wedge bar. Since the two sides of the wedge were put on the plate at different intensities, the wedge values on one side were scaled up or down to interleave them between adjacent points on the other side. The composite curve was then fit with five terms of a Laurent series, a typical result of which is shown in Figure 7. The series was finally applied to each point in each spectral vector converting the plate transmission to intensity.

The second part of Sys 4 calibrated the index scale in terms of wavelength Each comparison spectrum was displayed on the 2250 Display Console and the centers of selected lines were located with the console light pen. The corresponding wavelength of each line was then plotted on the 2250 screen as a function of index. Since the dispersion is highly linear over the ~ 10Å traced in the vicinity of each interstellar line, these points appeared on the screen in a straight line. A straight line least-square fit was also displayed on the screen, which aided in the correction of any line misidentification The output of Sys 4 was finally two parallel vectors of intensity and corresponding wavelength appropriate to the laboratory frame.

In general, high resolution Coudé spectrographs are rather well matched to the emulsions used in astrophysical spectroscopy, and grain noise which is "high frequency" with respect to sharp interstellar lines is not conspicuous. In order to extract the maximum amount of statistical information from the data at hand, however, a considerable amount of thought was given to the problem of numerically filtering the final spectra. A description of the statistical analysis appears in Appendix 4. The final result of the analysis

was to prescribe a filter function to be used to filter the calculated synthesis.

Thus, Sys 5 was designed to take the successive outputs from Sys 4 and to add these together with the appropriate statistical weights. It then filtered out the "high frequency" noise by convolving the synthesis with the above filter function. The final output of Sys 5 for each star and molecule was three vectors:

1. Wavelength in the molecular rest frame
2. Unfiltered spectrum
3. Filtered spectrum

CHAPTER 5

RESULTS OF SYNTHESIS

A. Curve of Growth Analysis

Figures 9, 10, and 11, show the results of adding together, in the manner just described, the available spectra of interstellar CN, CH, and CH+ for a number of stars. As just mentioned the wavelength scales in these plots are those of the molecular rest frame, and the final spectra except for ζ Persei CN and ζ Ophiuchi CN have been numerically filtered. The number of individual spectra included in each synthesis and the corresponding vertical magnification factor are indicated on the left side of Figure 9.

Table 4 lists the visual magnitudes, MK spectral types galactic latitudes as well as the equivalent widths W and optical depths τ, for the interstellar lines measured. The uncertainties of W in all instances result from a statistical analysis of the grain noise, and represent a level of confidence of 95.5% (see Appendix 4). Also all upper limits set on the strengths of unobserved lines represent the more conservative confidence level 99.7%.

For ζ Ophiuchi the equivalent widths of the interstellar molecular lines listed in Table 4 are systematically smaller by $\sim$ 30% than the values obtained by Herbig (1968a) from plates taken at the 120-inch Coude We note, however, that Dunham (1941) reported W = 6mÅ for the CN R(0) line and W = 14mÅ for the CH $R_2(1)$ line in ζ Ophiuchi, and O. C. Wilson (1948) reported W = 16 ± 2mÅ for the CH+ R(0) line in ζ Ophiuchi, both from Mt. Wilson plates and both in good agreement with out values of 6 62, 13.4, and 19.6 mÅ respectively.

Since most of the spectra from which our values are derived were also obtained with the 100-inch telescope about thirty years ago, this gives us some confidence that the discrepancy is not a result of an error in calibrating or adding together the spectra, but represents instead a systematic difference between equivalent widths obtained with the 100-inch Coude then and the 120-inch Coude now.* Our main interest, however, is only in the ratio of line strengths, which in the limit of weak lines is independent of systematic uncertainties of this kind, and it is accordingly unnecessary to explore this point further. But we emphasize that the uncertainties listed in Table 4 can only be taken seriously in a relative sense, and are liable to be considerably less than absolute uncertainties.

Also included in this Table for completeness are several late B and early A type stars whose rotational temperatures have been estimated by other workers.

The calculation of the optical depths in Table 4 requires some knowledge or assumption concerning the true shape and width of the interstellar molecular lines. In general the lines we are considering are not quite resolved, and it is thus necessary to make several assumptions concerning the curve of growth Fortunately the CN lines are usually so weak that the correction for saturation is small, and our final results are not very sensitive to these assumptions.

---

* It is interesting to note, however, that Adams (1949) was led to suggest that the molecular absorption spectra may be time variant.

We assume a gaussian line shape in all cases (see Appendix 4) and use the curve of growth due to Strömgren (1948) and Spitzer (1948), and the tabulation of Ladenburg* (1930). For ζ Ophiuchi we adopt for the linewidth parameter b = 0.61km/sec, which is the value b = 0.85km/sec found by Herbig (1968a), for interstellar CH+ in the spectrum of this star, corrected for the apparently systematic difference in the measured equivalent widths of the CN R(0) line. In lieu of any other information we assign b = 0.85km/sec tothe CN lines of ζ Persei, since this star lies at a distance comparable to ζ Ophiuchi, and is also well off the galactic plane. ** (We have also found with the 300-foot transit radio telescope at Green Bank, that the 21cm profile in the direction of this star closely resembles that in the direction of ζ Ophiuchi - see Chapter 9.)

The signal strengths for the CN lines of the remaining stars shown in Figure 9 scarcely justify correction for line saturation: we simply adopt b = 1km/sec for all remaining stars except BD+66°1674 and BD+66°1675, to which we assign b = 5km/sec, on the basis of their great distance and low galactic latitude.

The excitation temperatures of interstellar CN may now be calculated from the ratios of the optical depths listed in Table 4 from equation (3.4).

---

* This was rechecked and a finer tabulation made.

** Further work should be done to obtain a good curve of growth for this star due to its importance here.

B. CN ($J = 0 \rightarrow 1$) Rotational Temperature and Upper Limit to the Background Radiation at λ 2.64mm

Table 4 now shows the results of the application of equation (3.4) to this data, taking $\nu_{10} = 1.134 \times 10^{11} sec^{-1}$ ($\lambda = 2.64mm$) corresponding to the $J = 0 \rightarrow 1$ transition in CN. The listed value of $T_{10}(CN)$ results from the ratio of the optical depths listed in Table 4. The entry labeled ΔT lowers $T_{10}(CN)$ by an amount which is at most comparable to the uncertainty due to the plate grain noise and , therefore, our final results as mentioned above do not critically depend on the assumptions that were made concerning the curve of growth

To get an upper limit on the radiation intensity we need consider only ζ Ophiuchi, where the molecular absorption lines have the greatest signal-to-noise ratio. For this star the weighted mean of the values found from the line strength ratios R(1)/R(0) and P(1)/R(0), given respective weights of 4 to 1, the square of the corresponding values of s (see Chapter 3), yields $T_B(2.64mm) \leq T_{10}(CN) = 2.74 \pm 0.22°K$. In terms of the intensity of radiation this becomes

$$I_\nu(2.64mm) \leq 3.42 \times 10^{-15} erg\ cm^{-2}\ sec^{-1}\ ster^{-1}\ Hz^{-1}$$

C. Upper Limit to Background Radiation at $\lambda = 1.32mm$

The observed absence in the spectrum of ζ Ophiuchi of the CN R(2) line at λ 3873.369Å places an upper limit to the background intensity at $\lambda = 1.32mm$. From the spectrum of Figure 9 it is found that the equivalent width of the CN R(2) line is less than 0.44mÅ, to a level of confidence of 99.7%. The curve of growth analysis described above then yields $\tau < 0.031$, and the rotational temperature found from equation (3.4) and the R(2)/R(1) ratio is

$$T_B\,(1.32\text{mm}) \leq T_{21}(\text{CN}) < 5.49^\circ\text{K}$$

and

$$I_\nu(1.32\text{mm}) < 2.75 \times 10^{-14}\ \text{erg cm}^{-2}\ \text{sec}^{-1}\ \text{ster}^{-1}\ \text{Hz}^{-1}$$

which is still a factor of 8.3 above the intensity of 2.74°K thermal radiation, but a factor of 1.6 below the intensity of 2.74°K greybody* radiation. This upper limit is shown in Figure 12.

D. Radiation Upper Limit at $\lambda = 0.359$mm

The observed absence of the CH+ R(1) line at λ 4229.341Å in the spectrum of ζ Ophiuchi synthesized from 19 spectra of this star and shown in Figure 11, allows an upper limit to be placed on the intensity of radiation at the wavelength of the CH+ $J = 0 \rightarrow 1$ transition (0.359mm).

As with CN the optical depths listed in Table 4 were calculated using Herbig's (1968a) value b = 0.85km/sec for the linewidth parameter, adjusted to take into account the apparently systematic difference between our and his equivalent widths.

For the CH+ R(1)/R(0) ratio it was found that $s = 3/2$, $\nu_{10} = 8.35 \times 10^{11}$Hz and

$$T_B(0.359\text{mm}) \leq T\ (\text{CH+}) \leq 9.01\ \text{K},$$

or

$$I_\nu(0.359\text{mm}) < 10.1 \times 10^{-14}\ \text{erg cm}^{-2}\ \text{sec}^{-1}\ \text{ster}^{-1}\ \text{Hz}^{-1}$$

---

* i.e. the extrapolation of the Rayleigh-Jeans intensity $I_\nu = 2kT\nu^2/c^2$ to short wavelengths. Radiation from an optically thin medium such as dust can approximate a spectrum of this type.

E. Detection of Interstellar $C^{13}H^+$

Also shown in Figure 11 is the faint trace of the R(0) line of $C^{13}H^+$ originally sought by Wilson (1948) and again by Herbig (1968b). A statistical analysis yields for the equivalent width $0.6 \pm .3$mÅ to a confidence level of 95%. Together with the R(0) line of $C^{12}H^+$ this yields for the isotopic abundance ratio along the line of sight $C^{12}/C^{13} = 62^{+100}_{-22}$ in agreement with the value 82^{+55}_{-15} independently found by Bortolot and Thaddeus (1969) and also with the terrestial value 89, but much greater than the equilibrium value ≈ 4, for the CN bi-cycle (Caughlin, 1965). This observation strengthens Herbig's (1968b) earlier conclusion that the material in the ζ Ophiuchi cloud did not come from C^{13} rich stars, but raises the question of how one explains the apparent agreement of this value with the terrestial one.

Bortolot and Thaddeus (1969) suggest that the coincidence of the terrestial C^{13} abundance with that of the interstellar abundance is due to the origin of the solar system out of an interstellar medium with a fixed C^{13} abundance. This notion is consistent with the coincidence of the atmospheric C^{13} abundance of Venus with the terrestial abundance (Connes et al 1968); however it is inconsistent with the recent observations of Lambert and Malia (1968) who find the solar abundance ratio to be $C^{13}/C^{12} = 150 \pm 30$, a value which exceeds the terrestial ratio by nearly a factor of two. *

Lambert and Malia believe that their observation represents at least

* There is considerable dispute on the question of the solar C^{13} abundance (Cameron, 1969).

a definite upper limit to the solar C^{13} abundance. Since there is no obvious process which might increase the solar C^{13} abundance, further work confirming their observations will represent strong evidence favoring the suggestion of Fowler et al (1961) that the planetary abundances are a product of spallation, and is otherwise unrelated to the interstellar C^{13} abundance.

F. Radiation Upper limits at $\lambda = 0.560$ and $\lambda = 0.150$mm

Figure 10 shows the result of the synthesis of seventeen spectra of ζ Ophiuchi in the vicinity of $\lambda = 4300$Å, the strongest lines of CH. The observed absences of the CH $R_1(1)$ and $R_2(2)$ lines at $\lambda = 4304.946$Å and 4296.636Å allow upper limits to be placed on background intensity at the wavelengths of the CH KJ = 1 1/2 → 1 3/2 ($\lambda = 0.560$mm) and KJ = 1 1/2 → 2 3/2 ($\lambda = 0.150$mm) transitions. We again use b = 0.85mm (corrected).

For the CH KJ = 1 1/2 → 1 3/2 transition s was calculated in Chapter 3 to be 1.525. Taking $\nu_{1\ 3/2,\ 1\ 1/2} = 5.37 \times 10^{11}$Hz ($\lambda = 0.560$mm), equation (3.4) and the data of Table 4 then yield

$$T_B(0.560\text{mm}) \leq T_{1\ 3/2,\ 1\ 1/2}(\text{CH}) < 6.33°\text{K}$$

or

$$I_\nu(0.560\text{mm}) \leq 3.91 \times 10^{-14} \text{erg cm}^{-2} \text{sec}^{-1} \text{ster}^{-1} \text{Hz}^{-1}$$

Finally for the CH KJ = 2 3/2 → 1 1/2 transition s = 0.820 and $\nu_{2\ 3/2,\ 1\ 1/2} = 2.00 \times 10^{12}$ Hz ($\lambda = 0.150$mm). Hence

$$T_B(0.150\text{mm}) \leq T_{2\ 3/2,\ 1\ 1/2}(\text{CH}) < 28.5°\text{K}$$

or

$$I_\nu(0.150\text{mm}) < 4.2 \times 10^{-12} \text{erg cm}^{-2} \text{sec}^{-1} \text{ster}^{-1} \text{Hz}^{-1}$$

G. Discussion of Upper Limits

At 150μ the most important source of background might be the contribution from young galaxies (Low and Tucker 1968, Partridge and Peebles 1967). However the CH upper limit at 150μ is $\sim 10^5$ greater than the expected integrated brightness of these objects and as a result is of little value.

The constraints which the other upper limits impose on the background radiation are shown in Figure 12. Except for the point at 2.64mm, they fall well above the blackbody curve at T = 2.7 °K, and all are considerably below the corresponding greybody curve. They immediately represent much of the information we possess on the radiative content of the universe at these wavelengths. It bears final emphasis that as upper limits, all of these points are virtually independent of any considerations concerning the location or environment of the molecules.

Shivananden, et. al. (1968), have recently reported the detection of a background flux in the wavelength interval from .4 to 1.3mm with a rocket-borne wide-band detector. They detected a flux of 5×10^{-9} W cm^{-2} ster^{-1} which yields a mean intensity over this frequency range of $\bar{I}_\nu = 9.6 \times 10^{-14}$ erg cm^{-2} ster^{-1} Hz^{-1}. This flux is represented in Figure 12 by the area under the line AA'. Since its mean value is nearly three times greater than the CH upper limit which falls right in the center of their frequency range, it may be concluded that either their observation is of a background with highly irregular spectrum (eg. spectral lines), or it is of a flux of quite local origin which does not extend as far as the major interstellar cloud in front of ζ Ophiuchi.

The important question which is unanswered at this point in the analysis is what is the meaning of the observed $J = 1$ level population of CN. In the remaining Chapters we will try to show that, in all probability, this population provides a good measure of the radiation intensity at λ 2 64mm, and the intensity at this wavelength is equal to that of a blackbody temperature $T_B = T_{10}(CN)$.

CHAPTER 6

ALTERNATE RADIATIVE EXCITATION MECHANISMS

In addition to direct rotational excitation of CN by microwave photons, radiative excitation is possible to both higher vibrational and electronic states by infrared and optical photons. The characteristic lifetimes of these higher states are very short, and virtually all of the molecules will be found in the ground electronic and vibrational states. However, indirect rotational excitation is possible by means of electronic and vibrational fluorescence. A CN molecule can be excited to a high vibrational or electronic level by an optical photon (from dilute starlight for example) and re-emit a photon while making a transition back to a rotational level different from the one in which it started. Hence, this cycle can effectively populate higher rotational levels, and contribute to the observed rotational temperature. Typical cycles are shown in Figure 13.

Such indirect processes are potentially very serious alternate mechanisms for the CN rotational excitation, in that they might provide an explanation for the observed rotational temperature invariance in eleven stars. This observed invariance provides the strongest single piece of evidence that the CN is not excited by processes other than the cosmic microwave background. (See Chapter 9)

The explanation for the invariance in terms of fluorescence could come in either of two ways. First, if the excitation is produced by galactic starlight, the inherent uniformity of this radiation might account for the observed invariance. Second, the process of CN formation in the interstellar medium

is not well understood (see, for example, Dieter and Goss 1968), and it seems plausible to suggest that the CN is only formed at certain distances from a star, and thus would always be subject to the same radiation field. In this respect* Münch (1964) has proposed that the CN is being flashed off interstellar grains by the advancing ionization front at an H I - H II boundary.

However, it will be shown in this Chapter that, (1) vibrational fluorescent excitation is negligible by more than six orders of magnitude. (2) Electronic fluorescence is insufficient to account for the observed CN rotational excitation by at least three orders of magnitude for galactic starlight. (3) If the CN is close enough to a star, perhaps the star used to observe it, for fluorescence to contribute materially to the rotational excitation of the ground state then the photo-dissociation rate will be so high that the molecules will be destroyed at a rate much faster than any suggested mechanism for their production. In addition, the idea that the molecules are circumstellar is inconsistent with out present ideas concerning the location of the molecules.

A. Criterion for Fluorescence to be Negligible

We saw in Chapter 2 that a sufficient criterion for a process to be negligible is for $R_{J'',J''+1} << A_{J''+1,J''}$, where J'' and $J''+1$ represent rotational levels in the electronic ground state ** e''.

---

* The suggestion by Merrill (1942, 1946) that the CN might be circumstellar was dispelled by Adams (1949, see Chapter 7).

** Unless otherwise specified, e'' will be used to denote either an electronic or a vibrational state.

Fluorescent excitation involves first a transition from rotational level J'' in the ground electronic and vibrational state e'', to a level J' in a higher electronic or vibrational state e'. This will occur at a rate given by $u_{e'J', e''J''}B_{e''J'', e'J'}$. Subsequently, the molecule decays to a rotational level J in the electronic ground state e''. Since the excited vibrational or electronic state lifetimes are very short, in general,

$$A_{e'J', e''J} >> u_{e'J', e''J''}B_{e''J'', e'J'}. \tag{6.1}$$

Thus for a given band system, the total rotational excitation rate is given approximately by

$$R_{J'', J} \approx \alpha_{e'J', e''J''} u_{e'J, e'J''} B_{e''J'', e'J'} \tag{6.2}$$

where $\alpha_{e'J', e''J}$ is the branching ratio of $e'J \rightarrow e''J$ electronic decays (including cascades through an intermediate electronic state) to all other possible electronic decays. α will generally be ~ 1 (always ≤ 1). Hence a sufficient criterion for fluorescence to provide negligible rotational excitation is for

$$u_{e'J', e''J''}B_{e''J'', e'J'} << A_{J'', J''+1} \tag{6.3}$$

for all e', J'.

B. Vibrational Fluorescence

We will assume that the galactic radiation field near $\lambda \sim 4.9\mu$ (the wavelength of the CN v= 0 → 1vibrational transition) is predominantly dilute starlight. Speculation about the existance of radiation from young galaxies (Partridge and Peebles 1967) suggests an additional contribution which is at most the same order of magnitude, so we will neglect this component.

The energy density of starlight at this wavelength is given by

$$u(4.9\mu) = 8.8 \times 10^{-28} \text{ erg cm}^{-1} \text{ Hz}^{-1}$$

The Einstein B coefficient for this transition is calculated in Appendix 3, and from it we calculate that

$$R_{v=0,1} \leq 4 \times 10^{-12} \text{ sec}^{-1} .$$

This rate is totally negligible with respect to the excitation rate necessary to produce the observed 2.7°K excitation $B_{01}\tilde{u}_{10} = 8.7 \times 10^{-6}$. Thus vibrational excitation falls short by six orders of magnitude in accounting for the observed excitation.

C. Electronic Fluorescence

For electronic transitions in which one electron is involved, we can write the Einstein B coefficient in terms of the electronic oscillator strength or "f value" (≤ 1)(Herzberg 1959) . Thus the upper limit for the excitation by optical photons of frequency $\nu = \nu_{e'v'J', e''v''J''}$ is given by

$$R_{J'', J''+1} \leq \frac{u(\nu)\ \pi e^2 f_{e''e'}\ |\mathfrak{M}^{(vib)}_{v'v''}|^2\ |\mathfrak{M}^{(rot)}_{J''J'}|^2}{mhc\ \nu\ (2J''+1)} \qquad (6.4)$$

where $|\mathfrak{M}^{(rot)}_{J''J'}|^2$ are the Honl - London factors, and $|\mathfrak{M}^{(vib)}_{v''v'}|^2$ are the Franck - Condon factors.

Then the usual sum rules apply

$$\sum_{J'} \sum_{M'M''} |\mathfrak{M}^{(rot)}_{J''J'}|^2 = 2J''+1 \qquad (6.5)$$

$$\sum_{v'} \left| \mathfrak{M}^{(vib)}_{v'v''} \right|^2 = 1 \quad . \tag{6.6}$$

$$\sum_{e'} f_{e''e'} = 1 \tag{6.7}$$

Since $u(\nu)$ is a slowly varying function of ν, and the excitation will be predominantly via the (0, 0) band, we may sum over allowed rotational and vibrational transitions to get

$$R_{01} \leq u(\nu) \frac{\pi e^2 f_{e''e'}}{mhc\nu} \quad . \tag{6.8}$$

where $\nu = \nu_{e' v=0 J''=1,\ e''v''=0 J''=0}$

C_a CN Band Systems

CN has two band systems in the visible, the well known red ($X^2\Sigma - A^2\Pi$) and violet ($X^2\Sigma - B^2\Sigma$) systems. The f values for these transitions have been measured to be 0. 0034 (Jeunehomme, 1965) and 0. 027 (Bennett and Dalby 1962) respectively.

Ultraviolet systems involving electronic states above $B^2\Sigma$ have been studied by Douglas and Routly (1954, 1955), and by Carroll (1956). Our current knowledge of the electronic term scheme of CN is shown in Figure 14.

It is of considerable importance to us to know the oscillator strengths of the CN ultraviolet systems. Douglas (1968) has searched unsuccessfully for these transitions in absorption down to $\lambda \sim 1400$Å, in a long path length "White-Cell". He has concluded that all of the oscillator strengths for these ultraviolet systems, which terminate in the ground electronic state, are less than the oscillator strength of the violet system (. 027). The CN dissociation

energy corresponds to $\lambda \sim 1500$ Å (Carroll 1956), thus any state with a large oscillator strength for transitions from the ground state must lie beyond the dissociation limit.

$C_b - R_{01}$ Upper Limits

It is revealing now to calculate the upper limit for R_{01} given by (6. 8) assuming f and α to be equal to 1. This is plotted in Figure 15 as a function of wavelength, for a radiation field corresponding to that of the galactic starlight background (Zimmerman 1964). For the red and violet bands the measured f values are also shown displacing these upper limits accordingly.

Thus it is clear that for any band system, the fluorescent excitation rate due to the galactic background will be $\sim 2 \times 10^{-9} \text{sec}^{-1}$, or smaller. This is $\sim$ 6000 times too small to yield the required excitation, and we may thus conclude, without further discussion, that the galactic starlight background is not responsible for the CN excitation. This is a most important point, since this is the only process which we have been able to find which might account for the observed independence of T_{10}(CN) with respect to galactic latitude, longitude or spectral type of the star against which the CN is observed.

Now consider the situation in which the star is the source of fluorescent radiation. Figure 15 also shows the upper limit for R_{01} given by (6. 8) for a radiation field corresponding to that of a line blanketed B0v star at a distance of 10pc (Hickok and Morton 1968). Again we assume f and $\alpha = 1$, and see that at this distance, the starlight intensity is of the same order as the galactic starlight. Thus if the CN is not circumstellar, the radiation field

of the star used to observe it is of insufficient strength to account for the observed rotational excitation.

In order to have the fluorescent excitation of the star play a dominant role in the rotational excitation of the CN, we need $R_{01} \sim 10^{-5} sec^{-1}$. There are two consequences of an excitation rate this high. First, the flux necessary to yield this high a rate would require the star to be as close as 0.2pc to the CN. This proximity is totally contrary to our present ideas concerning the location of interstellar clouds. A review of our present understanding of their location will be deferred to Chapters 7 and 9, however, the main feature which emerges from this work is that the clouds are not circumstellar, but rather broad layers spanning, in several instances, more than one star. For example, the interstellar CN lines of X Persei and ζ Persei appear to originate in the same interstellar cloud. These clouds appear to have the atoms and the molecules well mixed, and only a moderate radiation field incident upon them (see for example, Herbig 1968a).

Secondly, since we know that all of the f values are small electronic states which lie below the dissociation limit, the sum rule (6.7) implies the existance of at least one electronic state above the ionization limit with an f value approaching unity. If a molecule makes a transition to this state, it will have a certain probability for dissociation. It is difficult to estimate what this probability is, but we believe a value of $\sim 1\%$ to be a conservative guess.

Then, since the f value of the dissociating state is greatest, this state will produce the fluorescence, and the molecules will be destroyed at a

rate $\sim 10^{-7}$ sec^{-1} per CN molecule. (They will be excited at a rate 10^{-5} sec^{-1}, and 1% of these will dissociate.) In order to maintain an equilibrium population of CN, we must have a continuous production rate for these molecules of equal magnitude.

The production of interstellar molecules is unfortunately not well understood (see for example Dieter and Goss 1966), and only with difficulty is it possible to get CH production rates comparable to CH dissociation rates ($\sim 10^{-11}$ sec^{-1} per molecule, for the CH existing in the interstellar radiation field). Assuming similar processes to be responsible for the formation of CN, it would appear, then, hard to understand even the existance of the CN. Hence it appears highly improbable that the observed excitation could be due to the fluorescence.

CHAPTER 7

COLLISIONAL EXCITATION IN H I REGIONS

In this Chapter we summarize briefly those properties of H I and H II regions which are pertinent to the problem at hand, and we review work devoted to the location and environment of the interstellar molecules. We then proceed to consider in some detail the possible rotational excitation mechanisms of the CN if it resides in an H I region of the interstellar medium.

A. Difference Between H I and H II Regions*

Almost 10% of the galactic mass is in gas clouds $\sim$ 4pc in diameter which comprise about 10% of the volume of the galactic plane. These tend to be irregular in concentration and composition, but are composed mainly of atomic hydrogen, (although H_2 may predominate at higher densities). This gas is divided into two distinct types of regions: H I and H II regions (Strömgren, 1939, 1948). H I regions are neutral atomic hydrogen with a kinetic temperature $\sim 125°K$, and hydrogen number density rarely exceeding $10^4 cm^{-3}$ and usually $\sim$ $1cm^{-3}$.

H II regions, on the other hand, are the emission nebulae which surround hot, luminous O and B stars which have sufficient ultraviolet flux to fully ionize the surrounding atomic hydrogen. These regions, then, have a temperature $\sim 10^4 °K$ and density $\sim 10cm^{-3}$. Since O and B stars are com-

---

* For a review of the interstellar medium see Dieter and Goss (1966) and Vol. VII of Stars and Stellar Systems: Nebulae and Interstellar Matter (Middlehurst and Aller, 1968)

paratively uncommon, and stars later than B 0 have only limited H II regions associated with them, H II regions only involve ~ 10% of the mass of the interstellar gas near the galactic plane.

A well known but noteworthy feature of the interstellar medium is that the boundary between the two types of regions is relatively sharp (Strömgren, 1939, 1948). This is due to the fact that the radiant energy density beyond the Lyman limit falls off inversely as the square of the distance from the star, where as the total opacity due to the non-ionized component of the gas increases exponentially with the path length to the star. These two effects, when included in the equations for ionization equilibrium produce a very sharp transition between H I and H II.

B. Earlier Work on the Place of Origin of the Molecular Interstellar Lines

Prior to Adams' work (1943; 1949) Merrill (1942, 1946) had suggested that there might be a difference in the place of origin of the molecular absorption lines and those of Na I and Ca II, known to be interstellar in origin. The latter would presumably originate in the "true interstellar clouds", far from the star against which the lines were observed, while the molecular lines might be produced in circumstellar clouds, and be affected by the stellar radiation field.

To clarify this situation, Adams measured the velocity correlation between the H and K lines of Ca II and the molecular lines. He found that all of the evidence suggested a common origin for molecular and atomic lines in the same clouds, and in the same portions of the same clouds. He showed that the molecular lines, when present, almost invariably correspond to the

strongest components of complex H and K lines Thus there is a close relationship between the Ca II and the molecular lines as regards both position and in most cases, relative intensities as well.

Also contributing to his conclusion were the presence of the same molecular lines with nearly the same intensities in wide double stars and numerous pairs of physically unrelated stars. He also found no evidence that the occurrence of the lines is related to the spectral types of stars which appear to lie nearest the clouds of their origin.

To further support this work, Bates and Spitzer (1951) subsequently showed that Adams' visual estimates of the intensities of the molecular lines yield a correlation with the intensities of the interstellar reddening, the latter is presumably due to the presence of grains. * Taking advantage of the new and more accurate atomic and molecular f values, Herbig (1968a) has recently considered this problem for one particular star ζ Ophiuchi. This was chosen because it has a single well resolved interstellar cloud in front of it He has arrived at a similar conclusion that the place of origin of both the molecular and atomic lines is an interstellar H I cloud. His arguements for this conclusion are as follows:

---

* Bates and Spitzer (1951) also suggest that the stars in the Pleades represent a unique case, in that the CH+ in the spectra of these stars is probably circumstellar.

1. The pattern of Ca II absorption lines in ζ Ophiuchi is repeated in at least seven stars in this direction, many of them well outside the H II region surrounding ζ Ophiuchi. Since this is the only star in the group involved in an H II region, these lines must be formed in a rather extensive foreground layer not associated with these stars

2. A similar arguement applies to H I 21cm emission feature which is not appreciably affected by, and extends well beyond the ζ Ophiuchi H II region. This feature is identified with the same cloud containing the other absorbing molecules.

3. If the Na I lines were formed in an H II region, the increased electron presure would depress the sodium ionization and imply an order of magnitude deficiency in the Na/H ratio. If one assumes an H I region as the origin of the Na I lines, one gets the solar system Na/H and K/H abundance ratios.

4. A comparison of the 109 α and Hα emission lines originating in the H II region shows no turbulent width correlation with any of the interstellar species.

Thus Herbig has concluded that for the case of ζ Ophiuchi at least, which is probably the most important star for our work, the place of origin of the molecular lines is an interstellar H I region.

C. Collisional Mechanisms in H I Regions

We now turn to a consideration of the various collisional excitation mechanisms of the CN, assuming that it does reside in an H I region. Since

the kinetic temperature here is $\sim 125°K$, and particles will have kinetic energies $\sim 4kT/\pi = 229cm^{-1}$, it is clear that we need to consider only direct rotational excitation. Indirect rotational excitation by way of higher electronic and vibrational states can be immediately ruled out on energetic grounds alone, as the thresholds for excitation of these states are $2024cm^{-1}$ and $9114cm^{-1}$ respectively.

D. Excitation by H Atoms

We shall consider first the collisional excitation by neutral hydrogen atoms. We can write for the excitation rate

$$R_{01} = \int v N'_H(v)\, \sigma'_{01}(v)\, dv \approx N_H \bar{v}\, \sigma_{01} = N_H r_{01} \qquad (7.1)$$

where:

N_H is the total H I number density

$\bar{v}$ is the mean atomic velocity

σ_{01} is the total cross section for rotational excitation

The calculation of σ_{01} in terms of molecular parameters is a difficult problem in the theory of atomic collisions. Fortunately, the problem is one which in another guise has been studied from both an experimental and theoretical point of view. This is the problem of microwave pressure broadening (Townes and Schawlow, 1955 p. 338).

Virtually all of the experimental work of this subject has been devoted to an understanding of the interaction between chemically stable systems which can be conveniently studied under laboratory conditions, while H I and CN are both free radicals. The particular short range forces responsible for pressure

broadening, however, do not basically distinguish between free radicals and chemically stable molecules, and it is thus possible to estimate the cross section for CN rotational excitation by H to an accuracy of perhaps 50% by an appeal to the laboratory data of similar molecules.

A rather similar process which has been described in the literature is that of the pressure broadening of the H Cl $J = 0 \rightarrow 1$ rotational line by collisions with He atoms at room temperature (Rank et al. 1963). The resulting cross section for the $J = 0 \rightarrow 1$ rotational excitation has been calculated from the experimental results to be 1.6×10^{-15} cm^2 (Gordon, 1966).

H Cl, like CN, is a highly polar molecule with $\mu_{HCl} = 1.085$D (Bell and Coop, 1938). The bond lengths of the two molecules are also similar - $r_e(HCl) = 1.274$Å versus $r_e(CN) = 1.172$ Å (Herzberg, 1959, Table 39).

Unfortunately the quantum-mechanical description of the collision between a polar molecule and a spherically symmetric atom results in a slowly converging expression for the excitation cross section (Anderson 1949). Since each term scales in a different way with the molecular dipole moment μ, the atomic polarizability α, and the projectile velocity v, there is no precise way in which we can deduce the CN - H or CN - H_2 excitation cross sections from those of H Cl - He. However on the basis of the leading term in the expression,* due to the dipole - induced dipole interaction, we can estimate that an upper limit, at least, for the cross section will scale as $(\alpha\mu^2/v)^{2/5}$.

---

*Actually for CN - H_2 collisions there is a comperable term due to the direct interaction between the CN dipole moment and the H_2 quadrupole moment.

In addition to σ_{01} for HCl - He collisions, Gordon (1966) also gives the corresponding cross sections for OCS - He and OCS - Ar collisions The OCS electric dipole moment is small, and consequently we have not used this molecule as a comparison since interactions other than the dipole induced - dipole type probably are moreimportant. But it is encouraging to note that these data scale according to our prescription.

The polarizability α of the colliding atom may be calculated from the quadratic stark effect of its ground state and has been calculated for both H and He, as well as having been measured for the latter atom (Bethe and Salpeter, 1957). It is found that $\alpha_H/\alpha_{He} = (9/4) / .074 = 30.4$.

The ratio of the velocities of 125°K H atoms to 300°K He atoms is 1.29. Thus we expect a cross section for this process of $\sigma_{01}(H - CN) = \sigma_{01}(He - HCl) \times 4.5 = 7.1 \times 10^{-15} cm^2$

Taking Herbig's (1968a) upper limit of $900 cm^{-3}$ for the neutral hydrogen number density in the cloud containing the CN in front of ζ Ophiuchi, and $\bar{v} = \sqrt{8kT/(\pi m_H)} = 1.6 \times 10^5$ cm/sec for the mean velocity of 125°K hydrogen atoms, we get the excitation rate $R_{01} \approx 1.03 \times 10^{-6}$ sec^{-1} which is smaller than $B_{01} \tilde{u}_{10} = 8.7 \times 10^{-6}$ sec^{-1} by a factor of 8.4. Thus it appears improbable, although not by a large margin, that collisional excitation by hydrogen atoms could account for the observed rotational temperature. At most a small portion of the observed excitation can be attributed to collisions with H atoms *

---

* There also exists the possibility that a fraction of the interstellar hydrogen may be in the form of H_2 molecules The ratio of the polarizabilities of He and H_2 is given by $\alpha_{H_2} / \alpha_{He} = 3.95$ (Margenau, 1939), so we expect a cross section

$$\sigma_{01}(CN - H) / \sigma_{01}(CN - H_2) = 1.97.$$

E. Electron Density

In H I regions, the ultraviolet flux is of insufficient magnitude to ionize the hydrogen gas there, however, there is sufficient radiation to ionize such more loosely bound but considerably less abundant species as C, Mg, Si, and Fe, primarily C. It is generally assumed that the electron density is due to photoionization of these elements (Middlehurst and Aller, 1968). More recently, cosmic rays also have been suggested as a possible source of ionization (Potash, 1968; and Spitzer and Tomasko, 1968).

In H I regions of typical density (1 cm^{-3}) the electron density is thus quite small. For example recent dispersion measurements made with the help of pulsars yield electron densities of order $N_e \approx 2 \times 10^{-2} cm^{-3}$ (Shuter et al, 1968) averaged over hundreds of thousands of parsecs in the galactic plane. However, in the cloud containing the CN in front of ζ Ophiuchi where the density may be as high as 900 atoms/cm^3, the density of these elements and hence the corresponding electron density will be proportionately higher. From a consideration of the expected carbon to hydrogen ratio, Herbig (1968a) has estimated that here it may be as high as $N_e \sim .4 cm^{-3}$.

If either of the optical lines of Na II or Ca I were observed, one could calculate the actual electron density in this cloud from the equations for

---

It thus appears that two H atoms are roughly four times as effective in exciting molecular rotation acting alone, as they are when bound together in a molecule. Thus we have assumed,for the sake of an upper limit, that all of the hydrogen is in the atomic form.

ionization equilibrium Since only Na I and Ca II are seen (due to their difference in ionization potentials), to use the Na I/Ca II ratio one would have to assume the abundance ratio of Na to Ca. However the calcium abundance is often anomalously low, and in the case of the ζ Ophiuchi cloud Herbig points out that this effect is probably exaggerated. The easiest way to measure the electron density here would be to attempt to observe the Ca I resonance line at 4227Å for this star. Herbig has calculated from his upper limit of <3mÅ for the equivalent width of this line that $N_e < 1.9 cm^{-3}$.

It is unfortunate that this line was just off the bottom of the CH+ synthesis described in Chapter 5 of this thesis (this synthesis terminates at 4228Å). Further effort should be made for the detection of this line.

F Cross Sections for Excitation of CN by Electrons

In order to estimate the excitation cross section for 125°K electrons, we must consider the problem quantum mechanically, and will use the Born approximation for this. Because these results are used later when we consider H II regions, we will solve this problem for the general case of a diatomic molecule with both spin and orbital angular momentum, and specialize to the case of a rigid rotor for CN. Although Massey (1932) derived a similar expression earlier, his results appear to be in error by a factor of 2/3, hence, we shall present the calculation here.

The usual condition for the validity of this approximation applied to the excitation of a point dipole is that $2\mu em/\hbar^2 \ll 1$, or $\mu \ll 1.27D$ (Massey, 1932). While we adopt $\mu(CN) = 1.45D$, and $\mu(CH) = 1.46D$, (Table 3.2) it is known,

however, that Massey's condition is often too stringent a restriction on the use of the Born approximation. Altshuler (1957) for example, obtained good agreement with experiment by calculating the diffusion cross section of NH_3 and H_2O in the adiabatic Born approximation, and these molecules have dipole moments (1.468D and 1.94D respectively), as large and larger than CN and CH. Mittleman and von Holdt (1957) have moreover calculated the exact cross section for elastic scattering from a point dipole, and find that even at $\mu = 1.46$D the diffusion cross section is only 60% higher than the result in the Born approximation.

Let us first write the initial and final assymptotic wave functions for the electron - molecule system. Normalizing the electron wave function to a box with edge of length L, we have

$$\Psi_i = L^{-3/2} e^{i\underset{\sim}{k}_i \cdot \underset{\sim}{R}} \psi_{\hat{\Lambda}KSJM}$$
$$\Psi_f = L^{-3/2} e^{i\underset{\sim}{k}_f \cdot \underset{\sim}{R}} \psi_{\hat{\Lambda}K'SJ'M'} \qquad (7.2)$$

where:

$\psi_{\hat{\Lambda}KSJM}$ is the molecular wave function

$\underset{\sim}{R}$ is the electron's position vector

and

$\underset{\sim}{k}_i$ and $\underset{\sim}{k}_f$ are the initial and final electron propogation vectors

The interaction Hamiltonian for a point dipole in the field of an electron is

$$\mathcal{H} = \frac{e\mu \cos \chi}{R^2} \qquad (7.3)$$

where χ is the angle between the molecular axis and $\underset{\sim}{R}$ as shown in Figure 16a

Following Schiff (1955, equation 30.6) we may write the expression for the excitation cross section in first order perturbation theory

$$\frac{2J+1}{2\pi \sin \theta_s} \frac{d\sigma}{d\theta_s} = \frac{k_f}{k_i} \left(\frac{m}{2\pi \hbar^2} \right)^2 L^6 \sum_{M_i M_f} |\mathcal{H}'_{if}|^2 \qquad (7.4)$$

where θ_s is the scattering angle of the electron, and we take the z axis to be in the direction of $\delta\underset{\sim}{k} = \underset{\sim}{k}_i - \underset{\sim}{k}_f$ as shown in Figure 16b. Then the matrix element in (7.4) may be expressed simply as

$$\mathcal{H}'_{if} = \frac{1}{L^3} \int e^{i\delta\underset{\sim}{k}\cdot\underset{\sim}{R}} \langle \psi_{\Lambda \hat{K} SJM} \left| \frac{e\mu \cos\chi}{R^2} \right| \psi_{\Lambda \hat{K}'SJ'M} \rangle \, R^2 \sin\Theta \, d\Theta d\Phi \tag{7.5}$$

$$= \frac{e\mu}{L^3} \int e^{i\delta kR\cos\Theta} \sin\Theta \langle \psi_{\Lambda \hat{K} SJM} \left| \cos\chi \right| \psi_{\Lambda \hat{K} SJ'M} \rangle dR d\Theta d\Phi$$

with all other terms defined in the Figure. Note also that $(\delta k)^2 = k_1^2 + k_f^2 - 2k_i k_f \cos\theta_s$. We can now expand $\cos\chi$ in terms of spherical harmonics:

$$\cos\chi = \frac{4\pi}{3} \sum_{\mu=-1}^{1} (-1)^{\mu} Y_{1\mu}(\theta\phi) \, Y_{1-\mu}(\Theta\Phi) \tag{7.6}$$

Since Φ appears nowhere else in (7.5) the only term which will contribute to this sum is the one with $\mu = 0$. Hence we have for the matrix element, using the Wigner-Eckart theorm (Edmonds, 1968, equation 5.4.1),

$$\mathcal{H}'_{if} = \frac{2\pi e\mu}{L^3} \sqrt{4\pi/3} \int_0^{\infty} \int_0^{\pi} e^{i\delta kR\cos\Theta} \sin\Theta \cos\Theta \, d\Theta dR$$

$$\cdot \langle \Lambda \hat{K} SJM \left| Y_{10} \right| \Lambda \hat{K}' SJ'M' \rangle \tag{7.7}$$

$$= (-1)^{J-M} \frac{4\pi e\mu i}{L^3 \delta R} \begin{pmatrix} J & 1 & J' \\ -M & 0 & M' \end{pmatrix} \langle \Lambda \hat{K} SJ \| \underset{\approx}{C}(1) \| \Lambda \hat{K}'SJ' \rangle$$

Using Edmonds (3.7.8) and integrating, equation (7.4) then reduces to

$$\sigma_{\hat{K}J,\hat{K}'J'} = \frac{8\pi m^2 e^2 \mu^2}{3(2J+1)\hbar^4} \left| \langle \Lambda \hat{K} SJ \| \underset{\approx}{C}(1) \| \Lambda \hat{K}'SJ' \rangle \right|^2 \frac{k_f}{k_1} \int_0^{\pi} \frac{\sin\theta_s \, d\theta_s}{k_1^2 + k_f^2 - 2k_1 k_f \cos\theta_s} \tag{7.8}$$

$$= \frac{8\pi m^2 e^2 \mu^2}{3(2J+1)\hbar^4} \left| \Lambda \hat{K} SJ \| \underset{\approx}{C}(1) \| \Lambda \hat{K}'SJ \rangle \right|^2 \cdot \frac{1}{k_1^2} \ln \left| \frac{k_1 + k_f}{k_1 - k_f} \right|$$

The evaluation of the reduced molecular matrix element is carried out in Appendix 2, hence for a diatomic molecule, such as CH, intermediate between Hund's cases (a) and (b)

$$r_{\hat{KJ},\hat{K'J'}} = v\sigma_{\hat{KJ},\hat{K'J'}} = \frac{8\pi\mu^2e^2}{3\hbar^2v} \ln\left|\frac{k_i+k_f}{k_i-k_f}\right| (2J'+1)$$
$$\cdot\left[\sum_{K'K} U_{\hat{K'K'}} U^*_{\hat{KK}} (2K'+1)^{1/2}(2K+1)^{1/2} \begin{Bmatrix} K' & J' & S \\ J & K & 1 \end{Bmatrix} \begin{pmatrix} K & 1 & K' \\ -\Lambda & 0 & \Lambda \end{pmatrix}\right]^2 \quad (7.9)$$

where $k_i = mv/\hbar$, and $k_f^2 = k_i^2 - 2m\omega_{\hat{KJ},\hat{K'J'}}/\hbar$. When specialized to the linear rotor (7.9) yields

$$r_{JJ'} = \frac{8\pi\mu^2e^2}{3\hbar^2v} \ln\left|\frac{k_i+k_f}{k_i-k_f}\right| (2J'+1) \begin{pmatrix} J & 1 & J' \\ 0 & 0 & 0 \end{pmatrix} \quad (7.10)$$

which is a factor 2/3 smaller than Massey's (1932) result.

Using the approximation that

$$(k_i + k_f) / (k_i - k_f) \approx 2mv^2/\hbar\omega_{ij} \quad (7.11)$$

we can average the cross sections over the Maxwell-Boltzmann *velocity* distribution. Thus for a molecule such as CH

$$\langle r_{\hat{KJ},\hat{K'J'}} \rangle = \frac{32\mu^2e^2}{3\hbar^2\bar{v}(2J+1)} \left[\ln\left|\frac{\pi m\bar{v}^2}{2\hbar\omega_{\hat{K'J'},\hat{KJ}}}\right| - \gamma\right]$$
$$\cdot\left[\sum_{K'K} U_{\hat{K'K'}} U^*_{\hat{KK}} (2K'+1)^{1/2}(2K+1)^{1/2} \begin{Bmatrix} K' & J' & S \\ J & K & 1 \end{Bmatrix} \begin{pmatrix} K & 1 & K' \\ -\Lambda & 0 & \Lambda \end{pmatrix}\right]^2 \quad (7.12)$$

and for the rigid rotor

$$\langle r_{JJ'} \rangle = \frac{32\mu^2e^2}{3\hbar^2\bar{v}} \left[\ln\left|\frac{\pi m\bar{v}^2}{2\hbar\omega_{\hat{K'J'},\hat{KJ}}}\right| - \gamma\right] \quad (7.13)$$

where $\gamma = 0.577$ (Euler's constant)

and $\bar{v} = \sqrt{8kT/\pi m}$

The use of the approximation (7.11) results in an error of less than one percent in the average rate, and we neglect the slight difference between the electron mass and the reduced electron mass.

G. Excitation Rate from Electrons

Application of equation (7.13) for Herbig's (1968a) estimate of $N_e \sim .4 cm^{-3}$ yields the excitation rate $R_{01} \approx 5.6 \times 10^{-7} sec^{-1}$, which is 15 times lower than $B_{01}\tilde{u}_{10}$. On the other hand it is only 3.3 times smaller if we use Herbig's upper limit of $N_e < 1.9\ cm^{-3}$. Thus it appears improbable although again not by a large margin that slow electrons could provide sufficient excitation to account for the observed rotational excitation of CN. It also appears that for a normal C/H abundance ratio, electrons are approximately as effective as H atoms in exciting molecular rotation.

Since the Born approximation satisfies electric-dipole selection rules, the rate equations may be solved by an equivalent increase of radiative intensity at the corresponding wavelength (this proceedure was described in Chapter 2).

The increase in temperature due to excitation by slow electrons is given in Figure 17 as a function of electron density and observed temperature, and for H I atoms assuming that the CN - H interaction predominantly obeys electric-dipole selection rules. For Herbig's estimate of $N_e = .4 cm^{-3}$, the correction to T_{10} and T_{21} due to electron excitation is 0.14°K and 0.12°K respectively, just comparable with the statistical error of the temperature measurement.

If the electron density is as high as Herbig's upper limit $N_e < 1.9 cm^{-3}$, the corrections are still less than 0.75°K and 0.77° K, with the result that the major part of the excitation must be due to some other process. Further study of λ 4227Å of Ca I should allow the upper limit to be considerably depressed.

H. Comparison of T_{21} with T_{10} to Determine Electron Density

Since collisional excitation is a nonthermal process, the resulting distribution of level populations will not be thermal. In principle, this departure from thermal distribution can be measured and additional information about the collisional mechanism obtained.

The expected T_{21} for excitation by a mixture of microwave background and 125° K electrons has been plotted in Figure 18 as a function of electron or H I density and observed T_{10}. It can be seen that the departure from thermal equilibrium of the J = 2 level population is too small to be measured with the present precision of T_{21} measurement; the temperature differences are at most ≈ 0.1°K for reasonable electron densities, comparable to the statistical errors involved. Thus with the present observational accuracy, a partial contribution from electrons or H atoms cannot be ruled out

I. Excitation by Ions

In the next Chapter, we will describe a numerical calculation of the cross section for rotational excitation by particles with the mass of a proton or greater. Figure 19 shows the results of this method applied to the cross section for excitation of the CN J = 0 → 1 transition. In this curve the abcissa is in units of the most probable velocity of 10^4°K protons. For an H I region the excitation will be primarily due to C II ions at 125°K, hence the most probable velocity of these will be down by a factor 1/31.

It can be seen that the cross section is falling off very rapidly with velocity, and at the most probable velocity of the ions, it will be at least two orders of magnitude below the value at the most probable velocity of 10^4°K protons.

In the next Chapter it will be shown that a number density of approximately 1.37 protons/cm^3 at 10^4°K is sufficient to provide 3°K excitation of the CN. Assuming charge neutrality in the H I region the ion density will be the same as the electron density ($\approx$. 4e/cm^3). Thus the excitation rate here will be smaller by a factor of approximately 10^4, and will clearly be negligible.

J. Discussion

It is thus seen that if the CN resides in an H I region typical of the major interstellar cloud in front of ζ Ophiuchi, its excitation probably provides a good measure of the background radiation at 2.64mm. No other excitation mechanisms appear to be of sufficient strength to provide this excitation, although the margin for e^- and H excitation in the case of ζ Ophiuchi is not as high as one might like. There is good evidence that the CN does in fact reside in an H I region, as we discussed earlier in this Chapter. Further discussion of this point will follow in Chapter 9 after we consider the alternative possibility of the CN residing in an H II region.

CHAPTER 8

COLLISIONAL EXCITATION IN H II REGIONS

In H II regions virtually all of the collisions experienced by a molecule will be with charged particles. We will now show that, as a result of the long range of the Coulomb force, the excitation cross section is sufficiently large that all of the observed CN excitation could be produced in an H II region of reasonable ($\sim 1 cm^{-3}$) density.

Our analysis of Chapter 2 showed that even though the CN may not yield reliable temperature measurements, in this case it will set a reliable upper limit to it. In addition we will now show that if protons are the sole exciting agent for the interstellar CN, the resulting rotational temperature will be a sensitive function of the density of exciting protons. Since the interstellar medium is a highly inhomogeneous place with respect to density, the observed invariance of the rotational temperature against eleven stars (see Chapter 9) speaks strongly against the suggestion that the excitation is collisional.

We will calculate here the CN J = 1 and, J = 2 and the CH KJ = 1 3/2 level populations which result if the CN J = 1 population is due solely to excitation by 10^4 K protons. Following Chapter 7, we are interested to see if the present observational upper-limits on these levels might be useful in shedding further light on the CN excitation mechanism. Hence our calculations will be for the most complicated case of interest, a diatomic molecule, such as CH, with both spin and orbital angular momentum which lies intermediate between the Hund's case (a) and (b) coupling schemes. We can easily specialize this to the simpler coupling scheme of CN.

A. Semi Classical Approximation

Our calculation of the excitation of molecular rotation will treat the projectile trajectory classically. Such a proceedure is usually valid in scattering theory when the impact parameter b is large with respect to the projectile de Broglie wavelength $\lambda = \hbar/Mv$ (here M and v are the projectile mass a velocity relative to the scattering center). For $v \approx 10^6$ cm/sec, the maximum excitation of CN and CH occurs when $b \approx 50$Å, so this condition is well satisfied. In addition, since the projectile energy is $\sim$ 1ev, while the lower energy level separations of CN and CH are $\sim 10^{-2}$ to 10^{-3} ev, the energy loss of the projectile will be small. Hence its deflection will also be small, and we may assume it to follow a classical straight line trajectory.

The transition rate $R_{JJ'}$ for a density of N_p incident projectile ($N'_p(v)$ at velocity v) is given by

$$R_{JJ'} = N_p r_{JJ'} = \int_o^\infty v\sigma_{JJ'}(v)\, N'_p(v)\, dv \qquad (8.1)$$

where v is the relative velocity of the molecule and the projectiles, and $\sigma_{JJ'}(v)$ is the (velocity dependent) cross section for excitation of a molecule initally in level J to level J'. The cross section is found by summing the transition probability $P_{JM,J'M'}$ over all initial and final states, integrating over impact parameter, and dividing by the statistical weight of the initial level. Written in the differential form this is

$$\frac{2J+1}{2\pi b}\,\frac{d\sigma_{JJ'}}{db} = \sum_{M'M} P_{JM,J'M'}. \qquad (8.2)$$

The dynamical variables of the molecule, on the other hand, must

be treated quantum mechanically. The molecular state vector during the encounter with the projectile is described by Schrodinger's equation in the form (see for example Schiff 1955, p. 196).

$$i\hbar \frac{da_i}{dt} = \sum_j a_j \mathcal{H}'_{ij}(t)\, e^{i\omega_{ij} t} \tag{8.3}$$

Even with the simplifying assumptions already made, no analytic solution exists for these coupled differential equations for arbitrary values of v, b and the molecular constants B or μ. We must therefore solve these equations numerically, and use a Runge Kutta scheme to do this (see below). First the requisite matrix elements of the interaction Hamiltonian $\mathcal{H}'(t)$ must be calculated. The excitation cross sections may then be found numerically, and averaged over the velocity distribution of the 10^4°K protons typical of an H II region. Since the computer time required for the Runge Kutta integration is large, for a check of the resulting rates at other temperatures we use a hybrid of first-order perturbation theory and the quantum mechanical sudden approximation. This has yielded the same cross sections to an accuracy of $\sim$ 1% near 10^4°K (Thaddeus and Clauser, to be published).

B. Matrix Elements of Interaction Hamiltonian

The matrix elements of the Hamiltonian are taken to be those of the interaction of a point charge with a point dipole. Following equations (7.3) and (7.6) we take the operator to be given by

$$\mathcal{H}'(t) = \frac{4\pi\mu e}{3R^2} \sum_{\mu=-1}^{1} (-1)^{\mu}\, Y_{1\mu}(\theta\phi)\, Y_{1\mu}(\Theta, \bar{\Phi}) \tag{8.4}$$

where R, Θ, and Φ describe the time dependent spherical polar coordinates of the position of the projectile in the laboratory frame with origin at the molecular center of mass, and θ and ϕ represent the spherical polar coordinates specifying the molecular orientation in the laboratory frame.

For a classical straight line trajectory of a projectile with impact parameter b and relative velocity v, the $Y_{1\mu}(\Theta(t), \Phi(t))$ may be written for the coordinate scheme shown in Figure 20, as

$$Y_{1\pm1}(t) = \mp (3/8\pi)^{1/2} \frac{vt}{(v^2t^2 + b^2)^{1/2}}, \quad Y_{10}(t) = (3/4\pi)^{1/2} \frac{b}{(v^2t^2 + b^2)^{1/2}} \tag{8.5}$$

Hence the matrix elements of the Hamiltonian (8.4) may be written

$$\langle \Lambda \hat{K} SJM \,|\, \mathcal{H}'(t) \,|\, \Lambda \hat{K}' SJ' M' \rangle = (4\pi/3)^{1/2} \frac{\mu e}{R^2(t)} \cdot \sum_{\mu=-1}^{1} (-1)^{\mu} Y_{1\mu}(t) \langle \Lambda \hat{K} SJM | \, C_{1-\mu}(\theta, \phi) | \, \Lambda \hat{K}' SJ' M' \rangle \tag{8.6}$$

The $C_{1-\mu}$ are the components of a tensor operator, so we can apply the Wigner-Eckart theorem (Edmonds 1968, equation 5.4.1.) to factor off the M', M dependence. Thus

$$\langle \Lambda \hat{K} SJM | \mathcal{H}'(t) | \Lambda \hat{K}' SJ' M' \rangle = (4\pi/3)^{1/2} \frac{\mu e}{R^2(t)} \cdot \langle \Lambda \hat{K} SJ \,\|\, \underset{\approx}{C}(1) \,\|\, \Lambda \hat{K}' SJ' \rangle \sum_{\mu=-1}^{1} Y_{1\mu}(t) (-1)^{J-M+\mu} \begin{pmatrix} J & 1 & J' \\ -M & -\mu & M' \end{pmatrix} \tag{8.7}$$

The reduced matrix element in (8.7) has been evaluated in Appendix 2 so that the matrix elements of $\mathcal{H}'$ may be written

$$\langle \Lambda \hat{K} SJM \mid \mathcal{H}'(t) \mid \Lambda \hat{K}' SJ' M' \rangle = (4\pi/3)^{1/2} (-1)^{\Lambda+S+J+J-M+1} (2J'+1)^{1/2} (2J+1)^{1/2}$$

$$\cdot \left[\frac{\mu e}{R^2(t)} \sum_{\mu=-1}^{1} (-1)^{\mu} Y_{1\mu}(t) \begin{pmatrix} J & 1 & J' \\ -M & -\mu & M' \end{pmatrix} \right] \tag{8.8}$$

$$\cdot \sum_{K' K} U_{\hat{K}' K} U^{*}_{\hat{K} K} (2K'+1)^{1/2} (2K+1)^{1/2} \begin{Bmatrix} K & J' & S \\ J & K & 1 \end{Bmatrix} \begin{pmatrix} K & 1 & K' \\ -\Lambda & 0 & \Lambda \end{pmatrix}$$

Letting $\Lambda = S = 0$, $K' = J'$, $K = J$, and using Edmonds (1968) equation 6. 3. 2), we obtain the matrix elements for the linear rotor:

$$\langle JM \mid \mathcal{H}'(t) \mid J' M \rangle (4\pi/3)^{1/2} (-1)^{M} (2J'+1)^{1/2} (2J+1)^{1/2} \tag{8.9}$$

$$\cdot \begin{pmatrix} J & 1 & J \\ 0 & 0 & 0 \end{pmatrix} \frac{\mu e}{R^2(t)} \sum_{\mu=-1}^{1} (-1)^{\mu} Y_{1\mu} \begin{pmatrix} J & 1 & J' \\ -M & -\mu & M' \end{pmatrix}$$

C. First Order Perturbation Theory

The differential cross section of equation (8. 2) for a molecule such as CH has been calculated using first order perturbation theory* to be (Thaddues and Clauser, to be published)

$$\frac{dr_{\hat{K}J,\, K'J'}}{db} = v \frac{d\sigma_{\hat{K}J,\hat{K}'J'}}{db} = \frac{8\pi\mu^2 e^2 \omega^2_{\hat{K}'J',\hat{K}J}}{3\hbar^2 v^3} (2J+1)$$

$$\cdot \left[\sum_{K' K} U_{\hat{K}' K'} U^{*}_{\hat{K} K} (2K'+1)^{1/2} (2K+1)^{1/2} \begin{Bmatrix} K' & J' & S \\ J & K & 1 \end{Bmatrix} \begin{pmatrix} K & 1 & K' \\ -\Lambda & 0 & \Lambda \end{pmatrix} \right]^2 \tag{8.10}$$

$$\cdot \left[K_0^2 \left(\frac{\omega_{\hat{K}'J',\hat{K}J} b}{v} \right) + K_1^2 \left(\frac{\omega_{\hat{K}'J',\hat{K}J} b}{v} \right) \right] b$$

*It should be noted that first order perturbation theory is in all respects equivalent to analyzing the pulse associated with the passage of the projectile into virtual quanta.

where K_0 and K_1 are modified Bessel functions. The transition probability for this process obeys the usual symmetric-top selection rules for electric dipole transitions. To apply equation (8. 10) to the simple rotor we again let $\Lambda = S = 0$, $K' = J'$, and $K = J$, and use Edmonds (1968 equation 5. 3. 2) to evaluate the 6j symbol,

$$\frac{dr_{JJ'}}{db} = v\frac{d\sigma_{JJ'}}{db} = \frac{8\pi\mu^2 e^2 \omega_{J'J}^2}{3\hbar^2 v^3}(2J+1)\begin{pmatrix} J & 1 & J' \\ 0 & 0 & 0 \end{pmatrix}^2 \cdot\left[K_0^2\left(\frac{\omega_{J'J}b}{v}\right) + K_1^2\left(\frac{\omega_{J'J}b}{v}\right)\right]b \tag{8.11}$$

Again, the 3j symbol leads to the selection rule $\Delta J = \pm 1$ for the linear rotor.

Figure 21 shows the application of equation (8. 11) to the $J = 0 \rightarrow 1$ transition of CN, and Figure 22 shows the application of equation *(8. 12) to the $KJ = 1\ 1/2 \rightarrow 1\ 3/2$ transition of CH. In both cases a logarithmic divergence of the cross section results at small impact parameters.

D. Quantum Mechanical Sudden Approximation

The integrated cross section has been calculated for the collision of a proton with a molecule such as CH using the quantum mechanical sudden approximation, and the result is

$$r_{\hat{KJ},\ \hat{K'J}} = \sigma_{\hat{KJ},\hat{K'J'}} = \frac{\pi^2\hbar v^2}{2\mu e}(2J'+1)\sum_L (2L+1)\int_0^\infty J^2_{L+1/2}\frac{2\mu e}{\hbar bv}\,b^2 db \cdot\left[\sum_{K'K\ K'K'\ KK} U_{\hat{\ }}\ U^*_{\hat{\ }}\ (2K'+1)^{1/2}(2K+1)^{1/2}\begin{Bmatrix} K' & J' & S \\ J & K & L \end{Bmatrix}\begin{pmatrix} K & L & K' \\ -\Lambda & 0 & \Lambda \end{pmatrix}\right]^2 \tag{8.12}$$

The integral over impact parameter in equation (8.12) (Gröbner and Hofreiter 1958, p. 202) converges for $L > 1$. If K and K' are such that the second line of (8.12) vanishes for $L \leq 1$, we can write

$$r_{\hat{K}J,\,\hat{K}'J'} = \frac{8\pi\mu^2 e^2}{3\hbar^2 v}(2J'+1)\sum_L \frac{2L+1}{(L-1)L(L+1)(L+2)} \cdot \left[\sum_{K'K} U_{\hat{K}'K}\, U^*_{\hat{K}K}\,(2K'+1)^{1/2}(2K+1)\begin{Bmatrix} K' & J' & S \\ J & K & L \end{Bmatrix}\begin{pmatrix} K & L & K' \\ -\Lambda & 0 & \Lambda \end{pmatrix}\right]^2 \tag{8.13}$$

For this case, letting $\Lambda = S = 0$, $K' = J'$, $K = J$ we obtain the excitation rate for the simple rotor

$$r_{JJ'} = \frac{8\pi\mu^2 e^2}{3\hbar^2 v}(2J'+1)\sum_L \frac{(2L+1)}{(L-1)L(L+1)(L+2)}\begin{pmatrix} J & L & J' \\ 0 & 0 & 0 \end{pmatrix}^2 \tag{8.14}$$

On the other hand, if the second line of (8.12) does not vanish for $L \leq 1$, the rate diverges at large b, and we cannot evaluate the integral in (8.12) from $b = 0$ to ∞ we use the latter approximation.

Using (8.14) the sum of the many-quanta transition rates from a given level to all other levels can be calculated exactly. For excitation of a rigid rotor from the ground state to a level with $J \geq 2$ (8.14) yields

$$r_{0J} = \frac{8\pi\mu^2 e^2}{3\hbar^2 v}\frac{(2J+1)}{(J-1)\,J\,(J+1)(J+2)} \tag{8.15}$$

and by means of partial fractions we may write

$$\sum_{J=2}^{\infty} r_{0J} = \frac{8\pi\mu^2 e^2}{3\hbar^2 v} \cdot 1/2 \sum_{J,=2}^{\infty}\left(\frac{1}{J-1} - \frac{1}{J} - \frac{1}{J+1} + \frac{1}{J+2}\right) \tag{8.16}$$

The series terminates and is easily evaluated:

$$\sum_{J=2}^{\infty} r_{0J} = \frac{8\pi\mu^2 e^2}{3\hbar^2 v} \cdot \frac{1}{3} \tag{8.17}$$

In the same way it is found that

$$\sum_{J=3}^{\infty} r_{1J} = \frac{8\pi\mu^2 e^2}{3\hbar^2 v} \cdot \frac{9}{40} \tag{8.18}$$

and

$$\sum_{J=4}^{\infty} r_{2J} = \frac{8\pi\mu^2 e^2}{3\hbar^2 v} \cdot \frac{4}{21} \tag{8.19}$$

Finally, the simple $1/v$ velocity dependence of the excitation rate in the sudden approximation allows the Maxwell-Boltzmann velocity average to be done analytically. The average rates $\langle r_{KJ,K'J'} \rangle$ and $\langle r_{J\,J'} \rangle$ are given by equations (8.13) and (8.14) with the factor $8\pi\mu^2 e^2 / 3\hbar^2 v$ replaced by

$$\frac{32\mu^2 e^2}{3\hbar^2 v} \tag{8.20}$$

where the average reduced projectile velocity

$$\bar{v} = (8kT/\pi m^*)^{1/2} \tag{8.21}$$

and m^* is the reduced projectile mass, and T is the kinetic temperature of the projectiles (temperature of the H II region).

Figures 21 and 22 show the differential cross section in the sudden approximation, the derivative of equation (8.12) evaluated for the specific case of excitation from the CN and CH ground states. The divergence of the sudden approximation for $\Delta J = \pm 1$ transitions ($L \leq 1$) at large impact parameters is evident, but the finite value of the many-quanta cross sections, as revealed in

equations (8. 13) and (8. 14), is also illustrated for the $J = 0 \rightarrow 2$ CN transitions.

E. Numerical Solution of Schrodinger's Equation

The descrete points shown in Figures 21 and 22 result from a numerical integration of Schrodinger's equation (8. 3), and at least to the accuracy inherent in the numerical analysis, they represent an exact solution of the excitation problem.

The amplitude of the state vector in equation (8. 3) is first separated into real and imaginary parts,

$$a_j(w) = p_j(w) + iq_j(w) \tag{8. 22}$$

and a change in independent variables is made (Winther and de Boer 1965):

$$\sinh w = vt/b \tag{8. 23}$$

Since the matrix elements of the Coulomb interaction, given by equations (8. 8) or (8. 9) are real, Schrodinger's equation can then be written as an infinite system of first order coupled differential equations in the real variable w,

$$\frac{dq_j(w)}{dw} = b\frac{\cosh w}{\hbar v} \sum_i \langle j | \mathcal{H}(w) | i \rangle \left[q_i(w) \sin \frac{\omega_{ji} b \sinh w}{v} - p_i(w) \cos \frac{\omega_{ji} b \sinh w}{v} \right] \tag{8. 24}$$

$$\frac{dp_j(w)}{dw} = b\frac{\cosh w}{\hbar v} \sum_i \langle j | \mathcal{H}'(w) | i \rangle \left[q_i(w) \cos \frac{\omega_{ji} b \sinh w}{v} + p_i(w) \sin \frac{\omega_{ji} b \sinh w}{v} \right]$$

Here j and i denote the set of quantum numbers $\Lambda K'SJ'M$ and $\Lambda KSJM$, respectively (or $J'M'$ and JM for the simple rotor), and the initial conditions are prescribed at $a_j(-\infty)$ while the transition probability is calculated from $a_j(+\infty)$.

In practice, the infinite set of equations (8. 24) are truncated at some rotational level of the molecule, such that the inclusion of higher levels has a

negligible result on the transition probability of interest. In addition, the integration is confined to a finite range, $-w_0 \leq w \leq w_0$. The resulting finite set of 2N real first order differential equations is then solved over a finite integration range by the Runge-Kutta method, subject only to the initial condition $q_i(-w_0) = 0$ and $p_i(-w_0) = \delta_{ik}$, or $q_i(-w_0) = \delta_{ik}$ and $p_i(-w_0) = 0$, for all i (i. e., the molecule is in a definite state k prior to the collision). The transition probability due to the collision is then

$$P_{kj} = p_j^2(w_0) + q_j^2(w_0) \tag{8.25}$$

The specific numerical prediction scheme was a generalization of Hildebrand's (1956, p. 236) equations(6. 16 7) through (6. 16 10) to the solution of 2N simultaneous differential equations. Writing equations (8. 24) in the form

$$\frac{dp_j}{dw} = F_j(p_i, q_i, w) \text{ and } \frac{dq_j}{dw} = G_j(p_i, q_i, w) \tag{8 26}$$

and defining

$$a_{jn} = p_{jn} + iq_{jn} = p_j(w_n) + iq_j(w_n) \tag{8. 27}$$

then the equations for the $a_{j,n+1}$ in terms of the a_{jn} are the following:

$$p_{j,n+1} = p_{jn} + 1/6\,(k_{1jn} + 2k_{2jn} + 2k_{3jn} + k_{4jn})$$

and

$$q_{j,n+1} = q_{jn} + 1/6\,(m_{1jn} + 2m_{2jn} + 2m_{3jn} + m_{4jn}) \tag{8. 28}$$

where

$$k_{1jn} = \delta w\, F_j(p_{in}, q_{in}, w_n)$$

$$k_{2jn} = \delta w\, F_j(p_{in} + k_{1in}/2,\ q_{in} + m_{1in}/2,\ w_n + h/2)$$

$$k_{3jn} = \delta w\, F_j(p_{in}+k_{2in}/2,\ q_{in}+m_{2in}/2,\ w_n+h/2)$$

$$k_{4jn} = \delta w\, F_j(p_{in}+k_{3in},\ q_{in}+m_{3in},\ w_n+h)$$

and

$$m_{1jn} = \delta w\, G_j(p_{in},\ q_{in}, w_n)$$

$$m_{2jn} = \delta w\, G_j(p_{in}+k_{1in}/2,\ q_{in}+m_{1in}/2,\ w_n+h/2)$$

$$m_{3jn} = \delta w\, G_j(p_{in}+k_{2in}/2,\ q_{in}+m_{2in}/2,\ w_n+h/2)$$

$$m_{4jn} = \delta w\, G_j(p_{in}+k_{3in},\ q_{in}+m_{3in},\ w_n+h)$$

and

δw = the increment in w

To calculate the cross section of excitation rate for a given initial level via equations (8. 1) and (8. 2), the Runge-Kutta integration must be repeated starting from each state of the level in turn, unless it is possible to exploit the symmetry of the interaction For the simple rotor, for example, the rates are symmectrical with respect to $\pm$ M.

For CH, where only excitation from the ground state is important, the Runge-Kutta calculation included the interaction between all the states of the lowest seven rotation-fine structure levels of the molecule, while for CN, where excitation from the three lowest levels is of interest, the lowest ten rotational levels were included in the calculation. The integration over w was confined to the range $-4 \leq w \leq 4$, and the increment δw in the Runge-Kutta scheme was adjusted in the range 0. 005 to 0. 1, depending on b, to provide the desired convergence of the solution. Adequate convergence was furthur demonstrated by varying the number of levels, and w_0, and by comparing the solution with the sudden approximation and first order perturbation theory in the appropriate

limiting cases. Using this scheme each of the points shown in Figures 21 and 22 required approximately one minute of computation on an IBM 360/75 computer.

Figure 21 shows for CN how the solution calculated from first order perturbation theory converges for large impact parameters to the numerical solution and for small impact parameters how the sudden approximation converges to the numerical solution. From a consideration of the orders of magnitude involved (Thaddeus and Clauser, to be published) it might be expected that the hybrid technique would yield accurate results when applied to CN,but be of only marginal value for CH. This contention is in fact born out as can be seen by comparing Figures 21 and 22.

Figure 21 also shows, specifically for the $J = 0 \rightarrow 2$ transition of CN how well the sudden approximation alone is able to describe many-quanta transitions. Comparable close agreement between the exact and sudden approximation solutions is obtained for the $J = 0 \rightarrow 3$ and higher many-quanta CN transitions not shown in the Figure.

F. Numerical Results

We now turn to the excitation of interstellar CN and CH, and specifically calculate (a) the number density of protons and electrons necessary to provide the observed 3°K excitation temperature of the J = 1 CN level, and the temperature of the J = 2 and J = 3 levels which then results, and (b) the excitation temperature of the KJ = 1 3/2 state of CH which this particle density produces. Charge neutrality and a common kinetic temperature for protons and electrons are assumed, and it is supposed that CN and CH are well mixed together, and thus subject to the same density of charged particles.

a) CN

Since for this molecule the population of several levels is appreciable, we are obliged to solve the rate equations (2.14) which reduce to

$$\frac{dn_J}{dt} = 0 = -n_J \left(N_p \sum_{J'=0}^{\infty} R_{JJ'} + A_{J,J-1}\right) + n_{J+1} A_{J+1,J} + N_p \sum_{J=0}^{\infty} n_{J'} R_{J'J} \qquad (8.29)$$

where n_j is the population of level J, N_p is the proton (or electron) number density, and $R_{JJ'}$ is now the sum of the electron and proton collision rates. These equations are to be solved for N_p, n_2 and n_3 under the condition $n_1/n_0 = 3 \exp(-2hB/kT_B)$, $B = 5.7 \times 10^{10} \text{sec}^{-1}$, $T_B = 3°K$, and the normalization condition $\sum_{J=0} n_J = 1$. That is, we assume that when levels with $J > 3$ are collisionally excited they immediately relax radiatively to the J = 3 level, and that the population of these higher levels is effectively zero. In view of the rapid increase of the spontaneous emission probability with J this approximation pro-

duces a negligible error in the final results. The rate for many-quanta transitions from the levels $J = 0, 1, 2$ to higher levels is thus simply added on to the transition rate to the $J = 3$ level. The last column of the rate matrix in equation (8.29) is thus

$$R_{J\,3} = \langle r^{(e)}_{J\,3} \rangle + \sum_{J'=3}^{\infty} \langle r^{(p)}_{J\,J'} \rangle \tag{8.30}$$

for $J = 0, 1, 2$, where (e) denotes electrons, and (p) protons.

The electron rates were already calculated in Chapter 7 using the Born approximation. The summation does not extend over the electron rate since only $\Delta J = \pm 1$ transitions are permitted in the first Born approximation. Note that $\langle r^{(e)}_{JJ'} \rangle$ and $\langle r^{(p)}_{JJ'} \rangle$ satisfy the principle of detailed balance, but for terms which involve the $J' = 3$ column, $R_{JJ'}$ does not.

The proton contribution to the rate matrix is found by two techniques. In the first, or approximate, method the many-quanta rates are calculated from the sudden approximation, employing equations (8.14), (8.17), (8.18) and (8.19), since the integral over velocity as given by (8.20) is expressed in closed form. These terms are listed in Table 5 for an H II temperature of 10^4°K.

For the $\Delta J = \pm 1$ $(L \leq 1)$ approximate rates we employ the hybrid solution described in the section on the sudden approximation. Fine intervals for both the integrations over b ($\delta b = 1$Å) and v ($\delta v = 0.1 v_m = 0.1(2kT/m^*_p)$ were used where v_m is the most probable proton velocity), and no appreciable error is introduced by the numerical integration. The approximate single-quanta rates for CN, were calculated in this way for H II temperatures from 5000° to 15,000°K, at 1000° intervals; the rates for 10,000°are listed in Table 5.

In the second, or exact, method both the single and many-quanta transition rates were calculated by means of the numerical integration of Schrödinger's equation. Since the calculation of dr/db at a given value of b and v requires a substantial amount of computer time by this technique (at least one minute), an economical scheme for the double integration must be employed. Simpson's rule was used for the integration over b, with interval δb ranging from 2Å to 10Å. The second integration over the velocity distribution was then done by a four point quadrature scheme -- a modification of Gauss-Hermite quadrature to deal with integration over the domain 0 to ∞. Since in terms of v_m the average over the velocity distrbution is

$$\langle r_{J\,J'} \rangle = 4\pi^{-1/2}\, v_m^{-3} \int_0^{\infty} \exp(-v^2/v_m^2)\, r_{J\,J'}(v) v^2 dv \qquad (8.31)$$

an n point quadrature scheme will exactly integrate the first $2n - 1 = 7$ terms in a power series expansion of $r_{JJ'}(v)\, v^2$ in terms of v. In the sudden approximation $r_{JJ'}(v)\, v^2$ is exactly proportional to v, thus high accuracy might be expected with a small number of quadrature divisions. The divisions of v/v_m and corresponding weights used here are those calculated by Huang and Giddens (1968). The adequacy of only four points in this integration can be demonstrated by comparing the quadrature velocity average of the approximate rates with the result of the fine-interval numerical integration given in Table 5: agreement to better than one per cent is found in all instances.

The exact rates averaged in this manner over the velocity distribution, for an H II temperature of 10^4°K, are also listed in Table 5. The tendency of the average exact rates to be smaller than the average approximate rates is due

to the divergence of the sudden approximation at low velocities, where the exact rates instead vanish (since the low frequency photons associated with the passage of the projectile cannot produce transitions).

Using the results of Table 5 and the molecular constants* of Table 2, the rate equations (8.29) truncated at $J = 3$, are solved numerically, and yield Figures 23, 24, and 25. First of all, we find from the exact rates that a number density $N_p = 1.37\text{cm}^{-3}$ (and 1.37cm^{-3}) at a kinetic temperature of 10^4°K is adequate to account for the observed 3°K excitation of the $J = 1$ CN level. Such a density of charged particles is easily attainable in an H II region, so that the observed excitation could be produced collisionally if the CN resides in such a region.

Next, in Figure 24, we see that if collisions excite the $J = 1$ CN level to 3°K, the $J = 2$ level will show very nearly the same temperature, again over a wide range of H II temperatures. The first significant departure from thermal equilibrium occurs with the $J = 3$ level, whose fractional population is only $\sim 10^{-3}$, and as such is not observable with present techniques.

Finally, Figure 25 shows that the temperature T_{10} of the $J = 1$ CN level is a rapidly varying function of N_p. Since the density of the interstellar medium is highly inhomogeneous, the invariance of T_{10} against eleven widely separated stars would tend to disprove the hypothesis that the excitation is

---

* Note that the calculations in this Chapter used the value μ=1.1D (Arpigney 1964) for the CN dipole moment instead of the more recently measured value 1.45D (Thomson and Dalby 1968). The reason is that this was the best available value at the time the work for this Chapter was done, but the slight difference between these values should not affect appreciably the final values for the proton density and T_{21} which we calculate.

collisionally induced by heavy charged particles.

b) CH

For this molecule we are only interested in the temperature of the KJ = 1 3/2 first excited state. The numerical integration of Schrodinger's equation, averaged over the velocity distribution by quadrature, yields for the proton excitation rate at an H II temperature of 10^4°K, $r^{(p)}_{1\ 1/2,\ 1\ 3/2} = r^{(p)} = 9.97 \times 10^{-8}$ cm^3/sec. The many quanta transitions to higher levels, and the single quantum transition KJ = 1 1/2 - 2 3/2, produce only slight additional excitation of the KJ = 1 3/2 level, and will be neglected.

For the electron excitation rate we use equation (7.12) and find $r^{(e)}_{1\ 1/2,\ 1\ 3/2} = r^{(e)} = 4.11 \times 10^{-8}$ cm^3/sec. The total excitation rate is thus $R = r^{(e)} + r^{(p)} = 1.41 \times 10^{-7}$ cm^3/sec. Since the Einstein coefficient for the KJ = 1 3/2 level is 9.184×10^{-5} sec^{-1}, the fractional population of this level is

$$n = N_p R/A = 2.10 \times 10^{-3} \tag{8.32}$$

for $N_p = 1.37$ cm^{-3}, and the excitation temperature in turn is

$$T = h\nu/k \ln (2/n) = 3.76°K \tag{8.33}$$

for $\nu = 5.336 \times 10^{11}$ Hz. The resultant fractional population is, however, still well below the limit of the present threshold of detectability.

CHAPTER 9.

FURTHER EVIDENCE THAT THE CN EXCITATION ORIGINATES NON-COLLISIONALLY IN AN H I REGION

In the previous three Chapters we have seen that neither infrared nor optical photons nor collisions with atoms, ions, nor electrons are sufficient to account for the observed rotational excitation of the CN in an H I region. We found, however, that if the CN is in an H II region, the observed excitation could be produced solely by collisions with charged particles. The location of the molecules is thus of crucial importance to our arguement.

As we learned in Chapter 7, the question of the place of origin of the molecular lines was first investigated by Merrill (1942, 1946), and subsequently by Adams (1949) and Bates and Spitzer (1951). Herbig (1968a), has more recently considered this question, with specific reference to the interstellar lines of ζ Ophiuchi. With the possible exception of the CH and CH+ interstellar lines in the direction of the Pleades, all of the evidence pointed to an H I origin of the molecular lines.

We will now present further evidence that the CN excitation originates non-collisionally in an H I region:

1 Probably the strongest evidence yet that the excitation is not collisional is the observed invariance of the CN rotational temperature in eleven stars.

2. We present the results of H I 21cm observations made in the direction of these stars. The CN velocity profiles are shown to correlate well with the H I velocity profiles in the same direction. This is consistent with the

contention that the CN is well embedded in an H I region of the interstellar medium.

A. T_{10} Invariance

Let us first consider the observed invariance of the rotational temperature for eleven widely separated stars. This is probably the most cogent arguement that the place of origin of the molecular lines is not an H II region, and that the source of the rotational excitation of the CN is not collisional.

Listed in Table 4 are the optical depths of the interstellar CN lines, as well as the rotational temperatures calculated from them. The saturation corrections used in calculating these values were described in Chapter 3, and appear in this Table under the column labeled ΔT.

In Chapter 8, it was shown that the assumption that the excitation is due solely to 10^4°K protons (the dominant exciting agent in an H II region) yields a rotational temperature which is for example, from 2.5° K to 3.5° K as the proton number density varies from only 0.9 to 1.9cm^{-3} (see Figure 24).

Considering that the density of the interstellar medium is highly inhomogeneous, one would expect a wide variation in CN rotational temperature from one cloud to the next if its excitation were local. However, the present data do not support this suggestion. On the contrary, the observed CN rotational temperature appears to be invariant and independent of cloud location. For all of the entries in Table 4, including a total of eleven stars, the data may be said to be consistent with the idea that the spectrum of the background is thermal, and that the excitation is not due to a local process, but rather a universal one.

Also included in this list for completeness are three late B and A type stars, that have recently been observed by other workers at the 120-inch Coude. Although T_{10} has been left uncorrected for saturation in these cases, it is evident that the excitation here is also $\sim 3°K$. These three stars represent the first observation of CN in front of stars later than B. Since extensive H II regions are only associated with stars earlier than B 0, the very restricted ionization associated with stars of such comparatively late spectral type as these three provides very good evidence that collisions with charged particles do not materially contribute to T_{10}.

Hence the temperature invariance, while not conclusive, is to be considered to be very strong evidence that the observed interstellar CN excitation is due to a universal mechanism, which is an invariant property of the universe and independent of the CN location within the interstellar medium

B. H I - CN Velocity Correlations

For CN well embedded in an H I region, we expect a velocity correlation between the CN absorption lines and the H I 21cm emission of this cloud. It should be noted that a HI- CN velocity correlation does not prove that the CN is in fact embedded in an H I region, since an H II region will also emit 21cm line radiation (Riegel 1967), however, it would seem to be a necessary condition.

Herbig (1968a) has shown that there is such a velocity correlation for the cloud in front of ζ Ophiuchi. We have also observed the CN and the H I 21cm velocity profiles for ζ Ophiuchi, as well as those for several other stars showing interstellar CN. The results are presented in Table 4, and Figures

25, 26, and 27 with the velocities referred to the solar rest frame.

The H I 21cm radio observations were made with the 300 foot transit telescope of the National Radio Astronomy Observatory (Findlay 1963), with the 100 channel autocorrelation receiver (Shalloway 1964) at an angular resolution of 10'.

The frequency resolution of the system for these scans was set between 2.5 kHz and 5 kHz, depending upon the desired total frequency range for the scan. This corresponded to a velocity resolution of between .53 and 1.06 km/sec/channel. On the other hand the velocity resolution of the optical observations was ~5km/sec, and the optical absorption lines were barely resolved. However, when we superpose the velocity profiles of CN, Ca II, and H I, we see a reasonable correlation.

Figure 26 shows these profiles in the direction of ζ Ophiuchi. Note that the optical absorption lines have approximately the same velocity maxima, but that the 21cm counterpart to these occurs as an assymetrical bump on the side of the H I peak. This peculiarity was noticed by Herbig (1968a). Presumably the H I emission originates both in front of and behind ζ Ophiuchi, and represents two independent partially resolved clouds. That the 29km/sec Ca II cloud appears to have no strong counterpart in either CN or H I is probably due to the rather high degree of saturation of the Ca II lines, not shared by the H I emission of the CN absorption. In addition the highly irregular occurrence of CN absorption suggests that a lack of occurrence of CN absorption for this cloud should not be considered surprising.

In Figure 27 the H I and CN velocity profiles are given for both ζ Persei and X Persei, which are located within 1° of each other. Adams (1949) noted the identical interstellar velocities as well as other similarities in the spectra of these two stars. We now see that this similarity also holds for the 21cm velocities as well.

Finally Figure 28 shows the Ca II, CN, and H I profiles in the direction of 20 Aquilae. To the extent that the signal-to-noise ratio of the CN tracing permits, one can say that there appear to be three distinct clouds: the first at -23km/sec containing Ca II, and possibly CN, a second at -12km/sec containing Ca II, H I, and CN, and a third at -2km/sec containing only H I and CN.

The appearance of a CN feature at -2km/sec is somewhat curious, since no corresponding feature occurrs for Ca II. The fact that in this cloud H I is observed, but Ca II is not, might be explained through the assumption that this cloud is behind the star; however, to our knowledge there is no other case known of any interstellar cloud in which the CN absorption is stronger than that of Ca II, so that in this case the CN feature must only be noise.

There is a good possibility that this CN feature is merely a dimple in the plate grain. On the other hand it is tempting to suggest that this is a unique cloud. It appears that only future observations with higher signal-to-noise ratio profiles for the CN absorption in this star can settle this question.

These four stars are the only ones whose signal-to-noise ratio permitted a comparison of velocity profiles. The velocity maxima of these lines, as well as those of the CN lines in the spectra of several other stars,

are compared in Table 4 in the column labeled v. The entries in this column were made from traveling-microscope measurements of the CN lines on the spectral plates directly.

All of the entries in this column (except possibly the aforementioned cloud in front of 20 Aquilae, whose existance appears dubious) shows a reasonable correlation of the molecular Ca II, and H I velocity. From these observations (and from the previous work) we get the picture of discrete H I clouds, in which the molecules are well mixed with the Ca II and H, as being the place of origin of the interstellar lines.

Thus all of our data are consistent with the idea that the CN is well embedded in a normal H I region, and that the observed rotational excitation of the interstellar CN is not due to collisional or local mechanisms.

CHAPTER 10

CONCLUSIONS

In this dissertation $T_{10}(CN)$, the $J = 0 \rightarrow 1$ excitation temperature of interstellar CN, has been determined to varying degrees of accuracy in the direction of eight stars. The primary data for this analysis consisted largely of old plates found in the Mt. Wilson files, but included six spectra of ζ Ophiuchi obtained by Herbig with the Lick 120-inch telescope and four spectra of BD+66° 1674 and BD+66° 1675 obtained by Münch with the 200-inch telescope. This excitation temperature has also been determined in three other directions by other workers. A summary of these results is listed in Table 4 and discussed in Chapters 5 and 9.

The important result of these measurements is that, to within observational uncertainties, $T_{10}(CN)$ appears to be independent of direction, as would be expected if the molecules were excited by cosmic background radiation alone. Unfortunately the uncertainty of $T_{10}(CN)$ is often of the order of 1.0°K. New observational work on the stars listed in Table 4 is therefore of high priority, and, of course, interstellar CN lines should be sought in the spectra of other stars.

In the two cases with best signal-to-noise ratio, in which CN is observed against the 2nd magnitude stars ζ Ophiuchi and ζ Persei, $T_{10}(CN)$ is in remarkable agreement with the direct radio observations of the background at wavelengths longer than 3.3mm (Figure 1). Consider in particular the series of direct measurements made by Wilkinson and his collaborators at Princeton, which represent the most extensive collection of direct observations made by a

single group, and those which extend to shortest wavelength. A weighted mean of their four measurements (extending from λ 3. 2cm to λ 3. 2mm) yields for the brightness temperature of the background radiation $\bar{T}_B = 2\ 68 \pm 0.\ 11°K$, while we find for ζ Ophiuchi $T_{10}(CN) = 2.\ 74 \pm 0.\ 22°K$, and for ζ Persei $T_{10}(CN) = 2.\ 74 \pm 0.\ 30°$ K. A graphical comparison of the radio observations and CN temperatures is shown in Figure 29.

Although the invariance of $T_{10}(CN)$, and the velocity correlation of CN and H I, are the strongest evidence that the CN lies in normal H I regions, a major part of this thesis has been devoted to considering the possible role of other interstellar processes in the molecular excitation. All of the evidence we have been able to assemble points to the conclusion that the CN molecules lie in normal H I regions where collisions or the scattering of photons are unable to account for 3°K excitation.

We first considered radiative excitation in Chapter 6, and concluded that in general in the interstellar medium indirect radiative excitation mechanisms by way of fluorescent cycles are far too weak to account for the observed excitation.

Next we considered collisional excitation, and assumed that the CN in front of ζ Ophiuchi resides in the dense H I layer whose conditions are those found by Herbig (1968a). There is good evidence in favor of this assumption We find that ions may be neglected but electrons and H atoms may not. These latter two components provide roughly equal CN rotational excitation, however, using Herbig's upper limit for the densities of these in this cloud, we find that they can contribute at most a small portion of the observed excitation temperature.

This fractional upper limit is not as low as one might desire, however,

and it appears that for electrons at least, considerable improvement of this upper limit is possible by further observational work. In addition, it would be useful to know if the high H I density of this cloud is characteristic of the clouds associated with the other stars in our survey. In this respect observations and an analysis similar to that performed by Herbig for ζ Ophiuchi should be extended to these other stars.

We next assume that the CN resides in an H II region. We find in this case that a modest density of only 1.4 protons/cm^{-3} (and electrons) is sufficient to account for the $\sim 3^{\circ}$K observed CN excitation. However, we find that in this case the resultant excitation temperature is a sensitive function of the assumed proton density, and it is now hard to account for the observed invariance of T_{10} in eleven stars. In addition three of these stars are of rather late spectral type, and have fairly limited H II regions associated with them. This fact casts strong doubt on the suggestion that the CN is in such a region.

Thus on the basis of our current knowledge of interstellar conditions, the equilibrium between the CN molecules and $\sim 3^{\circ}$K background radiation is altogether intelligible. However, the interstellar molecular spectra offer still more valuable information on the spectrum of the background radiation at wavelengths inaccesible to ground-based observation. The absence of interstellar lines from the CN J = 2 level, and from the first excited states of CH and CH+ imposes low upper limits to the intensity of the radiation at $\lambda = 1.32$, 0.560 and 0.359mm. Since we are concerned only with upper limits to the background, other physical processes in the interstellar medium turn out to be of very slight consequence in the final analysis, and it is only necessary to consider the case of

ζ Ophiuchi where the lines can be observed with best signal-to-noise ratio. From the equivalent width measurements and upper limits listed in Table 4 and described in Chapter 5, we find that

$$I_\nu(2.64\text{mm}) \leq 3.24 \times 10^{-15} \text{ erg cm}^{-2} \text{ sec}^{-1} \text{ ster}^{-1} \text{ Hz}$$

$$I_\nu(1.32\text{mm}) < 2.75 \times 10^{-14} \text{ erg cm}^{-2} \text{ sec}^{-1} \text{ ster}^{-1} \text{ Hz}$$

$$I_\nu(0.560\text{mm}) < 3.91 \times 10^{-14} \text{ erg cm}^{-2} \text{ sec}^{-1} \text{ ster}^{-1} \text{ Hz}$$

$$I_\nu(0.359\text{mm}) < 10.0 \times 10^{-14} \text{ erg cm}^{-2} \text{ sec}^{-1} \text{ ster}^{-1} \text{ Hz}$$

$$I_\nu(0.150\text{mm}) < 4.2 \times 10^{-12} \text{ erg cm}^{-2} \text{ sec}^{-1} \text{ ster}^{-1} \text{ Hz}$$

The relevance of these upper limits to the result of the only attempt so far to detect the background radiation above the atmosphere (Shivananden et al 1968) was discussed in Chapter 5. It appears that their recent rocket observations of a large background flux with wavelength in the region of our upper limits must either be of radiation with a highly irregular spectrum, or of radiation which is quite local in origin, and does not extend as far as the -15Km/sec interstellar cloud in front of ζ Ophiuchi.

A final word should be said concerning some of the technical aspects of this dissertation. A large part of the data analysis consisted of devising a way of adding together a large number of spectra using a digital computer. These techniques are of potential value in a number of fields of astrophysics where signal-to-noise ratio is a principal problem. The techniques are described in Chapter 4.

In Appendix 4 there is also a long discussion of the problem of optimal signal processing of digitized spectrogram tracings. Relations are derived for the optimal filter function, the best estimate of spectral line strength, and an error estimate for this line strength.

Finally, a side benifit of this considerable improvement in signal-to-noise ratio, is the detection of $C^{13}H^{+}$ with an abundance which is in agreement with the value found on the earth and Venus.

APPENDIX 1

MATRIX ELEMENTS OF THE MOLECULAR HAMILTONIAN

We wish to calculate the matrix elements of the molecular Hamiltonian

$$\mathcal{H} = B(\underset{\sim}{K}^2 - \Lambda) + A\Lambda S_z \qquad \text{(equation 3. 3)}$$

in the Hund's case (b) coupling scheme

$$\underset{\sim}{K} = \underset{\sim}{N} + \underset{\sim}{\Lambda}, \quad \underset{\sim}{J} = \underset{\sim}{K} + \underset{\sim}{S} \qquad \text{(equation 3. 2)}$$

To calculate the matrix elements of the operator $S_{z'}$, we must first transform it into the laboratory frame.

$$S_{z'} = \sum_{q=-1}^{1} S(1q)\,(\mathfrak{D}^{-1})^{(1)}_{q0}\,(\alpha\,\beta\,\gamma) \qquad \text{(A1. 1)}$$

S(1q) are the tensor components of the spin operator in the laboratory frame, and $\mathfrak{D}$ is the finite rotation operator transforming the laboratory frame to the molecular frame (Edmonds 1968, Chapters 4 and 5). The particular matrix elements of the rotation operator which appear in equation (A1. 1) may be written as normalized spherical harmonics (Edmonds 1968 , equations 4. 1. 25 and 4. 2. 7).

$$\begin{aligned}(\mathfrak{D}^{-1})^{(1)}_{q0}\,(\alpha\beta\gamma) &= \mathfrak{D}^{(1)*}_{0q}(\alpha\beta\gamma) = (-1)^{-q}\,\mathfrak{D}^{(1)}_{0-q}(\alpha\beta\gamma) \\ &= \left(\frac{4\pi}{3}\right)^{1/2}(-1)^{-q}\,Y_{1-q}(\beta\alpha)\end{aligned} \qquad \text{(A1 2)}$$

$S_{z'}$ may then be expressed as the scalar product of two commuting tensor operators

$$\begin{aligned}S_{z'} &= \left(\frac{4\pi}{3}\right)^{1/2}\sum_{q=-1}^{+1}(-1)^{-q}\,S(1q)\,Y_{1-q}(\beta\alpha) \\ &= \sqrt{4\pi/3}\;\underset{\approx}{S}(1)\;\cdot\;\underset{\approx}{Y}(1)\end{aligned} \qquad \text{(A1. 3)}$$

The matrix elements of the scalar product of two such operators may be written (Edmonds 1968, equation 7. 1. 6)

$$\langle \Lambda K'SJ | S_{z'} | \Lambda KSJ \rangle = \left(\frac{4\pi}{3}\right)^{1/2} (-1)^{K+S+J} \begin{Bmatrix} J & S & K' \\ 1 & K & S \end{Bmatrix}$$

$$\langle S \| \underset{\approx}{S}(1) \| S \rangle \langle \Lambda K' \| \underset{\approx}{Y}(1) \| \Lambda K \rangle \qquad \text{(A1. 4)}$$

The first reduced matrix element in equation (A1. 4) has been evaluated by Edmonds (1957, equation 5. 4. 3), and the second is evaluated in the usual way by selecting the easiest to compute of the components $\langle \Lambda K'M | Y_{1q} | \Lambda K M \rangle$, and dividing by the appropriate 3j symbol. Thus

$$\langle \Lambda K' \| \underset{\approx}{Y}(1) \| \Lambda K \rangle = \langle \Lambda K' 0 | Y_{10} | \Lambda K 0 \rangle (-1)^{K'} \begin{pmatrix} K' & 1 & K \\ 0 & 0 & 0 \end{pmatrix}^{-1} \qquad \text{(A1. 4)}$$

The wave function $|\Lambda KM\rangle$ of the rotor may also be written in terms of the matrix elements $\mathfrak{D}^{(K)}_{M\Lambda}(\alpha\beta\gamma)$ of the finite rotation operator. Since $Y_{10}(\beta) = (3/4\pi)^{1/2} \mathfrak{D}^{(1)}_{00}(\beta)$ equation (A1. 4) then becomes

$$\langle \Lambda K' \| \underset{\approx}{Y}(1) \| \Lambda K \rangle = (-1)^{K' + \Lambda} \begin{pmatrix} K' & 1 & K \\ 0 & 0 & 0 \end{pmatrix}^{-1} \frac{1}{8\pi^2} \left(\frac{3}{4\pi}\right)^{1/2} [(2K'+1)(2k+1)]^{1/2} \qquad \text{(A1. 5)}$$

$$\times \int_0^{2\pi} \int_0^{\pi} \int_0^{2\pi} \mathfrak{D}^{(K')}_{0-\Lambda} \mathfrak{D}^{(k)}_{00} \mathfrak{D}^{(K)}_{0\Lambda} \sin\beta \, d\alpha \, d\beta \, \gamma$$

The integral over the three $\mathfrak{D}$ functions yields a simple product of two 3j symbols (Edmonds 1957, equation 4. 6. 2) and equation (A1. 5) simplifies to

$$\langle \Lambda K' \| \underset{\approx}{Y}(1) \| \Lambda K \rangle (-1)^{K'+\Lambda} (3/4\pi)^{1/2} [(2K'+1)(2K+1)]^{1/2} \begin{pmatrix} K' & 1 & K \\ -\Lambda & 0 & \Lambda \end{pmatrix} \qquad \text{(A1 6)}$$

Combining these equations, we obtain the requisite matrix elements of the molecular Hamiltonian (equation 3. 3) in the Hund's case (b) representation.

$$\langle \Lambda K'SJ | \mathcal{H} | \Lambda KSJ \rangle = B[K(K+1) - \Lambda^2] \delta_{K'K} + A\Lambda (-1)^{J+K'+K+S+J} \qquad \text{(A1. 7)}$$

$$\times [(2K'+1)(2K+1)(2S+1)(S+1)S]^{1/2} \begin{Bmatrix} J & S & K' \\ 1 & K & S \end{Bmatrix} \begin{pmatrix} K' & 1 & K \\ -\Lambda & 0 & \Lambda \end{pmatrix}$$

APPENDIX 2

EVALUATION OF THE REDUCED MATRIX ELEMENTS OF THE DIPOLE MOMENT OPERATOR

We wish to evaluate the reduced matrix element

$$\langle\, \Lambda KSJ\alpha \,\|\, \underset{\approx}{C}(1) \,\|\, \Lambda'K'SJ'\alpha' \,\rangle$$

in the Hund's case (b) coupling scheme

$$\underset{\sim}{K} = \underset{\sim}{N} + \underset{\sim}{\Lambda}, \quad \underset{\sim}{J} = \underset{\sim}{K} + \underset{\sim}{S}.$$

First we factor off the S dependence using Edmonds' (1968) equation (7. 1. 7)

$$\langle \Lambda KSJ\alpha \,\|\, \underset{\approx}{C}(1) \,\|\, \Lambda'K'SJ'\alpha \rangle = \tag{A2. 1}$$

$$(-1)^{K+S+J'+1} [(2J'+1)\,(2J+1)]^{1/2} \begin{Bmatrix} K' & J' & S \\ J & K & 1 \end{Bmatrix} \langle \Lambda K\alpha \| \underset{\approx}{C}(1) \| \Lambda'K'\alpha' \rangle$$

We evaluate, as before, by selecting one of the components, and dividing by the appropriate 3j symbol (Edmonds 1968, equation 5. 4. 1), whence

$$\langle \Lambda KJ\alpha \,\|\, \underset{\approx}{C}(1) \,\|\, \Lambda'K''J''\alpha \rangle = (-1)^{S+J'+1} \tag{A2. 2}$$

$$[(2J'+1)\,(2J+1)]^{1/2} \begin{Bmatrix} K' & J' & S \\ J & K & 1 \end{Bmatrix} \frac{\langle\, \Lambda K\alpha M_K = 0 \,|\, C_{10} \,|\, \Lambda'K'\alpha M_{K'} = 0 \,\rangle}{\begin{pmatrix} K & 1 & K' \\ 0 & 0 & 0 \end{pmatrix}}$$

In order to calculate the matrix element in equation (A2. 2), we must first transform this component into a frame (primed) which is fixed with respect to the molecule. Using Edmonds (1968, equations 4. 1. 25 and 4. 6. 5) we get

$$C_{10} = \sum_q \mathfrak{D}^{(1)}_{0q}(\alpha\beta\gamma)\; C'_{1q} \tag{A2. 3}$$

In a fashion similar to that of Appendix 1, since $C_{10}(\beta) = \mathfrak{D}^{(1)}_{00}(\beta)$, we can write

$$\langle\, \Lambda\, K\, \alpha M_K{=}0 \,|\, C_{10} \,|\, \Lambda K'\alpha' M_{K'}{=}0 \rangle = (-1)^{\Lambda} (3/4\pi)^{1/2} (1/8\pi^2)\; [(2K'+1)(2K+1)]^{1/2} \tag{A2. 4}$$

$$\times \sum_q \int_0^{2\pi}\int_0^{\pi}\int_0^{2\pi} \mathfrak{D}^{(K)}_{-\Lambda 0}\; \mathfrak{D}^{(1)}_{q0}\; \mathfrak{D}^{(K')}_{\Lambda' 0}\; \sin\beta\, d\alpha' d\beta' d\gamma' \,\langle \alpha \,|\, C'_{1q} \,|\alpha' \rangle$$

The integral over the three $\mathfrak{D}$ functions may again be evaluated by using Edmonds' (1968, equation 4. 6. 2). Integrating and transforming from the Hund's case (b) representation to the representation in which the molecular Hamiltonian is diagonal, we have

$$\langle \Lambda \hat{K} J\alpha \| \underset{\approx}{C}(1) \| \Lambda' \hat{K}' J'\alpha' \rangle = \sum_{K'K} U_{\hat{K}'K'} U^{*}_{\hat{K}K}$$

$$(-1)^{\Lambda+S+J'+1} [(2K'+1)(2K+1)(2J'+1)(2J+1)]^{1/2} \begin{Bmatrix} K' & J' & S \\ J & K & 1 \end{Bmatrix} \qquad \text{(A2. 5)}$$

$$\sum_{q} \langle \alpha | C^{1}_{1q} | \alpha' \rangle \begin{pmatrix} K & 1 & K' \\ -\Lambda & q & \Lambda' \end{pmatrix}$$

APPENDIX 3

VIBRATIONAL FLUORESCENCE RATE

The Einstein B coefficient for a vibration - rotation transition is given by

$$B_{J''v'',\,J'v'} = \frac{8\pi^3}{3h^2c} \; \frac{\left| \mathfrak{M}^{\text{vib-rot}}_{v''J'',\,v'J'} \right|^2 \left[J''\delta_{J''-1} + (J''+1)\,\delta_{J''+1,\,J'} \right]}{2J''+1} \qquad \text{(A3. 1)}$$

where $\mathfrak{M}^{(\text{vib-rot})}_{v''J'',\,v'J'}$ is the effective electric dipole moment for the transition (Herman and Wallis 1955). Since the P and R branches have approximately the same wavelength , we write the sum over rotational transitions as

$$B_{v=0,1} = \frac{8\pi^3}{3h^2c} \left| \mathfrak{M}^{\text{vib-rot}}_{v=0,1} \right|^2$$

Using Oppenheimer's (1926) model, for an upper limit to B we consider the effective charge to be at the internuclear spacing, whence

$$\left| \mathfrak{M}^{(\text{vib-rot})}_{v''=0,1} \right|^2 = \mu^2 \, \frac{B_e}{\omega_e} = 2.4 \times 10^{-3} \text{ Debye}^2$$

where μ is the permanent electric dipole moment of the molecule, and B_e and ω_e are molecular constants of its ground electronic state, found in Table 2 and Herzberg (1959, Table 39). Hence we calculate

$$B_{v=0,1} = 45.3 \times 10^{14} \text{ cm}^3 \text{ Hz erg}^{-1} \text{ sec}^{-1} \; .$$

APPENDIX 4

NOISE FILTERING AND STATISTICAL ANALYSIS OF ERRORS

In this Appendix we consider the problem of the optimal measurement of the strengths of spectral absorption lines embedded in photographic grain noise. This is a very similar problem to one which has been considered in the field of communication theory, i. e., the determination of the strength, position, and/or presence of radar echos in receiver noise. In the treatment which follows we shall make use of the literature of this field. *

The basic problem is (1) to determine the most probable value of the strength of a spectral line formed in the photographic grain noise noise of a microphotometer tracing of a spectrogram, and (2) to set error limits for this result Let us represent the intensity distribution recorded on the plate as a function of wavelength by

$$y(\lambda) = \alpha(\lambda) - \beta S(\lambda) + n(\lambda) \qquad \text{(A4. 1)}$$

where:

$\alpha(\lambda)$ is the continuum which is assumed to be known or measureable arbitrarily accurately,

$s(\lambda)$ is a spectral line whose shape is also assumed to be known. (The validity of this assumption will be discussed later.),

β is the height of the absorption line to be determined (the minus sign signifies absorption),

$n(\lambda)$ is continuous gaussian (Goetz and Gould 1937, Fellgett 1951) random noise (assumed wide-sense stationary), whose auto-correlation function

$$R_n(u) = \lim_{T \to \infty} \int_{-T}^{T} n^*(\lambda) n\ (u+\lambda)\ d\lambda \qquad \text{(A4. 2)}$$

is assumed to be measurable arbitrarily accurately.

---

* For a good review of this field see An Introduction to the Theory of Random Signals and Noise (Davenport and Root 1958), hereafter referred to as D & R.

Let us also represent by $y'(\lambda)$ our measurement of a spectrogram on a densitometer with a slit, whose transmission as a function of wavelength is given by $h_{slit}(\lambda)$. Then*

$$y'(\lambda) = [\, y * h_{slit} \,]_{\lambda} \qquad \text{(A4. 3)}$$

A similar and not unrelated problem which should also be considered is the removal of the slit scanning function h_{slit} introduced by the densitometer. As long as the slit is narrow with respect to the most narrow spectral features, one can neglect the signal distortion introduced by its finite width. A common proceedure has been to use a wide slit function as a crude noise filter. This is not an optimal proceedure (for a rectangular slit function), however, and it will be shown that a statistical estimation of line strength is inherently tied to the problem of optimal noise filtering. The maximum likelihood estimate of a line strength will be shown to be a function of certain parameters of an optimally filtered signal**. Our analysis will treat first the problem of processing the direct signal $y(\lambda)$, and then return to the problem of including the effect of a finite slit width.

A. Maximum Likelihood Estimation

As a starting point we shall use a maximum likelihood estimation for the most probable value of β (VonMises 1964, p. 547), and set our error limits according to the criterion of the Neyman-Pearson theory of hypothesis testing (VonMises 1964, p. 504).

---

* Here $a*b$ represents the convolution product given by

$$[\, a*b \,]_u = \int_{-\infty}^{\infty} a(u - \lambda)\, b(\lambda) d\lambda$$

** Fellgett (1953) has discussed the filtering of densitometer tracings of spectrograms, and come to the conclusion that the best filter is a "matched" filter. However, his filter is only derivable for an infinite length spectrogram, and he provides no suggestion for an estimate of spectral line strength.

If $\underset{\sim}{y} = y_1\ y_2\ \cdots,\ y_n$ is a given set of measurements*, from which we would like to estimate the parameter β, then the aposteriori probability density that our measurement will have occurred is

$$q(\underset{\sim}{y}) = p(\underset{\sim}{y} \mid \beta)\, p(\beta) \qquad \text{(A4.4)}$$

where $p(\beta)$ is the apriori probability density for the occurrence of β.

The apriori probability density $p(\beta)$ presents a problem because it is unknown. To find it, one would need a large ensemble of identical experimental situations, however we do not have such an ensemble. We do know, however, that $\beta \geq 0$, (i. e. we have no emission lines). Thus the apriori probability of an occurrence of β which does not satisfy this inequality is zero.

Outside of this restriction, $p(\beta)$ is unknown, and the usual practice** originally due to Gauss (1823) is to assume $p(\beta)$ to be constant in this region. Equivalently β may be regarded as an unknown positive "constant".

We define $\hat{\beta}$ to be the maximum likelihood estimate of β equal to the value of β which maximizes $p(y \mid \beta)$ (called the likelihood function). This is just equivalent to saying that we choose the value for β which makes our observation the most probable one.*** It is generally convenient to maximize $\log p(y \mid \beta)$ instead of $p(y \mid \beta)$. Since the logarithm is a real increasing function for positive arguements, the proceedure is equivalent to that of maximizing $p(y \mid \beta)$.

For an error estimate we must define an interval H, which for a given probability Q, the actual value of β lies within this interval. Usually in physics when gaussian statistics apply, the domain of a parameter is infinite or very great in comparison with the error limit range. Then the most probable

---

* For example the y_k may be the digitized intensity points of a spectrogram, or as we shall use later, the coefficients of an orthoganal expansion of y.

** Further justifications for the proceedure is given by VonMises (1964, p. 496, 548).

*** $p(y \mid \beta)$ is tacity assumed to possess one and only one maximum in the region where $p(\beta) \neq 0$.

value lies at the center of the interval and one says, for example, that for 95.5% probability the true value of β lies in the interval between $\hat{\beta} - 2\sigma$ and $\hat{\beta} + 2\sigma$ [or with a probability $Q = \text{erf}(n/\sqrt{2})$, the true value of β lies in the region $\hat{\beta} - n\sigma$ and $\hat{\beta} + n\sigma$], and the most probable value of $\beta = \hat{\beta}$. We shall adopt the 95.5% probability ($n = 2$), but find that $\hat{\beta} < n\sigma$', the region is no longer symmetrical about $\hat{\beta}$

The probability that the true value of β lies within the region H is just

$$Q(H) = \frac{\int_H p(y \subset A \mid \beta)\, p(\beta)\, d\beta}{\int_{H+\bar{H}} p(y \subset A \mid \beta)\, p(\beta)\, d\beta} \tag{A4.5}$$

where:

H is our error limit region

A is the region of y for which we will decide that β H and,

$H+\bar{H}$ is the allowed domain of $\beta (\beta > 0)$.

Since $p(\beta)$ is constant over $H+\bar{H}$ equation (A4.5) reduces to

$$Q(H) = \frac{\int_H p(y \subset A \mid \beta)\, d\beta}{\int_{H+\bar{H}} p(y \subset A \mid \beta)\, d\beta} \tag{A4.6}$$

What we wish to find is the minimum size region for H such that for a given probability Q the actual value of β is in H.

If $n(\lambda)$ is a gaussian random process, it can be shown (use is made of the results on pages 336 and 342 of D & R) by a rather involved analysis which will be omitted here for the sake of brevity (and to keep from having to type all of the equations) that $p(\lambda)\, p(y \mid \beta)$ is of the form

$$p(\beta)\, p(y \mid \beta) = N \begin{cases} \exp.\, [-(\beta - \beta_m)^2 / 2\sigma_\beta^2\ ] & \text{for } \beta > 0 \\ 0 & \text{otherwise} \end{cases} \tag{A4.7}$$

where N is a normalizing factor,

$$\beta_m(y) = \frac{\int_{\Lambda_L-\Lambda}^{\Lambda_L+\Lambda} [y(\lambda) - \alpha(\lambda)] f(\lambda)\, d\lambda}{\int_{\Lambda_L-\Lambda}^{\Lambda_L+\Lambda} s(\lambda)\, f(\lambda)\, d\lambda} \tag{A4. 8}$$

$$\sigma_\beta^2(y) = \frac{1}{\int_{\Lambda_L-\Lambda}^{\Lambda_L+\Lambda} s(\lambda)\, f(\lambda)\, d\lambda} \tag{A4. 9}$$

and $f(\lambda)$ is defined by the following integral equation

$$\int_{\Lambda_L-\Lambda}^{\Lambda_L+\Lambda} R_n(u-\lambda)\, f(\lambda)\, d\lambda = s(u) \tag{A4. 10}$$

Now consider the troublesome domain of β. To maximize the integral (A4. 6) and to find the maximum point of $p(y \mid \beta)$, we must consider the three cases which are illustrated in Figure 30. We must find an error limit region H of minimum size such that, with probability $Q = \text{erf}\,(n/\sqrt{2})$, β will be within H (our error criterion will yield the probabilities corresponding to the standard $\pm n\sigma$ criterion used in physics).

B. Case A

$$\text{If} \quad \beta_m \geq n\sigma' = \sigma\sqrt{2}\,\text{erf}^{-1}\left[Q/2-Q\right] \tag{A4. 11}$$

then $\hat{\beta} = \beta_m$ and it is easy to show that a minimum error probability occurs for limits symmetrical about $\hat{\beta}$. Then with probability Q the true value of β lies in the interval $\hat{\beta} - \eta \leq \beta \leq \hat{\beta} + \eta$.

As can be seen from Figure 30, in this case we have for equation (A4. 6)

$$\text{erf}\,\eta/\sqrt{2} = Q = \frac{\int_{\beta_m-\eta}^{\beta_m+\eta} p(y \mid \beta)\, d\beta}{\int_0^\infty p(y \mid \beta)\, d\beta} \tag{A4. 12}$$

Equation (A4. 12) may be solved for η to yield

$$\eta = \sigma\sqrt{2}\ \mathrm{erf}^{-1}\ \{\ [\ 1+\mathrm{erf}\ (\beta_m/\sigma\sqrt{2}\ )\ ]Q/2\} \qquad \text{(A4. 13)}$$

We can also see now the reason for the definition of $\eta\sigma'$. It is defined so that the lower limit of the integral in the numerator of (A4. 12) is greater than or equal to zero i. e. $\beta_m - \eta \geq 0$.

The limiting case occurs at $\beta_m = \eta$, and from (A4. 13) we may solve for η; thus $\eta\sigma' = \eta = \beta_m = \sigma\sqrt{2}\ \mathrm{erf}^{-1}\ [Q/2-Q]$.

For $n = 2$, $2\sigma' = 1.7116\sigma$.

Note that η reduces to the usual case encountered in physics for β_m well into the domain of β, then

$$\lim_{\beta_m \to \infty} \eta = \sigma$$

C. Case B

If $0 < \beta_m \leq \sigma$, then $\beta = \beta_m$ is still the most probable value of β, but it is no longer in the center of the error region, and equation (A4. 6) becomes

$$\mathrm{erf}\ n/\sqrt{2} = Q = \frac{\int_0^{\beta+\eta} p(y \mid \beta)\, d\beta}{\int_0^{\infty} p(y \mid \beta)\, d\beta} \qquad \text{(A4. 14)}$$

Solving (A4. 14) for η we get

$$\eta = \sigma\sqrt{2}\ \mathrm{erf}^{-1}\ [\ Q -(1 - Q)\ \mathrm{erf}\ (\ |\hat{\beta}|\ /\sigma\sqrt{2})\ ] \qquad \text{(A4. 15)}$$

D. Case C

If $\beta_m \leq 0$, the maximum value of $p(y \mid \beta)$ occurs for $\beta = \hat{\beta} = 0$, since $p(y \mid \beta)$ is never stationary in the allowed domain of β as can be seen from Figure 30. Then the lower limit of the region is zero, and the upper limit is again given by equation (A4. 15), as long as we include the absolute value

sign, and define η as is shown in Figure 30.

E. Interpretation

These results can be interpreted simply in terms of optimal linear "matched" filters (D & R p. 244, Zadeh and Ragazzini 1952, and Van Vleck and Middleton 1946).

Let us define

$$g(\Lambda_L - \lambda) = \begin{cases} \rho(\lambda) & \text{for } \Lambda_L - \Lambda \le \lambda \le \Lambda_L + \Lambda \\ 0 & \text{otherwise} \end{cases} \tag{A4. 16}$$

$$y''(\lambda) = -\int_{-\infty}^{\infty} [y(u) - \alpha(u)]\, g(\lambda - u)du = [(y-\alpha) * g]_{\lambda} \tag{A4. 17}$$

and

$$s''(\lambda) = \int^{\infty} s(u)\, g(\lambda - u)du = [s*g]_{\lambda} \tag{A4. 18}$$

Then β_m and σ_β are just given by

$$\beta_m = y''(\Lambda_L) / s''(\Lambda_L) \tag{A4. 19}$$

$$\sigma_\beta^2 = 1/s''(\Lambda_L) \tag{A4. 20}$$

It is clear that $y''(\lambda)$ is a representation of y which has been filtered by the function g. If the value $\beta_m s''(\Lambda_L) = y''(\Lambda_L) \ge 0$, it is just the maximum likelihood estimate of the signal strength. This is equal to the height of the filtered, zero restored, signal at the line center, if a normalized filter is used.

The integral equation for the filter function may be written by combining (A4. 15) and (A4. 16), whence we get

$$s(\Lambda_L - u) = \int_{\Lambda_L - \Lambda}^{\Lambda_L + \Lambda} R_n(\lambda - u)\, g(\lambda)\, d\lambda \quad \text{for } -\Lambda \le u \le \Lambda \tag{A4. 21}$$

$$= [R_n * g]_u = \bar{s}(u)$$

Here we have defined

$$\bar{s}'(u) = s(\Lambda_L - u)$$

F. Removal of Effect of Finite Slit Width

Let us now return to the problem of inverting the slit function. Instead of using the function g to filter our data, we will use the function h_c, whose purpose is to both remove the affect of h_{slit}, and to apply g. The tandem filter function for two linear filters applied sequencially is given by the convolution of the two individual filter functions (Cheng 1961, p. 245),

$$h_c * h_{slit} = g \tag{A4. 22}$$

Convolving both sides of equation (A4. 22) with $R^* \bar{h}_{slit}$, where $\bar{h}_{slit}(\lambda) = h_{slit}(-\lambda)$, and using equation (A4. 21) we have

$$\begin{aligned}(R_n * h_{slit} * \bar{h}_{slit}) * hc &= R_n * g * \bar{h}_{slit} \\ &= \bar{s}' * \bar{h}_{slit} = \bar{s}'\end{aligned} \tag{A4. 23}$$

where we have defined

$$\bar{s}'(\lambda) = [\bar{s} * h_{slit}]_\lambda = s'(\Lambda_L - \Lambda). \tag{A4. 24}$$

By the use of the Wiener-Khintchin theorem (D & R p 183) we can identify

$$R_n * h_{slit} * \bar{h}_{slit} = R'_n \tag{A4. 25}$$

as the autocorrelation for noise which has been filtered by h_{slit}; similarly s' is just the pure signal filtered by h_{slit}. Thus we have

$$[R'_n * h_c]_u = s'(\Lambda - u) \tag{A4. 26}$$

This will just be noted as the integral equation for the optimal filter for extracting a signal, which has been modified by convolving the slit function with it, from noise which has been modified in the same way. Thus all we need for the calculation of the optimal slit and noise removing filter function is R'_n, not R_n. This is fortuitous in that R'_n may be measured directly from the digitized tracings by

a simple numerical integration, where as R_n would require additional optical measurements.

G. Error Estimates for Spectral Line Depth

From equations (A4. 22) and (A4. 24) an error estimate for $\hat{\beta}$ (taking into account the three cases previously described) is given by

$$\sigma^2_{\beta} = [h_n * \bar{h}_n * R_n]_0 = \tilde{R}'_n(0) \tag{A4. 27}$$

where

$$h_n(\lambda) = \frac{h_c(\lambda)}{[h_c * s]_{\Lambda_c}} \tag{A4. 28}$$

is the normalized filter which applied to y yields y'' (normalized), then $\tilde{R}'_n$ is just the autocorrelation function of pure plate grain noise which has been acted upon by h_n. Thus a measurement of σ^2_{β} becomes very simple: just measure $\tilde{R}_n(0)$ i. e. the autocorrelation of filtered noise in an adjacent region of the plate where no signal is present. This is the way in which errors were calculated for Table 4.

APPENDIX 5

CALCULATION OF FILTER FUNCTIONS

Integral equation (A4. 26) becomes particularly easy to solve if one assumes that the noise spectrum is a constant (white noise), for which $R'_n(\lambda) = W_n \delta(\lambda)$, and W_n is given by

$$W_n = \int_{-\infty}^{\infty} R'_n(\lambda)\, d\lambda \tag{A5. 1}$$

Then we have the immediate solution

$$g(\lambda) = \begin{cases} s(\Lambda_L - \lambda) & \text{for } \Lambda_L - \Lambda \le \lambda \le \Lambda_L + \Lambda \\ 0 & \text{otherwise,} \end{cases} \tag{A5. 2}$$

and our likelihood test becomes simply a cross-correlation of the measured signal with the assumed signal.

In practice, $R'_n(\lambda)$ will be highly peaked at the origin with a peak width controlled by the slit width. The measured peak half widths are typically .015Å.

Using autocorrelation functions R'_n of similar form to those measured, equation (A4. 26) has been solved for a gaussian signal shape with a line width parameter .05Å, with a method described below. The equation for an optimal filter function is of the form

$$\int_{-\Lambda}^{\Lambda} \hat{R}'_n(u - \lambda)\, f(\lambda)\, d\lambda = s(u) \tag{A5. 3}$$

where

$$\hat{R}'_n = \frac{R'_n}{W_n}$$

In the case when $\hat{R}'_n(\lambda) \approx \delta(\lambda)$, we know immediately a good approximate solution is

$$h(\lambda) \approx s(\lambda) \tag{A5. 4}$$

Denote the linear integral operator of (A5. 3) by $\mathfrak{L}(h(\lambda))$ then (A5. 3) becomes

$$\mathcal{L}(h(\lambda)) = s(\lambda) \tag{A5.5}$$

let $h = s + h_1$ where $h_1 << h$, then $\mathcal{L}(h_1) = s - \mathcal{L}(s) = F(s) = s_1$ and $s_1 << s$. We now have a new integral equation to solve for the correction:

$$\mathcal{L}(h_1) = s_1 \tag{A5.6}$$

By iterating the same proceedure, we get for a solution

$$h = \sum_{n=0}^{\infty} s_n \tag{A5.7}$$

where

$$\begin{aligned} s_1 &= s - \mathcal{L}(s) = F(s) \\ s_2 &= s_1 - \mathcal{L}(s_1) = F(s_1) = F^2(s) \end{aligned} \tag{A5.8}$$

$$s_n = s_{n-1} - \mathcal{L}(s_{n-1}) = F(s_{n-1}) = F^n(s)$$

For the cases calculated, three iterations were sufficient to reduce the correction to less than .1%.

Filters were calculated using this technique assuming that the shape of a spectral line is gaussian (Strömgren 1948). Although this assumption has been criticized by Münch (1957) and Blaauw (1952), the actual velocity distribution within an interstellar cloud, and hence the resulting spectral line shape is peculiar to the cloud under consideration. Since most of the other high signal-to-noise ratio lines in the stars of our survey are well fit by a gaussian line shape, this assumption appears to be very good.

The difference between the assumed gaussian signal and the calculated filter function is found to be only about 5% (actually the solution closely approximates a gaussian slightly narrower). Since the signal shape is not known this accurately, a gaussian filter function was used for the processing throughout.

ACKNOWLEDGEMENTS

I would like to express my appreciation to Professor Patrick Thaddeus for his guidance on this project, and the education I gained from working with him. I express my special thanks to Drs. G. Herbig and G. Münch, and to Miss L. Lowen of the Mt Wilson and Palomar Observatories for the loan of the plates on which this work in based, and for helpful conversations. I acknowledge Dr. N. Woolf who first brought to our attention the fact that the interstellar CN rotational temperature would place an upper bound on the background intensity, and I also thank Dr. G. Field for helpful conversations.

I especially thank Mr. J. A Westphal for his making available to me the Caltech densitometer and for his advice and assistance in its use I also thank Mr. C. B. Ray of the Caltech Computing Center, and the Astrophysics Department and Biological Systems Group of Caltech for making the link-up possible; and Messrs. G. Snellen and N. Wright for their assistance in tracing the plates, and for making this part of the work enjoyable.

I wish to acknowledge the National Radio Astronomy Observatory and the Kitt Peak National Observatory for their generous grants of observing time, and the Mt. Wilson and Palomar Observatories for making their facilities available to me.

I also acknowledge Dr. R. Jastrow for his hospitality at the Goddard Institute for Space Studies, and for the generous grant of computer time needed for this work I also express my gratitude to Mr. M. Pine for his work in programming the numerical solution of Schrödinger's equation for the excitation of CN, and to the systems and operations staff of Computer Applications, Inc., for

their development of an effective computing facility.

I acknowledge the Columbia University Physics Department for financial support under a NASA grant, and Mr. T. Psaropulos for his fine illustrations.

Finally, I wish to express my sincerest appreciation to my wife Maralee for typing this manuscript, and for being constantly cheerful while under the strain of the Ph. D program.

BIBLIOGRAPHY

Adams, W. S. and Dunham, T. Jr., 1937, Pub. A.A.S. 9, 5

Adams, W. S. 1941, Ap. J., 93, 11
1943, Ap. J., 97, 105
1949, Ap. J., 109, 354

Allen, C. W. 1963 Astrophysical Quantities (2nd ed. London: The Athlone Press)

Alpher, R. A. and Herman, R. 1948, Nature 16, 2776
1950, Rev. Mod. Phys, 22, 153

Alpher, R. A., Herman, R., and Gamow, G. 1967, Proc. Nat'l Acad. Sci, 58, 2179

Altchuler, S. 1957, Phys. Rev., 107, 114

Arpigney, C. 1964, Ann. d'Ap., 27, 393

Bates, D. R. and Spitzer, L. Jr. 1951, Ap. J., 113, 441

Bell, R. P. and Coop, I. E. 1938, Trans. Faraday So., 34, 1209

Bennett, R. G. and Dalby, F. W. 1962, J. Chem, Phys., 36, 399

Bethe, H. A. and Salpeter, E. E. 1957 Handbuch der Physik (S. Flugge ed., Berlin: Springer Verlag 35 pt. 1)

Blaauw, A. 1952, B.A.N., 11, 459 No. 436

Bortolot, V. B. Jr., , Clauser, J. F., and Thaddeus, P., 1969, Phys. Rev. Letters, 22, 310

Bortolot, V. B. Jr., and Thaddeus, P. 1969, Ap. J., 155, L17

Boynton, P. E., Stokes, R. A., and Wilkinson, D. T. 1968, Phys. Rev. Letters, 21, 462

Burbidge, E. M., Burbidge, G. R., Fowler, W. A., and Hoyle, F. 1957, Rev. Mod. Phys., 29, 547

Cameron, A. G. W., 1969, private communcation

Carroll, P. K. 1956, Can. J. Phys., 34, 83

Caughlin, G. R. 1965, Ap. J. 141, 688

Cheng, D. K. 1961 Analysis of Linear Systems (Reading, Mass.: Addison Wesley Publishing Company, Inc.)

Clauser, J. F. and Thaddeus, P. 1969 Proceedings of the Third International Conference on Relativistic Astrophysics, (New York: Gordon & Breach)

Condon, E. U. and Shortley, G. C. 1951, The Theory of Atomic Spectra (Cambridge: Cambridge University Press)

Connes, P., Connes, J., Kaplan, L. D., and Benedict, W. S. 1968, Ap. J. 152, 731

Condon, E. U. and Shortley, G. C. 1951, The Theory of Atomic Spectra (Cambridge: Cambridge University Press)

Davenport, W. B. and Root, W. L. 1958, An Introduction to the Theory of Random Signals and Noise (New York: McGraw Hill Book Company Inc.

Dicke, R. H., Peebles, P. J. E., Roll, P. G., and Wilkinson, D. T. 1965, Ap. J., 142, 414

Dieter, N. H. and Goss, M. 1966, Rev. Mod. Phys., 38, 256

Douglas, A. E. and Herzberg, G. 1941, Ap. J. 94, 381
1942, Can. J. Res., 20A, 71

Douglas, A. E. and Routley, P. M. 1954, Ap. J., 119, 303
1955, Ap. J. Suppl. No. 9, 1, 295

Douglas, A. E. 1968, private communication

Doroshkevich, A. G. and Novikov, I. D. 1964, Dokl. Akad. Nauk. SSSR 154, 809 [English translation: Soviet Physics "Doklady" 9, 11(1964)]

Dunham, T. Jr. 1941, Pub. A. A. S. 10, 123

Edmonds, A. R. 1968, Angular Momentum in Quantum Mechanics (2nd ed; Princeton: Princeton University Press)

Ewing, M. S., Burke, B. F., and Staelin, D. H. 1967, Phys. Rev. Letters, 19, 1251

Fellgett, P. 1953 J. O. S. A. 43, 271

Fermi, E. and Turkevich, A. unpublished - see Alpher and Herman (1950)

Field, G. B., and Hitchcock, J. L. 1966a, Phys. Rev. Letters, 16, 817
1966b, Ap. J., 146, 1

Findlay, J. W. 1963, Sky and Telescope 25, 68

Fowler, W. A., Greenstein, J. L., and Hoyle, F. 1961, Geo. Phys. J., 6, 148

Friedman, A. 1922, Z. Physik, 10, 377
1924, Z. Physik, 21, 326

Gamow, G. 1948, Nature, 162, 680
1949, Rev. Mod, Phys., 21, 367
1953, Vistas, in Astronomy (A. Beer, editor, London: Pergamon Press, 2, 1726)

Gerò, L. I. 1941, Zts. f. Phys., 118, 27

Goetz, A., and Gould, J. 1937, J. Soc. Motion Picture Engrs. 29, 510

Gordon, R. G. 1966, J. Chem, Phys., 44, 3083

Grenander, U. 1950 Arkiv for Matematik 1, 195

Gröbner, W. and Hofreiter, N. 1958, Integraltafel (Vienna: Springer-Verlag)

Heiles, C. 1967, Ap. J. Suppl. No. 136, 15, 97

Heitler, W. 1954, The Quantum Theory of Radiation (3rd. ed., London: Oxford University Press)

Herbig, G. H. 1966, Zts. f. Ap. 64, 512
1968a, Zts. f. Ap., 68, 243
1968b, Contributions from the Lick Observatory No. 239

Herman, R. and Wallis, R. F. 1955, J. Chem. Phys., 23, 637

Herzberg, G. 1959, Spectra of Diatomic Molecules, (2nd ed:, New York: D. Van Nostrand Co., Inc.)

Hildebrand, F. B. 1956, Introduction to Numerical Analysis (New York: McGraw Hill Book Company Inc.)

Hill, E. and Van Vleck, J. H. 1928, Phys. Rev., 32, 250

Hickok, F. R. and Morton, D. C. 1968, Ap. J., 152, 203

Howell, T. F. and Shakeshaft, J. R. 1966, Nature, 210, 1318
1967, Nature, 216, 753

Huang, B. and Giddens, D. P. 1968, J. of Math. and Phys., 47, 213

Huo, W. 1967, private communication

Jenkins, F. A. and Wooldridge, D. E., 1938, Phys. Rev., 53, 137

Jeunehomme, M. 1965, J. Chem. Phys., 42, 4086

Ladenburg, R. von 1930, Zts. f. Phys., 65, 200

Lambert, D. L. and Mallia, E. A. 1968, Ap. Letters, 1, 85

Lighthill, M. J. 1959, Introduction to Fourier Analysis and Generalized Funcations (Cambridge: Cambridge University Press)

Low, F. J. and Tucker, W. H. 1968, Phys. Rev. Letters, 21, 1538

Massey, H. S. W. 1932, Proc. Camb. Phil. Soc., 28, 99

Margenau, H. 1939, Rev. Mod. Phys. 11, 1

McKellar, A. 1940, Pub. A. S. P., 52, 187
1941, Pub. Dominion Ap. Obs., 7, 251

Merrill, P. W. 1942, Ap. J., 95, 268
1946, Pub. A. S. P., 58, 354

Middlehurst, B. M. and Aller, L. H. 1968 Vol VII of Stars and Stellar Systems: Nebulae and Interstellar Matter (Chicago: University of Chicago Press)

Mittleman, M. H. and von Holdt, R. E. 1965, Phys. Rev., 140, A726

Münch, G. 1957, Ap. J. 57, 42
1964, Ap. J., 140, 107

Ohm, E. A. 1961, Bell System Tech, J., 40, 1065

Oppenheimer, R. J. 1926, Proc. Camb. Phil. Soc., 23, 327

Partridge, R. B. and Peebles, P. J. E. 1967, Ap. J., 148, 377

Penzias, A. A. and Wilson, R. W. 1965, Ap. J., 142, 949

Peebles, P. J. E. 1966, Ap. J. 146, 542
1968, Ap. J. 153, 1

Phelps, P. H. and Dalby, F. W. 1966, Phys. Rev. Letters 16, 3

Poletto, G. and Rigutti, M. 1965, Nuovo Cimento, 34, 519

Pottasch, S. R. 1968, B. A. N., 19, 469

Puzanov, V. I., Salomonovich, A. E. and Stankevich, K. S. 1967, Astr. Zh, 44, 1219 [English translation: Soviet Astronomy, A. J. 11, 905 (1968)]

Rank, D. H., Eastman, D. P., Rao, B. S. and Wiggins, T. A. 1963, J. Mol. Spect. 10, 34

Riegel, K. W. 1967, Ap. J., 148, 87

Roll, P. G. and Wilkinson, D. T. 1966, Phys. Rev. Letters, 16, 405

Schiff, L. I. 1955 Quantum Mechanics (New York: McGraw Hill Book Company, Inc.)

Shalloway, A. M. 1964, The NEREM Record

Shklovsky, I. S. 1966, Astron. Circular No. 364, Acad. Sciences USSR

Shivananden, K. G., Houck, J. R. and Harwit, M. O. 1968, Phys. Rev. Letters, 21, 1460

Shuter, W. L. H., Venugopal, V. R., and Mahoney, M. J. 1968, Nature, 220, 356

Spitzer, L. Jr. 1948, Ap. J., 108, 276

Spitzer, L. Jr. and Tomasko, M. G. 1968, Ap. J., 152, 971

Stokes, R. A., Partridge, R. B., and Wilkinson, D. T. 1967, Phys. Rev. Letters, 19, 1199

Strömgren, D. 1939, Ap. J. 89, 526
1948, Ap. J. 108, 242

Swings, P. and Rosenfeld, L. 1937, Ap. J., 86, 483

Thackery, A. D. 1961 Astronomical Spectroscopy (New York: The Macmillan Co.)

Thaddeus, P. and Clauser, J. F. 1966, Phys. Rev. Letters, 16, 819

Thomson, R. and Dalby, F. W. 1968, Can. J. Phys. 46, 2815

Tolman, R. C. 1938, Principles of Statistical Mechanics (London: Oxford University Press)

Townes, C. H. and Schalow, A. L. 1955 Microwave Spectroscopy (New York: McGraw Hill Book Company, Inc.)

Van Vleck, J. H. and Middleton, D. 1946, J. Appl. Phys., 17, 940

Van Vleck, J. H. 1951, Rev. Mod. Phys., 23, 213

Von Mises, R. 1964 Mathematical Theory of Probability and Statistics (New York: Academic Press)

Wagoner, R. W., Fowler, W. A., and Hoyle, F. 1967, Ap. J. 148, 3

Welch, W. J., Keachie, S., Thornton, D. D., and Wrixton, G., Phys. Rev. Letters, 18, 1068

Westphal, J. A. 1965, Ap. J., 142, 1661

Wilkinson, D. T. 1967, Phys. Rev. Letters, 19, 1195

Wilson, D. C. 1948, Pub. A.S. P., 60, 198

Winther, A. and deBoer, J. 1965 California Institute of Technology, Technical Reprint, reprinted in Coulomb Excitation (K. Alder and A. Winther editors, New York, 1966: Academic Press)

Zadeh, L. A. and Ragazzini, J. R. 1952, Proc. I. R. E., 40, 1223

Zimmerman, H. 1964, Astron. Nach. 288, 95

TABLE 1

IMPORTANT RESONANCE TRANSITIONS OF INTERSTELLAR MOLECULES

Molecule	Optical Transitions: Electronic Ground State levels	Lines Originating in that	Excited State levels	λ air (A°)	Observed Intensity Ratio		s	Microwave Transitions: Allowed Transitions within ground state	λ (mm)
CN	$(X^2\Sigma^+)$		$(B^2\Sigma^+)$						
	J = 0	R(0)	J = 1	3874.608[a]					
	J = 1	R(1)	J = 2	3873.998	R(1)/R(0)		*2	J=0 - J=1	2.644
		P(1)	J = 0	3875.764	P(1)/R(0)		1		
	J = 2	R(2)	J = 3	3873.369	R(2)/R(1)		*3/2	J=1 - J=2	1.322
		P(2)	J = 1	3876.312	P(2)/R(1)		1		
CH	$(X^2\Pi)$		$(A^2\Delta)$						
	KJ=1 1/2	$R_2(1)$	KJ=2 3/2	4300.321[b]					
	KJ=1 3/2	$R_1(1)$	KJ=2 5/2	4303.948	$R_1(1)/R_2(1)$	(9/5)[d]	*1.525	KJ=1 1/2 - KJ=1 3/2	0.560
		$^{R}Q_{12}(1)$	KJ=2 3/2	4303.621	$^{R}Q_{12}(1)/R_2(1)$	(1/5)	.392		
		$^{S}R_{21}(1)$	KJ=3 5/2	4287.620	$^{S}R_{21}(1)/R_2(1)$	(0)	.083		
	KJ=2 3/2	$R_2(2)$	KJ=3 5/2	4296.636	$R_2(2)/R_1(1)$	(20/27)	*.820	KJ=1 1/2 - KJ=2 3/2	0.150
		$Q_2(2)$	KJ=2 3/2	4312.705	$Q_2(2)/R_1(1)$	(1/3)	.267		
		$^{Q}R_{12}(2)$	KJ=2 5/2	4313.027	$^{Q}R_{12}(2)/R_1(1)$	(1/27)	.0224		
CH^+	$(X^1\Sigma^+)$		$(A^1\Pi)$						
	J = 0	R(0)	J = 1	4232.535[c]					
	J = 1	R(1)	J = 2	4229.336	R(1)/R(0)		* 3/2	J=0 - J=1	0.359
		Q(1)	J = 1	4237 555	Q(1)/R(0)		3/2		

[a] Jenkins and Wooldridge (1938)

[b] Gerö (1941)

[c] Douglas and Herzberg (1942)

[d] Hund's case (b)

TABLE 2

MOLECULAR CONSTANTS

	CN	CH	CH+
B (cm^{-1})	1.8909[a]	14.457[c]	13.9318[c]
A (cm^{-1})	---	27.95[c]	---
μ (D)	1.45 ±.08[b]	1.46 ± 0.06[d]	

[a] Poletto and Rigutti (1965)

[b] Thomson and Dalby (1968); note that μ = 1.1D (Arpigney, 1964) was used for the calcuations of Chapter 8.

[c] Herzberg (1950) Table 39

[d] Phelps and Dalby (1966)

TABLE 3

DATA ON PLATES USED IN NUMERICAL SYNTHESIS

Star	Plate No	Date	GCT(beg)	Exposure (minutes)	Slit Width	Emulsion	Camera (Grating)	Spectral Width	Seeing	Observer	Fraction of Synthesis (%) CN	CH	CH+
ξ Oph	Ce2313	5/13/40	10 55	240	6	E-33	114"	1 0	2-3	A	0 0	3 1	4 0
	Ce2317	5/14/40	10.31	270	6	Cr Cont	114"	0 5	3-2	A	0 0	4 1	16 0
	Ce2328	6/15/40	7 39	360	6	Cr Cont,	114"	0 7	1-2-3	A	5 5	0 0	0 0
	Ce2334	6/17/40	7 45	245	5 1/2	Cr Cont	114"	0 5	3-4	A	8 0	0 0	0 0
	Ce2381	7/26/40	9:08	127	6	Cr Cont	114"	0 8	3-2	D	28 9	23 6	1 0
	Ce2414	9/13/40	8 03	50	7	Cr Cont	114"	0 5	2	D	0 0	10 3	1 9
	Ce2495a	1/17/41	16 48	18	7	Cr Cont	114"	0 2	3	D	0 5	0 0	0 1
	Ce2495b	1/17/41	17 06	44	7	Cr Cont	114"	0 2	3	D	1 7	0 0	1 4
	Ce2516b	3/16/41	15:19	10	7	Cr Cont.	114"	0 2	3	D	0 0	0 2	0 0
	Ce2516c	3/16/41	15 29	48	7	Cr Cont	114"	0 2	3	D	7 3	1 7	4 9
	Ce2522	3/17/41	13 04	63	7	Cr Cont	114"	0 3	3	D	1 4	3 0	0 0
	Ce2538	4/16/41	11 42	106	8	Cr S C	114"	0 3	4-1	D	0 0	4 6	3 6
	Ce2542	4/21/41	10 09	365	6	Baked Process	114"	0 7	3-1	A	5 2	12.7	0 0
	Ce2569b	5/11/41	11:26	30	8	Exp 144-0 164,503	114"	0.2	2	D	3 3	0 0	0 0
	Ce2573	5/27/41	9 59	342	6	Cr. Cont	114"	0 7	2	A	0 6	4 7	2.3
	Ce2578	6/ 4/41	8:16	360	6	Cr. Cont.	114"	0 5	4-2	A	3 1	4 4	2.9
	Ce2581	6/ 5/41	8 50	332	6 1/2	Cr Cont.	114"	0 5	4-1	A	3 1	0 0	0 0
	Ce2582	7/ 4/41	7 39	231	6	Cr Cont	114"	0 3	6-5	A	4 1	14 7	21 2
	Ce3847	6/24/45	7:45	35	91	103-0	114"	0 8	2-3	A	1 6	0 0	2 8
	$EC28_1$	3/15/60					160"			H	4 4	0 0	0 0
	$EC28_2$	3/15/60					160"			H	3 2	0 0	0 0
	$EC38_1$	3/18/60					160"			H	0 0	4 1	1 7
	$EC38_2$	3/18/60					160"			H	0 0	6 1	18 3
	$EC55_1$	4/16/60					160"			H	0 9	0 0	0 0
	$EC55_2$	4/16/60					160"			H	1 5	0 0	0 0
	EC220	8/ 8/60					160"			H	2 1	0 0	0 0
	$EC162_1$	7/ 4/60					160"			H	4 1	0 0	5 4
	$EC162_2$	7/ 4/60					160"			H	3 7	0 0	4 1
	EC1890						160"			H	0 3	0.0	0 0
	EC1969	6/12/63					160"			H	5 5	3 1	8 4
ζ Per	Ce2432	10/13/40	10 57	50	96 5	Cr H S	114"	0 7	4	A	5 3		
	Ce2480a	12/20/40	7:15	40	7	Cr Cont	114"	0.2	3	D	17.3		
	Ce2480b	12/20/40	7 55	30	7	Cr Cont	114"	0 2	3	D	10 1		
	Ce2480c	12/20/40	8 25	20	7	Cr Cont	114"	0.2	3	D	1 5		
	Ce2481	12/20/40	9 33	150	7	3J + Am	114"	0 2	2	D	3 0		
	Ce2492a	1/17/41	8 18	36	7	Cr Cont	114"	0.3	4	D	41 2		
	Ce2492b	1/17/41	8 54	20	7	Cr. Cont.	114"	0 3	4	D	21 4		
55 Cyg	Ce2378	7/24/40	11 20	290	6	E-33	114"	0.5	3	D	59 0		
	Ce2390	8/18/40	10 07	378	9	Cr. Cont.	73"		3	D	30 0		
	Ce13793	8/18/60					73"			H E B	11 0		
AE Aur	Ce1281	12/ 6/36	9:22	150	91.5	III-F+Tri	32"		4-3	M	33 0		
	Ce3658	12/ 6/44	10.04	110	91.5	103-0Bak'd	114"		5	A	10 0		
	Ce9719	3/ 5/55	7 33	51	114	IIa-0	32"		2-3	Sl	57 0		
20Aql	Ce3554	9/ 4/44	8 21	90	92	103-0	114"	0 5	3-4	A	100 0		
X Per	Ce1534	10/22/37	13 40	90	12	E-33	32"		5	Sa	20 0		
	Ce2867	9/24/42					114"	0 3		A	80 0		
BD+ 66°1675	PC6056	8/ 1/61	13 03	167	2/40	IIa-0Baked	36"		2-3	Mu	78 0		
	PC6131	8/31/61	12 12	180	4/23	IIa-0Baked	36"		3	Mu	22. 0		
BD+ 66°1674	PC7520	9/ 5/63	9 32	200	2/50	IIa-0Baked	36"		2-3	Mu	46 0		
	PC9091	12/2&3/65	6 15& 6 05	359& 319	2/45	IIa-0Baked	36"		4 & 1-2	Mu	54 0		

Ce = Mt Wilson 100-inch, PC = Mt. Palomar 200-inch, EC = Lick 120-inch

TABLE 4

Star	v	MK Type	b^{II} (°)	ℓ^{II} (°)	b (Km/sec)	Mol/ Atom	Line	Equivalent Width(mÅ)[j]	τ^{j}	$\Delta\tau^{h}$	T(°K)[k]	v(Km/sec)[j]
ζ Oph	2 56	09 5v	+23 6	6 3		HI	21cm					-12 7[4]
					1 54[e]	CAII	K					-29 0[e][0 3/6]
					61[e]	CN	R(0)	6 62 ± 29	572 ± 032			-14 8[e][0 4/6]
						CN	R(1)	2 06 ± 29	155 ± 024	20	2 72 ± 22	-13 8[e][1 0/4]
						CN	P(1)	1 12 ± 29	082 ± 022	25	2 81 ± 31	-14 9[e][1 1/3]
						CN	R(2)	(0) < 44	(0) < 032	10	(0) < 5 49	
						CH	$R_2(1)$	13 40 ± 03	1 50 ± 03			-14 6[e][0 45]
						CH	$R_1(1)$	(11) < 53	(008) < 039	71	(4 54) < 6 33	
						CH	$R_2(2)$	(11) < 53	(008) < 039	1 8	(19 4) < 28 5	
						CH^+	R(0)	19 60 ± 08				-14 0[e][0 7/6]
						CH^+	R(1)	(14) < 72	(009) < 048	1 07	(6 86) < 9 01	
						$C^{13}H^+$	R(0)	60 ± 31	044^{+023}_{-013}	$C^{12}/C^{13} = 62^{+100}_{-22}$		
ξ Per	2 83	B1Ib	-16 7	162 3	61	HI	21cm					13 4[2]
						CN	R(0)	9 12 ± 57	$859^{+.079}_{-.070}$			12 3[1 3/2]
						CN	R(1)	3 02 ± 57	234 ± 049	30	2 72 ± 30	
						CN	P(1)	1 24 ± 57	092 ± 044	30	2.43 ± 54	
						CN	R(2)	(44) < 1 23	(032) < 091	29	(4 55) < 8 05	
						CH&CH+						13 8[f][7]
						CAII	H&K					13 5[f]
55 Cyg	4 83		B3Ia	85 7	1 0	CN	R(0)	6 6 ± 3.0	32 ± 16			
						CN	R(1)	(2 08) < 4 05	(09) < 23	14	(2 8) < 5 5	
AE Aur	5 30	08 5v	- 2 3	172.1	1.0	HI	21cm					2 5, 11 5(broad)
						CH&CH+						15 7[f][6]
						CAII	H&K					14 5[f]
						CN	R(0)	5 90 ±2.90	28 ± 15			
						CN	R(1)	2.67 ±2.57	12 ± .11	.2	3 5 ±2.3	
20 Aql	5 37	B3Iv	- 8.3	28 2	1 0	HI	21cm					-11 5, -2 0
						CA	K					-22 7[f], -12 1[f]
						CH&CH+						-13 4[f][3]
						CN	R(0)	22 9 ±8.0	$1\ 64^{+1\ 40}_{-.78}$			-12.2, -2.8[1 2/3]
						CN	R(1)	7 6 ±7.2	$38^{+.53}_{-.35}$	5	$2\ 5^{+1\ 8}_{-1\ 5}$	
HD 11953	5.68	AIIa	- 3 0	132 9		CN	R(1)				3 7 ± 7[c]	
HD 208501	5 79	B8Ib	1 7	100.4		CN	R(1)				2 8 ± 4[d]	
X Per	6 08		-17 1	163 1	1 0	HI	21cm					13 3, 22 8[1]
						CAII	H&K					15 4[f]
						CN	R(0)	18 4 ±3 1	$1\ 15^{+\ 33}_{-\ 26}$			13 5, 23 2[1]
						CN	R(1)	6 8 ±3 1	34 ± 15	.4	2 8 ± 8	
						CH&CH+						-15 2[f][6]
HD 26571	6, 10	B 8 II-III	-20 6	172 4		CN	R(1)				~ 3[a]	
BD+ 66° 1675[h]	9, 05	07	+ 4 8	118 0	5	HI	21cm					-14 2, -19 5[1]
						CAII	K					-15 1[g][2/2]
						CH	$R_2(1)$					-21 3[g][7/2]
						CN	R(0)	125 5 ± 14 0	1 95 ± 47			-17 2[g][1 0/1 5]
						CN	R(1)	39 6 ± 14 0	40 ± 16	56	2 39 ± 43	
BD+ 66° 1674[l]	9 5	0	+ 4 8	118 0	5	HI	21cm					-14 2, -19.5[1]
						CAII	K					-17 9[g][7/2]
						CH	$R_2(1)$					-17 6[g][1]
						CN	R(0)	55 9 ±7 3	60 ± 10			-17 4[g][1]
						CN	R(1)	13 8 ±7.3	.13 ± 07	.15	2 45 ± 63	

NOTES TO TABLE 4

[a] G. Herbig, Lick 120-inch Coude, private communcation

[b] From spectra taken by G. Munch (1964) with 200-inch Coude

[c] M. Peimbert, 120-inch Coude, private communication

[d] V. Bortolot Jr. and P. Thaddeus, 120-inch Coude, private communication

[e] Measured by G. Herbig (1968a)

[f] Measured by W. S. Adams (1949) reduced to the wavelength standards used by Herbig (1968a), Münch (1957)

[g] Measured by G. Münch (1964)

[h] ΔT is the correction (decrease) for line saturation

[i] Equivalenth width, optical depth, and temperature error limit ranges correspond to 95% confidence level except when a line has not specifically been detected with this confidence level. Then the upper limit given is to 99.7% and the number in parenthesis is the most probable value.

[j] Velocity errors follow the notation of Herbig (1968a) with the first number in brackets being the standard error and the second number being the number of plates measured.

[k] For a given pair of levels i and j the temperature calculated from n_i/n_j is listed beside optical depth $\tau_{ii'}$. n_j is always calculated from the strongest line originating in level j.

Figure 1. Direct measurements of the brightness temperature T_B of the fireball radiation. These are numbered in chronological order.

	Wavelength (cm)	T_B (°K)	Investigators
(11)	73.5	3.7 ± 1.2	Howell and Shakeshaft (1967)
(12)	49.2	3.7 ± 1.2	Howell and Shakeshaft (1967)
(4)	21 0	3.2 ± 1.0	Penzias and Wilson (1967)
(3)	20.7	2.8 ± 0.6	Howell and Shakeshaft (1966)
(1)	7.35	3.5 ± 1.0	Penzias and Wilson (1965)
(2)	3.2	3.0 ± 0.5	Roll and Wilkinson (1966)
(7)	3.2	$2.69^{+0.16}_{-0.21}$	Stokes, Partridge and Wilkinson (1967)
(8)	1.58	$2.78^{+0.12}_{-0.17}$	Stokes, Partridge and Wilkinson (1967)
(5)	1.5	2.0 ± 0.8	Welch, Keachie, Thornton, and Wrixton (1967)
(9)	0.924	3.16 ± 0.26	Ewing, Burke and Staelin (1967)
(6)	0.856	$2.56^{+0.17}_{-0.22}$	Wilkinson (1967)
(10)	0.82	2.9 ± 0.7	Puzanov, Salomonovich and Stankevich (1967)
(13)	0.33	$2.46^{+0.40}_{-0.44}$	Boynton, Stokes and Wilkinson (1968)

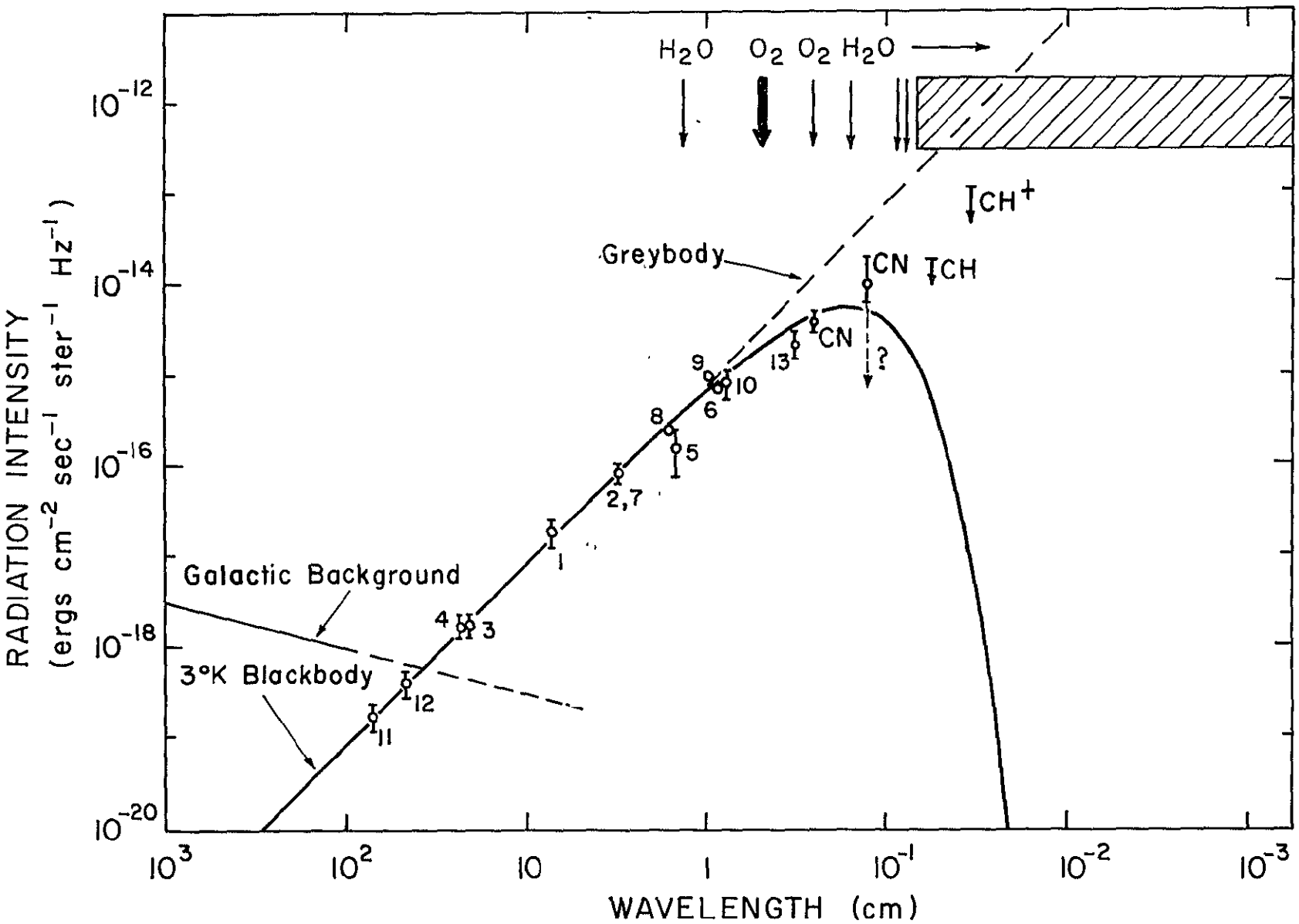
H_2O O_2 O_2 H_2O
CH+
Greybody
CN CH
CN
?
13
9
10
6
8
5
2,7
1
4
3
12
11
Galactic Background
3°K Blackbody
RADIATION INTENSITY
(ergs cm^{-2} sec^{-1} ster^{-1} Hz^{-1})
10^{-12}
10^{-14}
10^{-16}
10^{-18}
10^{-20}
10^{3}
10^{2}
10
1
10^{-1}
10^{-2}
10^{-3}
WAVELENGTH (cm)

Figure 2. Term diagram which is required for an atom or molecule to be able to be used to measure the cosmic microwave background with the techniques described here.

$\lambda_{i'i}$ and $\lambda_{j'j}$ are

mutually resolvable

optical transitions

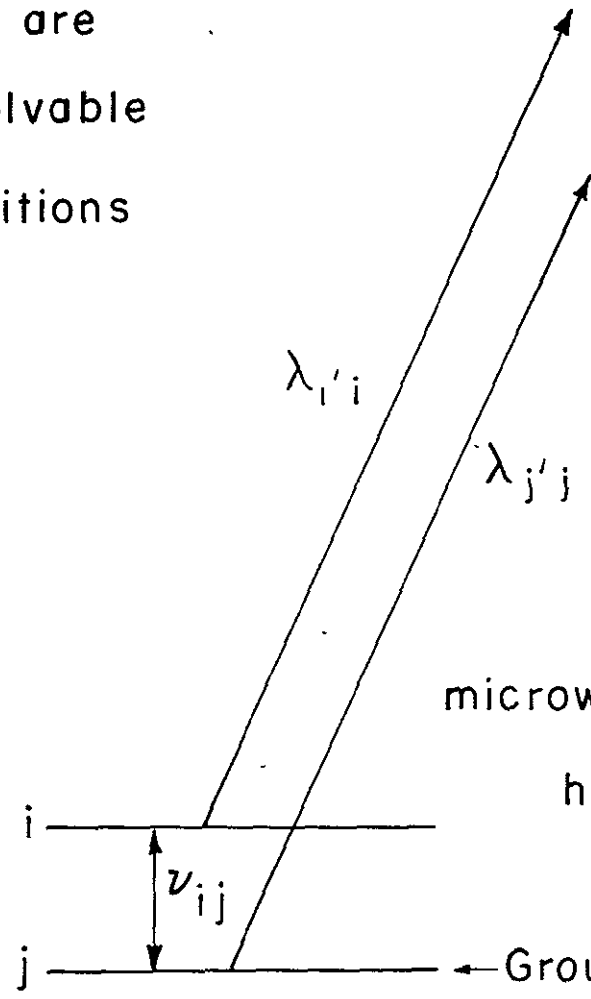

ν_{ij} is a

microwave transition with

$h\nu_{ij} \sim kT_B$

Figure 3. Partial term diagrams for molecules observed optically in the interstellar medium showing transitions which produce the strongest interstellar lines . All levels shown, in both the ground and excited electronic states, are in the ground vibrational state.

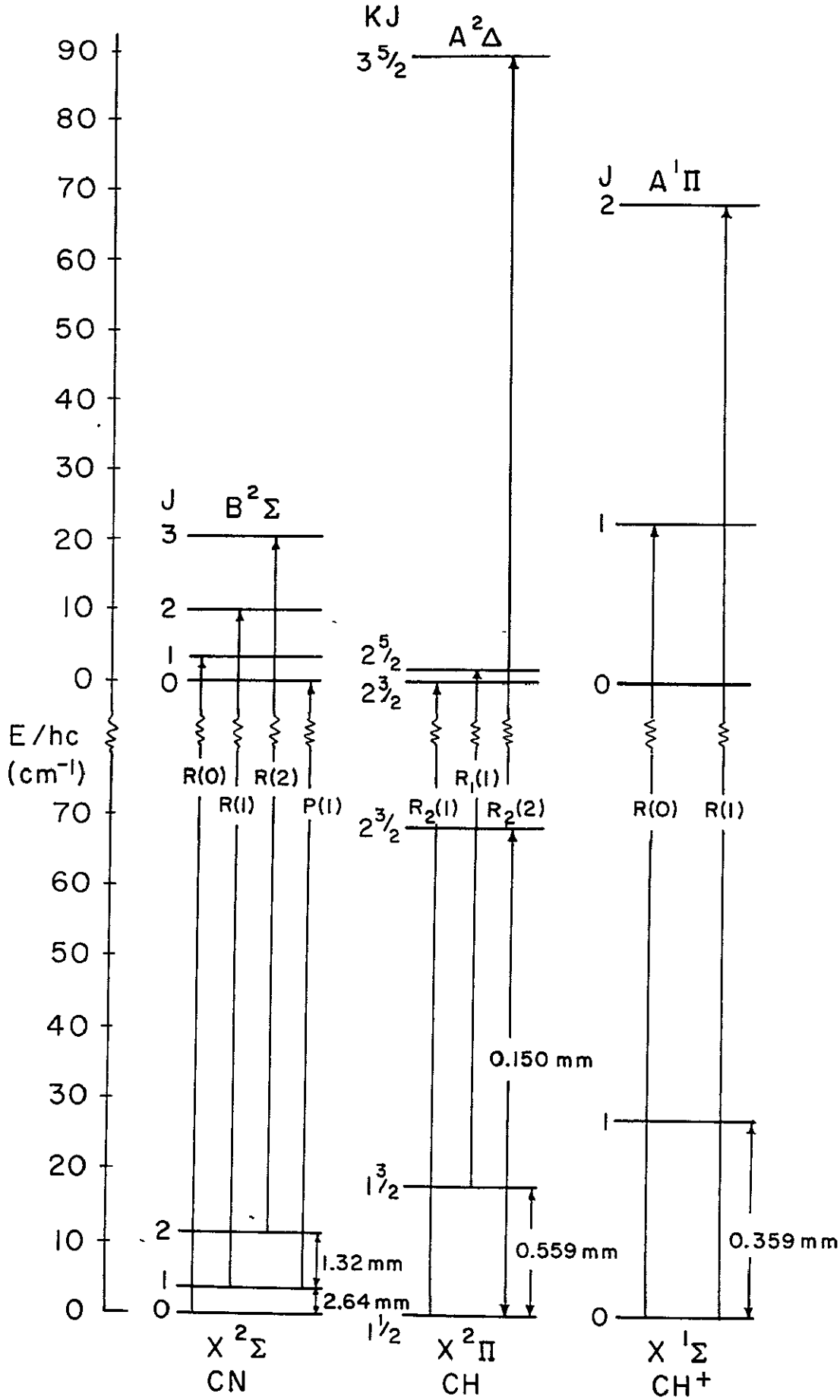
KJ
A ²Δ
3 5/2
2 5/2
2 3/2
1 3/2
1 1/2
J
B ²Σ
3
2
1
0
J
A ¹Π
2
1
0
E/hc
(cm⁻¹)
90
80
70
60
50
40
30
20
10
0
R(0)
R(1)
R(2)
P(1)
R₁(1)
R₂(1)
R₂(2)
0.150 mm
0.559 mm
1.32 mm
2.64 mm
0.359 mm
X ²Σ
CN
X ²Π
CH
X ¹Σ
CH⁺

Figure 4. Schematic diagram of equipment used for tracing plates at California Institute of Technology.

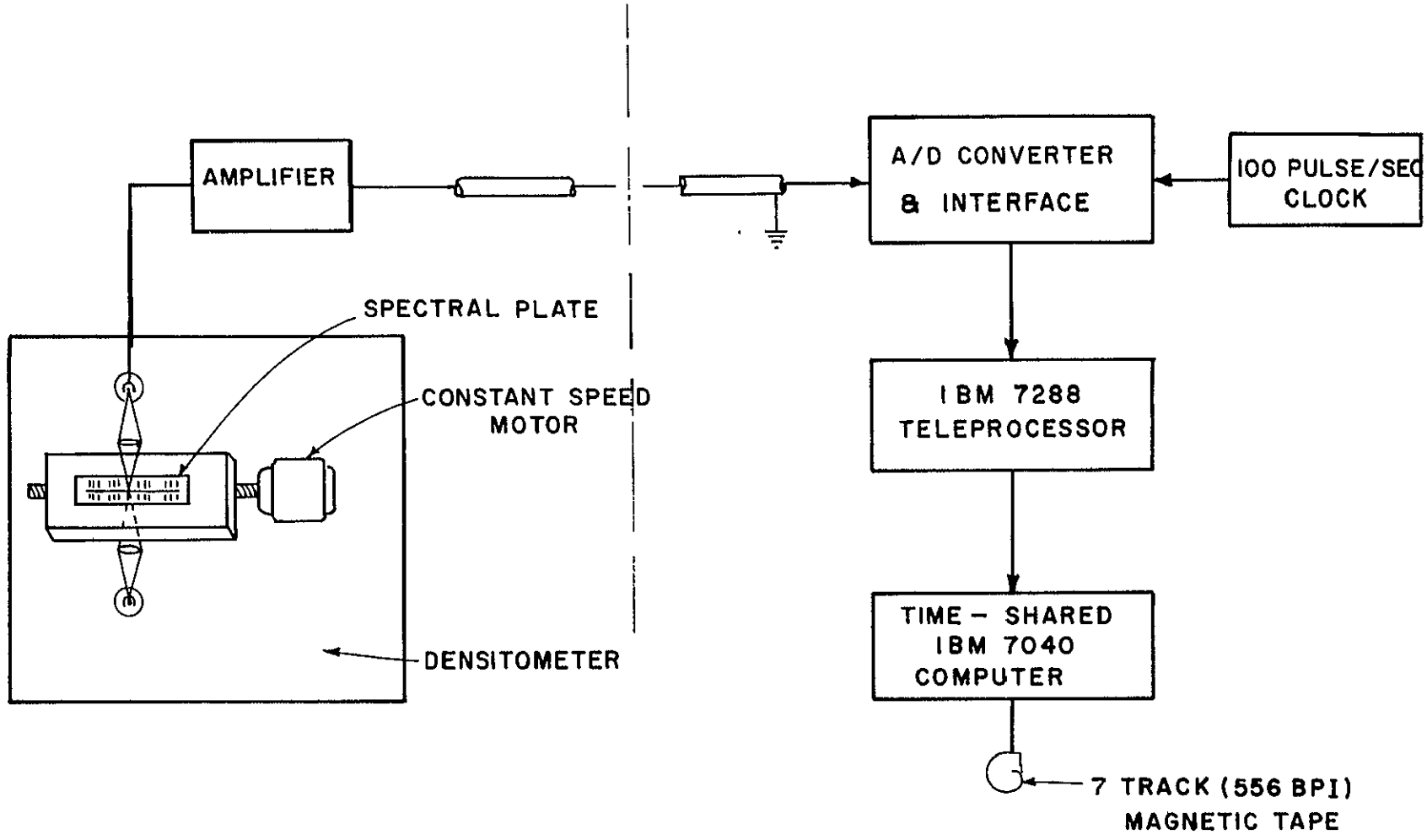
AMPLIFIER
A/D CONVERTER
& INTERFACE
100 PULSE/SEC
CLOCK
SPECTRAL PLATE
CONSTANT SPEED
MOTOR
DENSITOMETER
IBM 7288
TELEPROCESSOR
TIME – SHARED
IBM 7040
COMPUTER
7 TRACK (556 BPI)
MAGNETIC TAPE
ROBINSON LABORATORY
OF ASTROPHYSICS
WILLIS BOOTH COMPUTING
CENTER

Figure 5. Schematic diagram of the areas traced on each plate showing placement of razor blade for fiducial mark. Arrows show direction of scan and slit orientation.

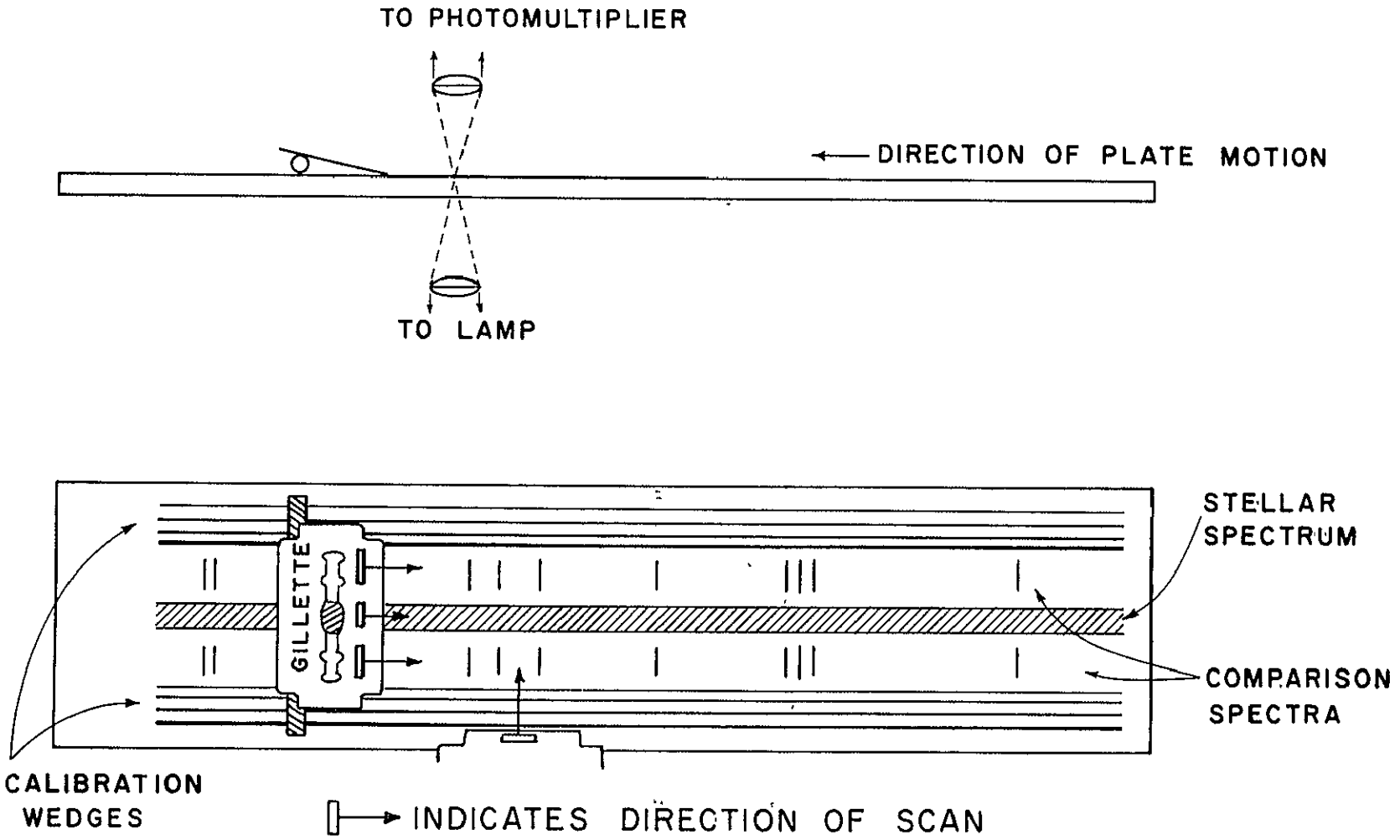
TO PHOTOMULTIPLIER
DIRECTION OF PLATE MOTION
TO LAMP
GILLETTE
STELLAR SPECTRUM
COMPARISON SPECTRA
CALIBRATION WEDGES
INDICATES DIRECTION OF SCAN

Figure 6 Wedge bars and corresponding intensities resulting from tracing plate perpendicular to stellar spectrum. Note that opposite sides of the wedge were put on at different intensities.

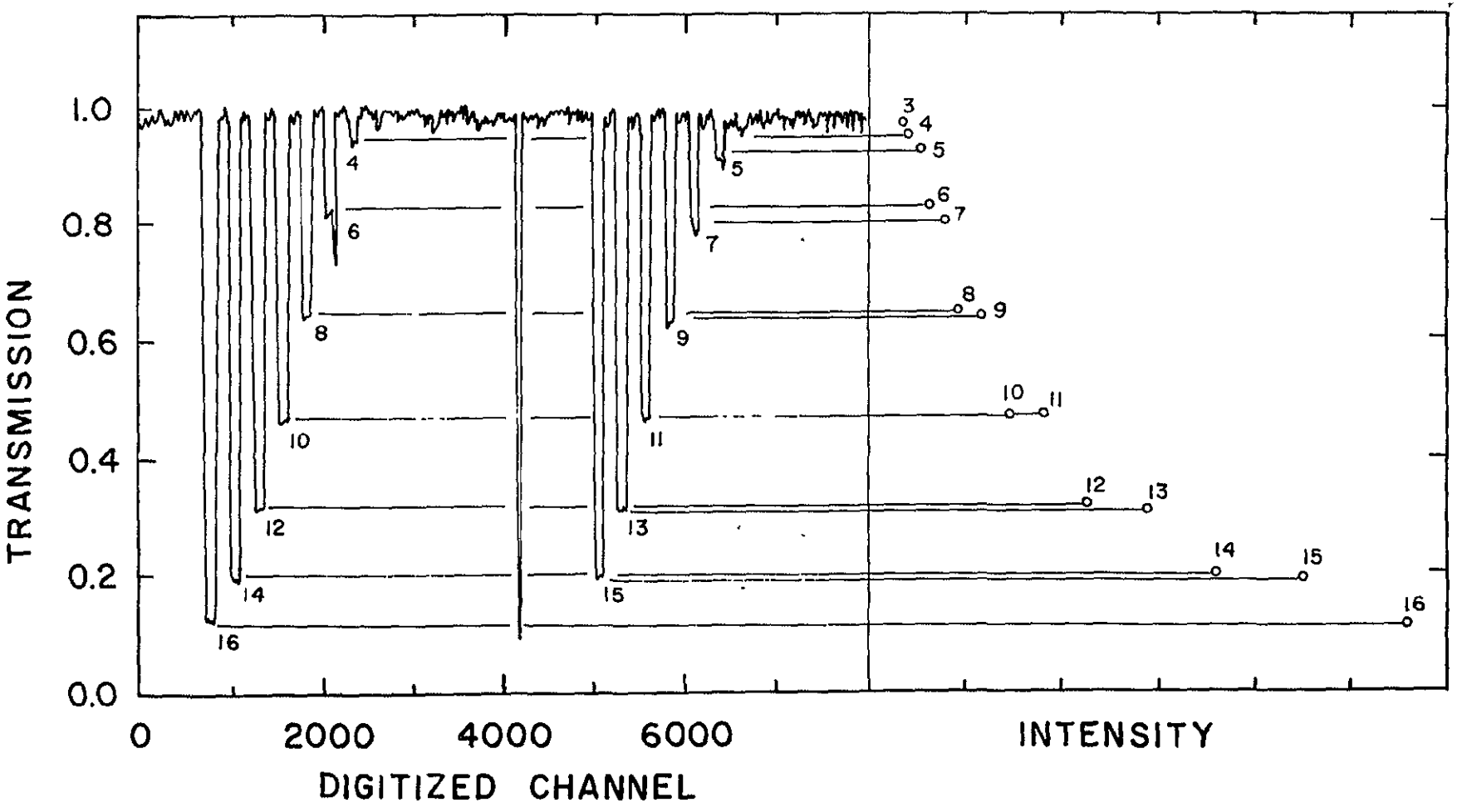
TRANSMISSION
1.0
0.8
0.6
0.4
0.2
0.0
0
2000
4000
6000
DIGITIZED CHANNEL
INTENSITY
3
4
5
6
7
8
9
10
11
12
13
14
15
16

Figure 7. Wedge after compensation for uneven intensities on opposite sides of plate. Square shows average continuum intensity.

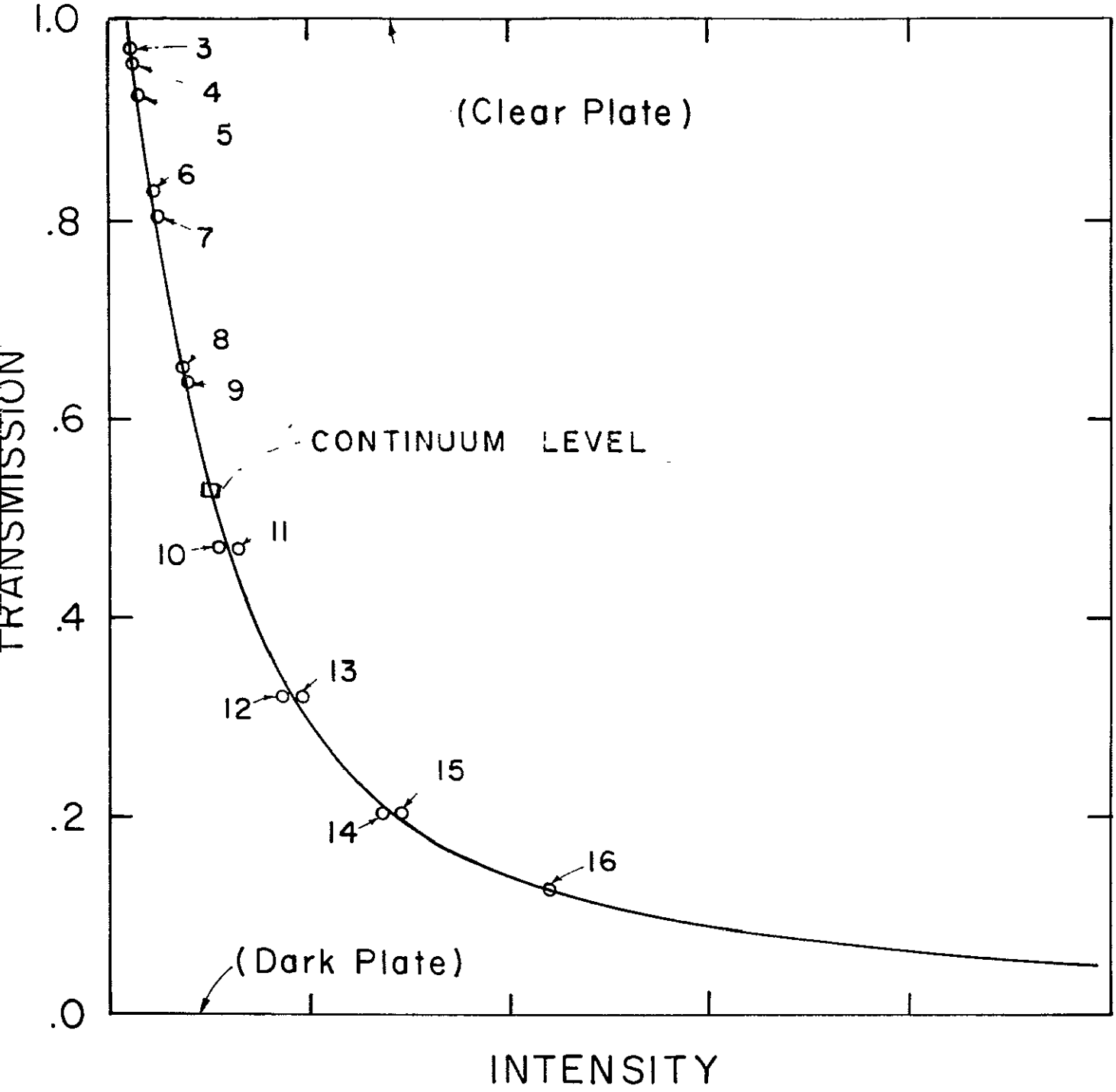
1.0
.8
.6
.4
.2
.0
TRANSMISSION
3
4
5
6
7
8
9
10
11
12
13
14
15
16
(Clear Plate)
CONTINUUM LEVEL
(Dark Plate)
INTENSITY

Figure 8. Plot of wavelength versus digitization index with least square straight line fits. Different initial wavelength resulted from fact that razor could not be placed exactly perpendicular to the stellar spectrum. Numbers refer to symbolic identifications of iron lines.

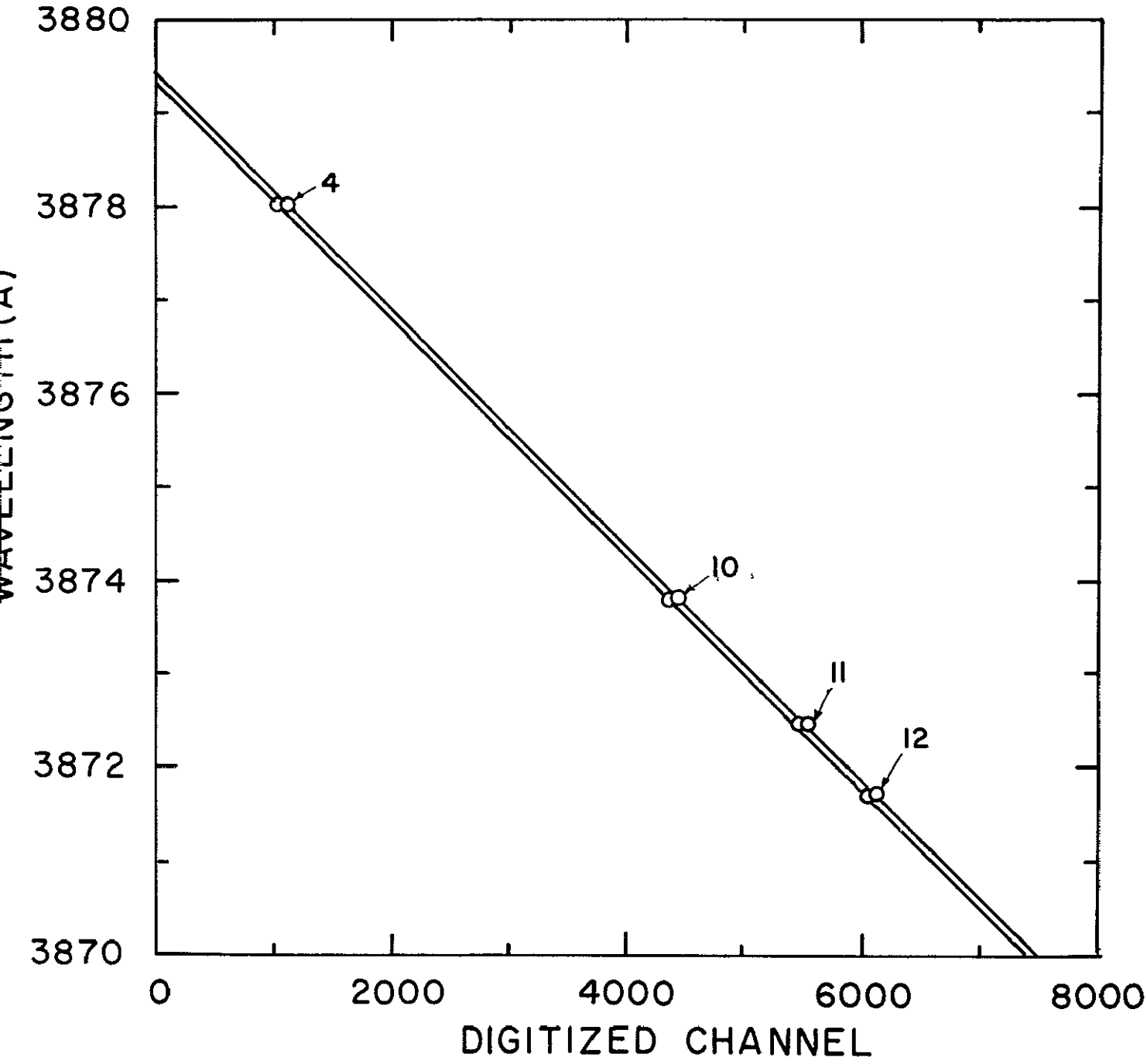
3880
3878
3876
3874
3872
3870
WAVELENGTH (A)
4
10
11
12
0
2000
4000
6000
8000
DIGITIZED CHANNEL

Figure 9. Syntheses of the spectra of several stars showing absorption of interstellar CN. All but ξ Ophiuchi and ζ Persei have been numerically filtered. Vertical magnification factor and number of spectra for each case are noted at left. Stellar lines are evident in the spectra of several of these, notably ζ Persei and 55 Cygni.

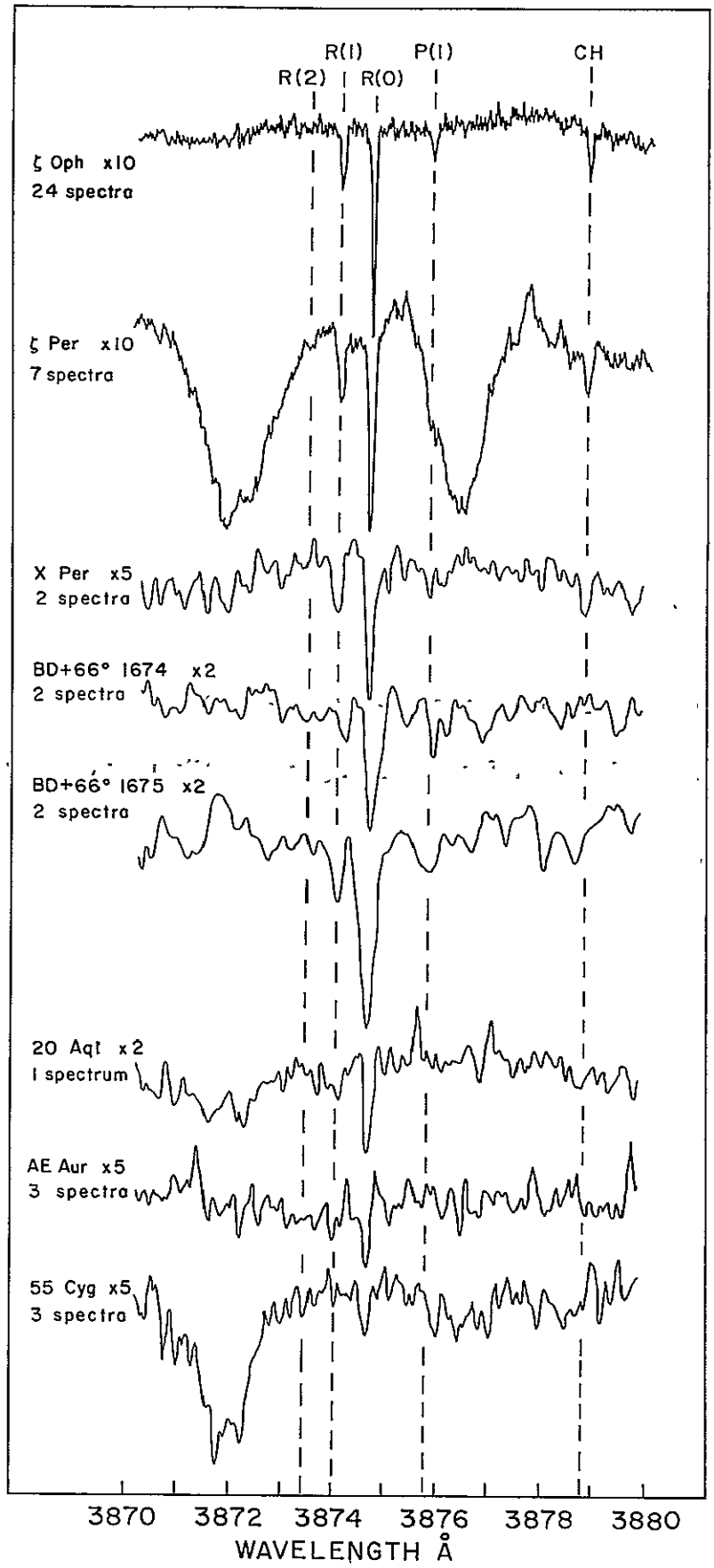
R(2)
R(1)
R(0)
P(1)
CH
ζ Oph x10
24 spectra
ζ Per x10
7 spectra
X Per x5
2 spectra
BD+66° 1674 x2
2 spectra
BD+66° 1675 x2
2 spectra
20 Aqt x2
1 spectrum
AE Aur x5
3 spectra
55 Cyg x5
3 spectra
3870
3872
3874
3876
3878
3880
WAVELENGTH Å

Figure 10. Synthesis of 17 spectra of ζ Ophiuchi showing absorption by interstellar CH. Spectrum has been filtered by a gaussian filter function of width .05 Å.

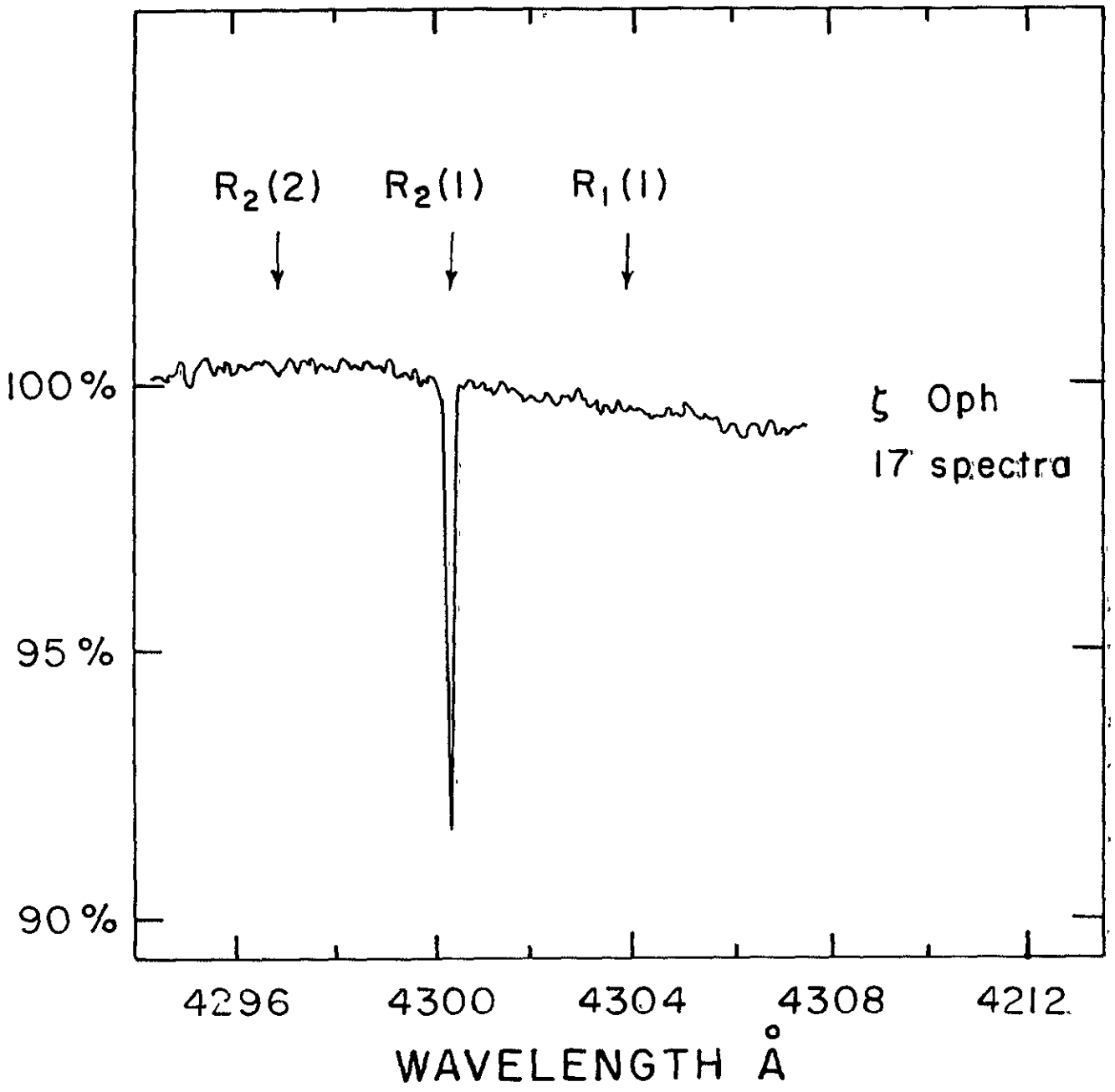
R2(2)
R2(1)
R1(1)
100%
95%
90%
ζ Oph
17 spectra
4296
4300
4304
4308
4212
WAVELENGTH Å

Figure 11. The result of adding together 19 spectra of ζ Ophiuchi showing absorption by interstellar CH+. Spectrum has been filtered by a gaussian width of .05Å. The location of the isotopically shifted R(0) line of $C^{13}H^{+}$ is also indicated.

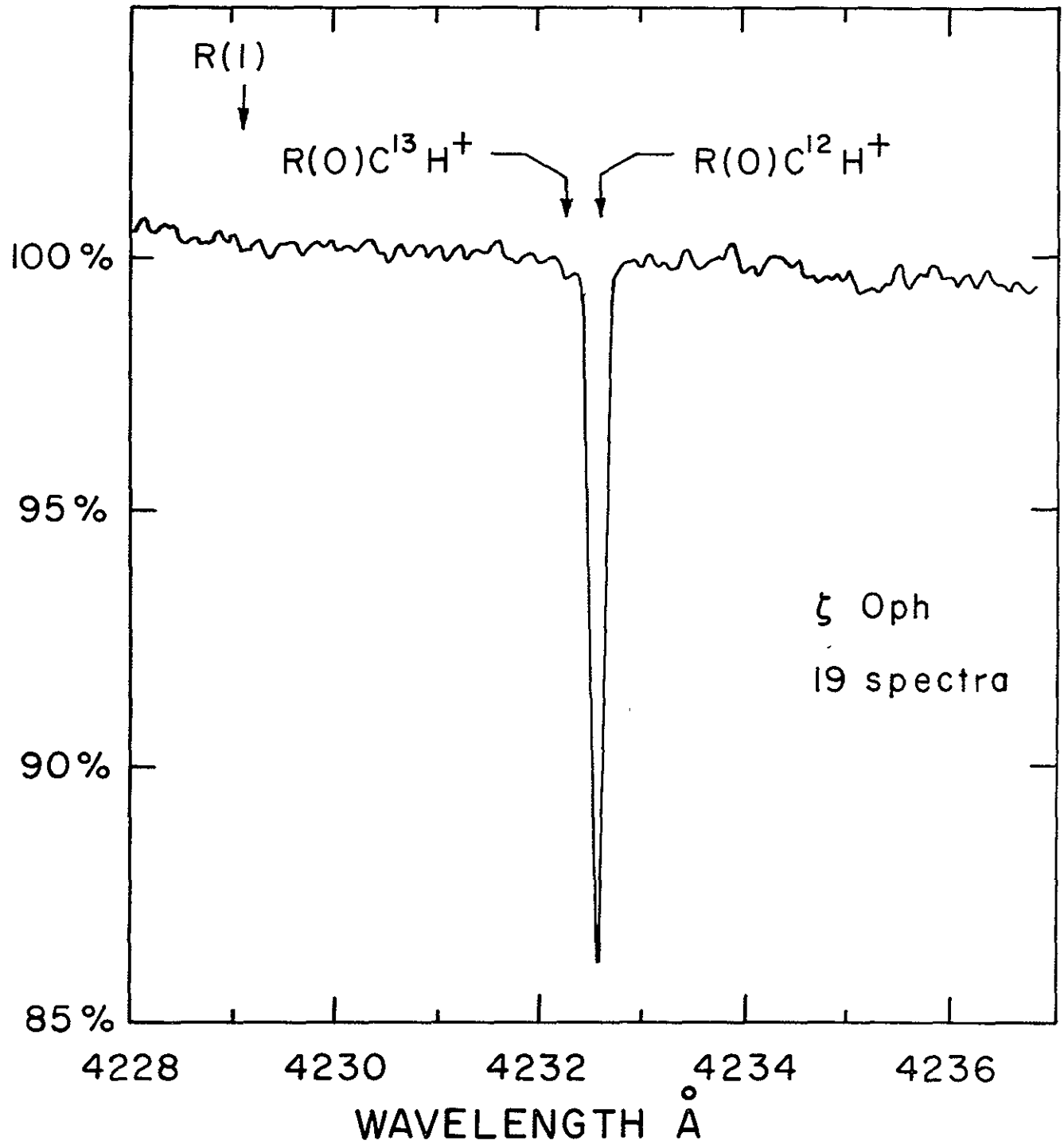
R(1)
R(0)C13H+
R(0)C12H+
100%
95%
90%
85%
ζ Oph
19 spectra
4228
4230
4232
4234
4236
WAVELENGTH Å

Figure 12. Limits on the intensity of radiation in the interstellar medium set by this work (M W) and by further observations by Bortolot et al (1969 - L). The area under the line AA' represents the flux 5×10^{-9} W cm^{-2} ster^{-1} observed by Shivananden et al (1968).

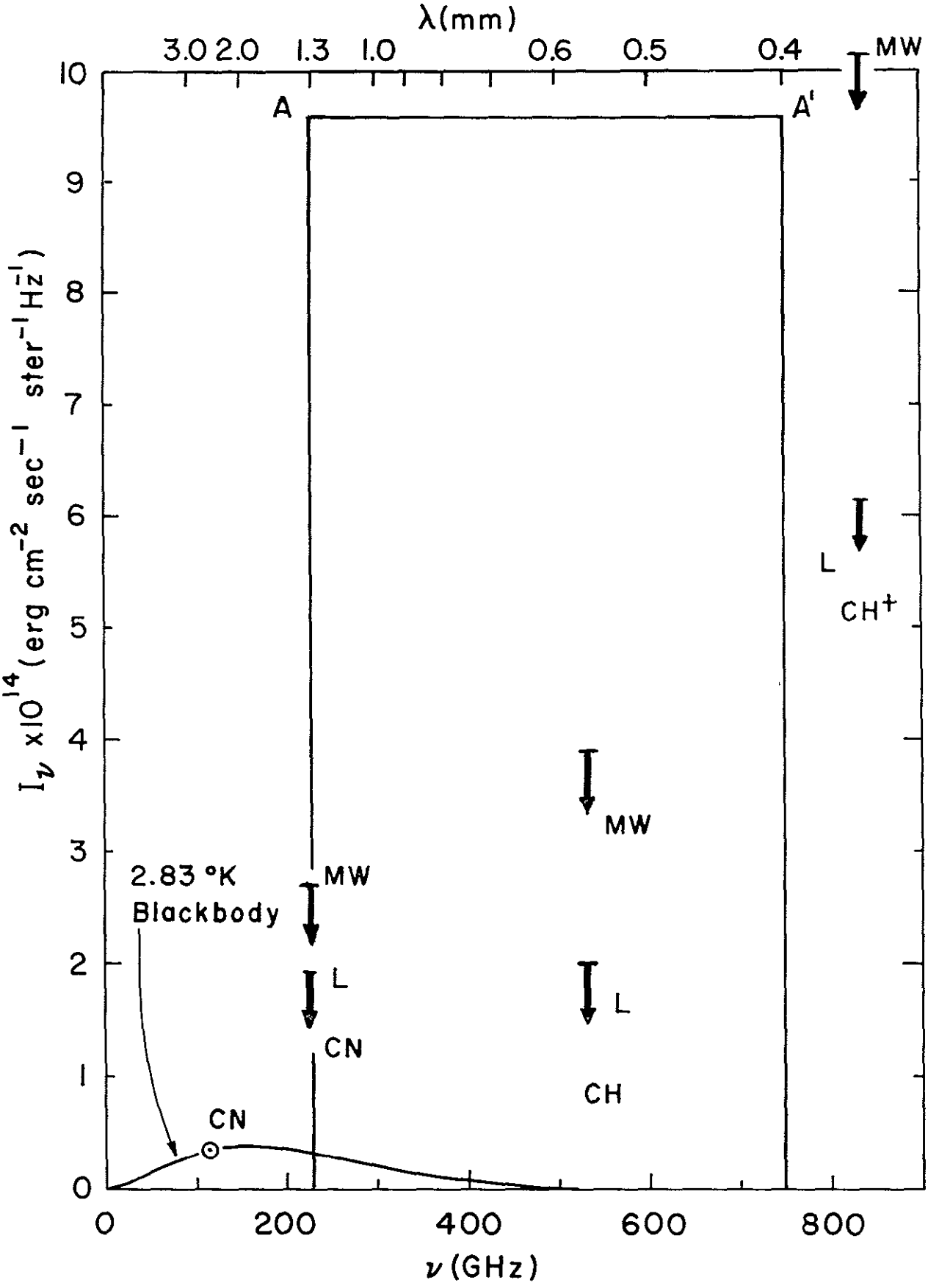
λ(mm)
3.0 2.0 1.3 1.0 0.6 0.5 0.4
MW
A
A'
L
CH+
MW
MW
2.83 °K
Blackbody
L
CN
L
CH
CN
I_ν x10^{14} (erg cm^{-2} sec^{-1} ster^{-1} Hz^{-1})
0 1 2 3 4 5 6 7 8 9 10
0 200 400 600 800
ν (GHz)

Figure 13. Typical fluorescent cycles through $^2\Pi$ and $^2\Sigma$ states which populate level J with respect to level J". Note for cycle through $^2\Pi$ state, $\Delta J = 0$ (Q branch) transitions are allowed.

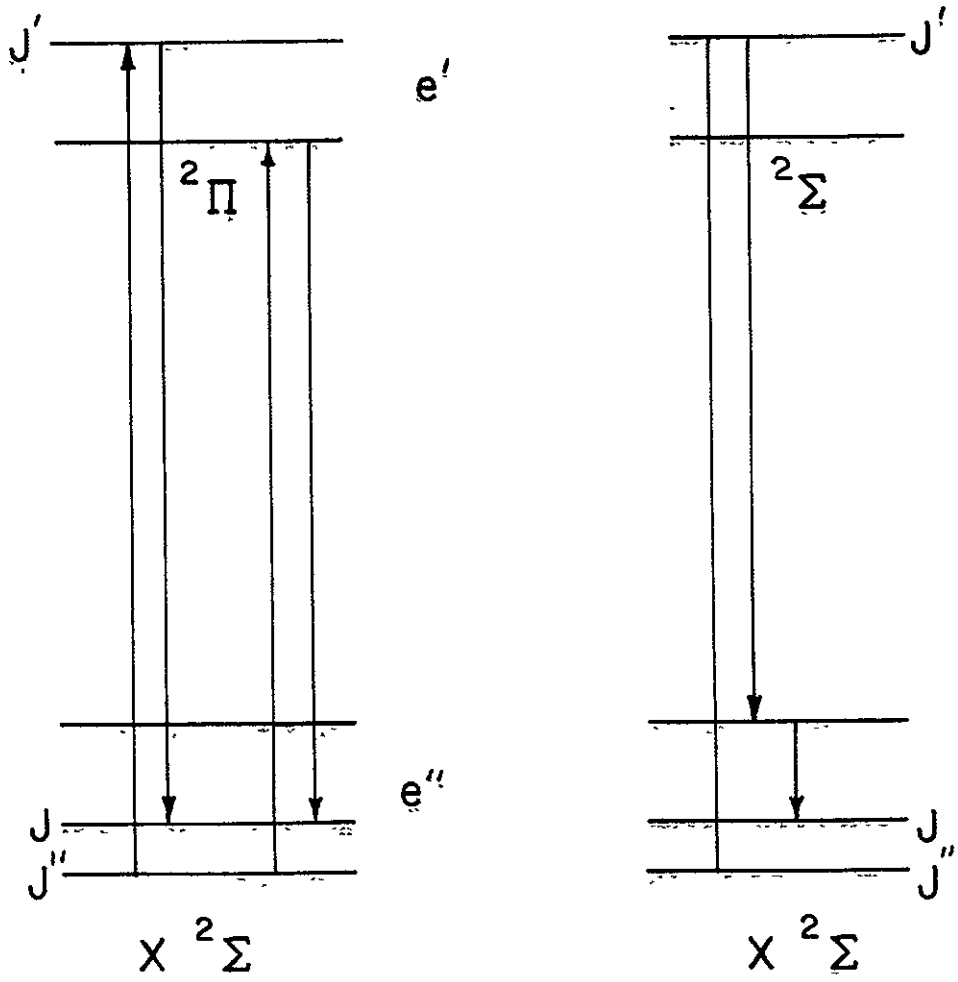
J'
e'
$^2\Pi$
e''
J
J''
X $^2\Sigma$
J'
$^2\Sigma$
J
J''
X $^2\Sigma$

Figure 14. Electronic term diagram for CN showing the well known red and violet systems and the ultraviolet systems studies by Douglas and Routly (1954, 1955) and Carroll (1956). (Figure after Carroll)

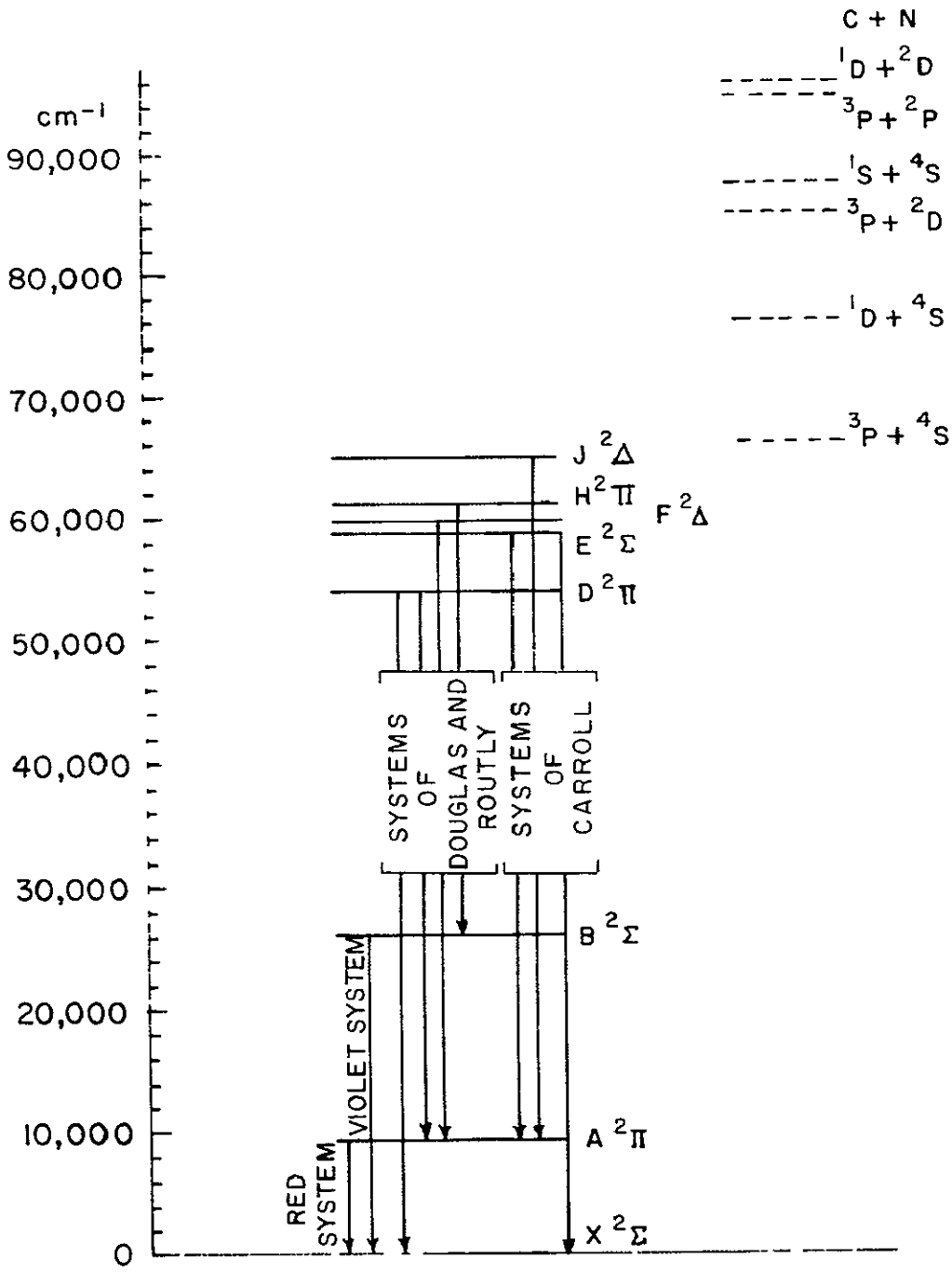
C + N
$^1D + ^2D$
$^3P + ^2P$
$^1S + ^4S$
$^3P + ^2D$
$^1D + ^4S$
$^3P + ^4S$
cm^{-1}
90,000
80,000
70,000
60,000
50,000
40,000
30,000
20,000
10,000
0
J $^2\Delta$
H $^2\Pi$
F $^2\Delta$
E $^2\Sigma$
D $^2\Pi$
SYSTEMS OF DOUGLAS AND ROUTLY
SYSTEMS OF CARROLL
B $^2\Sigma$
VIOLET SYSTEM
A $^2\Pi$
RED SYSTEM
X $^2\Sigma$

Figure 15. Upper limits to fluorescent excitation rates assuming f and α equal 1. For the known f values of the red and violet systems, the curve is displaced accordingly.

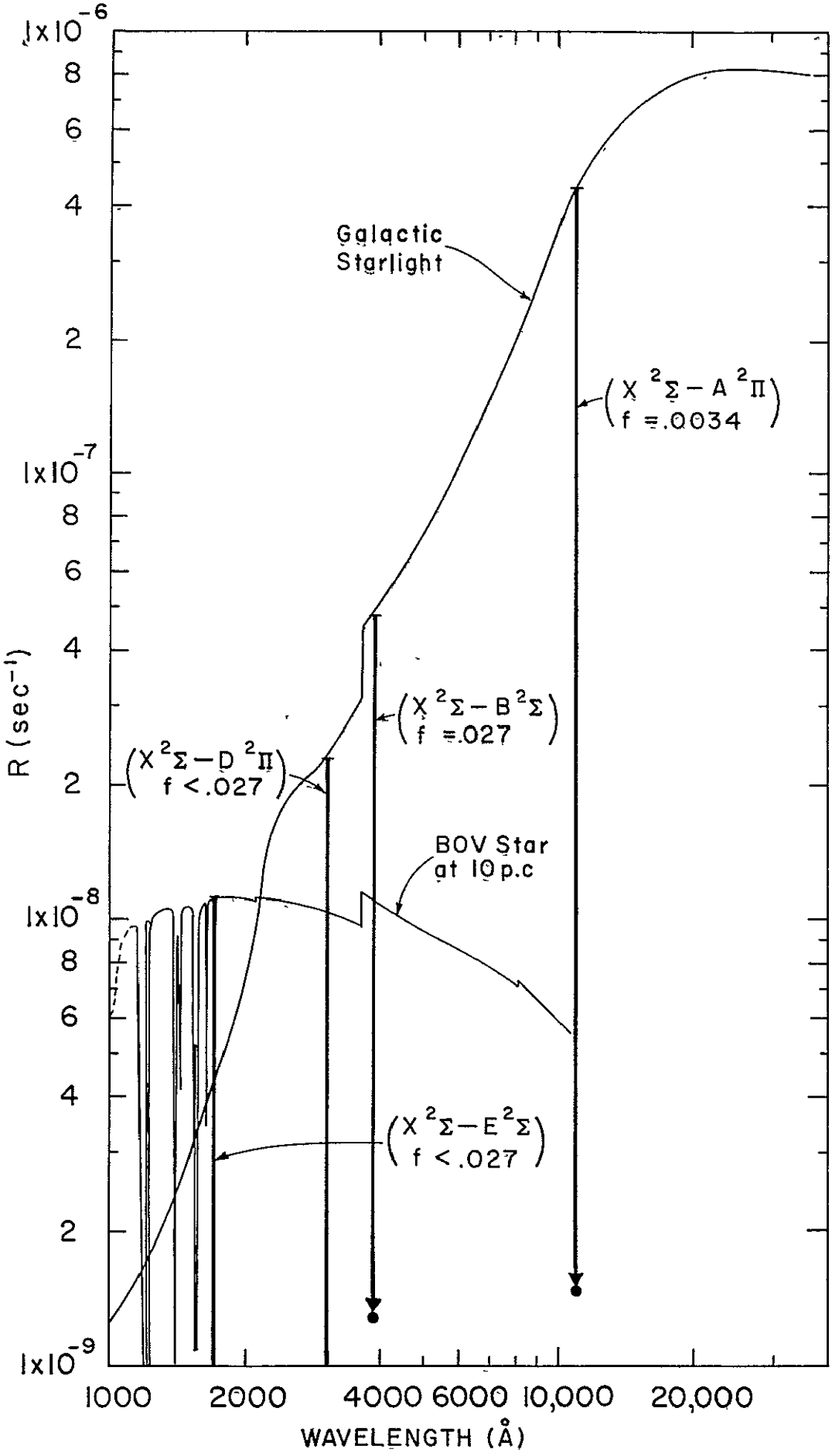
1x10⁻⁶
8
6
4
2
1x10⁻⁷
8
6
4
2
1x10⁻⁸
8
6
4
2
1x10⁻⁹
R (sec⁻¹)
Galactic Starlight
(X ²Σ − A ²Π f = .0034)
(X ²Σ − B ²Σ f = .027)
(X ²Σ − D ²Π f < .027)
BOV Star at 10 p.c
(X ²Σ − E ²Σ f < .027)
1000
2000
4000
6000
10,000
20,000
WAVELENGTH (Å)

Figure 16. (a) Coordinate system for treating the excitation of a polar molecule by electrons using the Born approximation (b) orientation of initial and final electron propogation vectors.

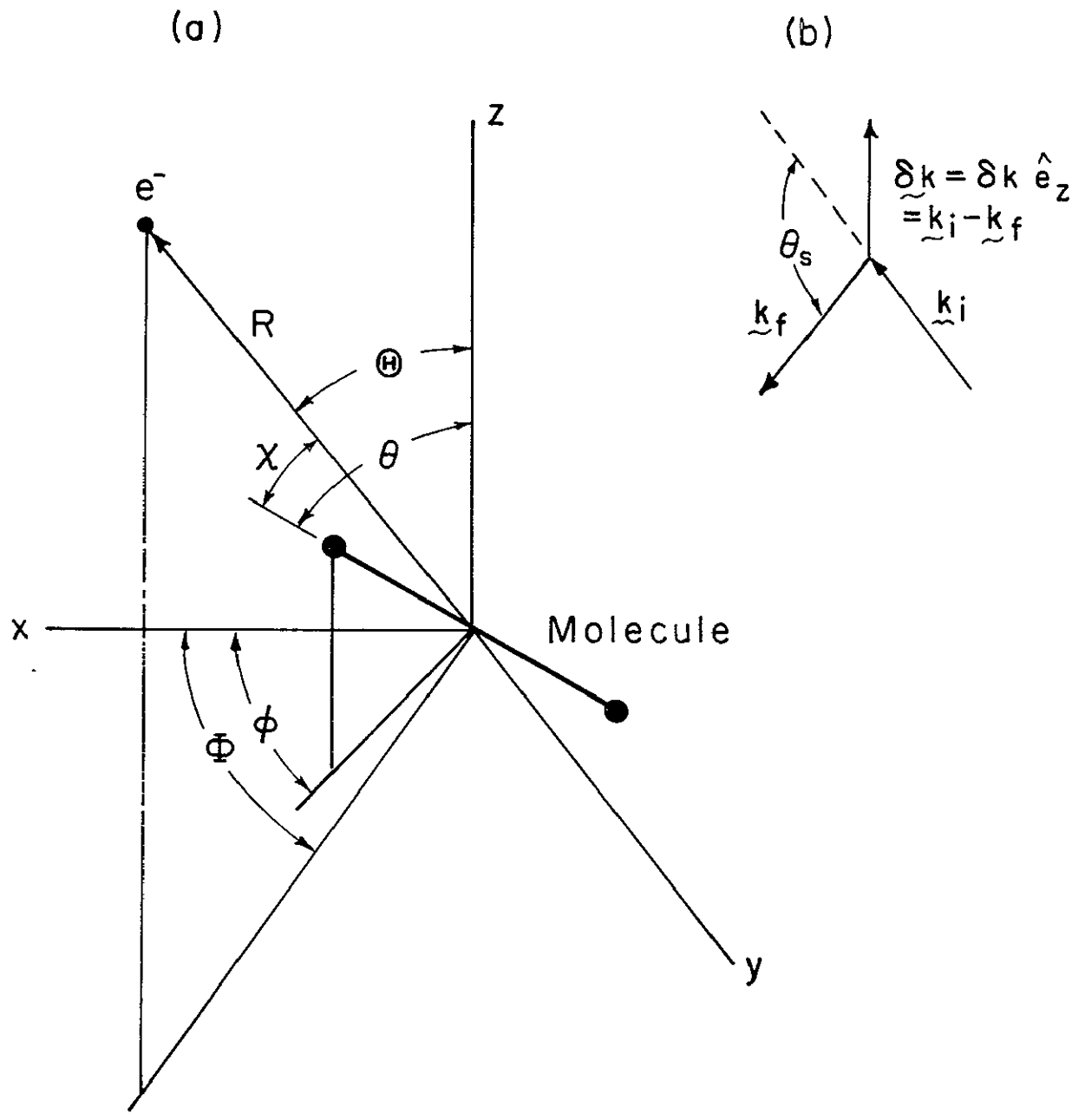
(a)
(b)
z
e⁻
R
Ⓗ
χ
θ
x
Molecule
Φ
φ
y
δk = δk ê_z
= k_i − k_f
θ_s
k_f
k_i

Figure 17. Temperature increase due to partical excitation by electrons and H I atoms. Each curve represents a constant observed excitation temperature so that the actual brightness is lower by this amount. Here we assume that H I - CN collisions predominantly satisfy electric dipole selection rules for CN excitation.

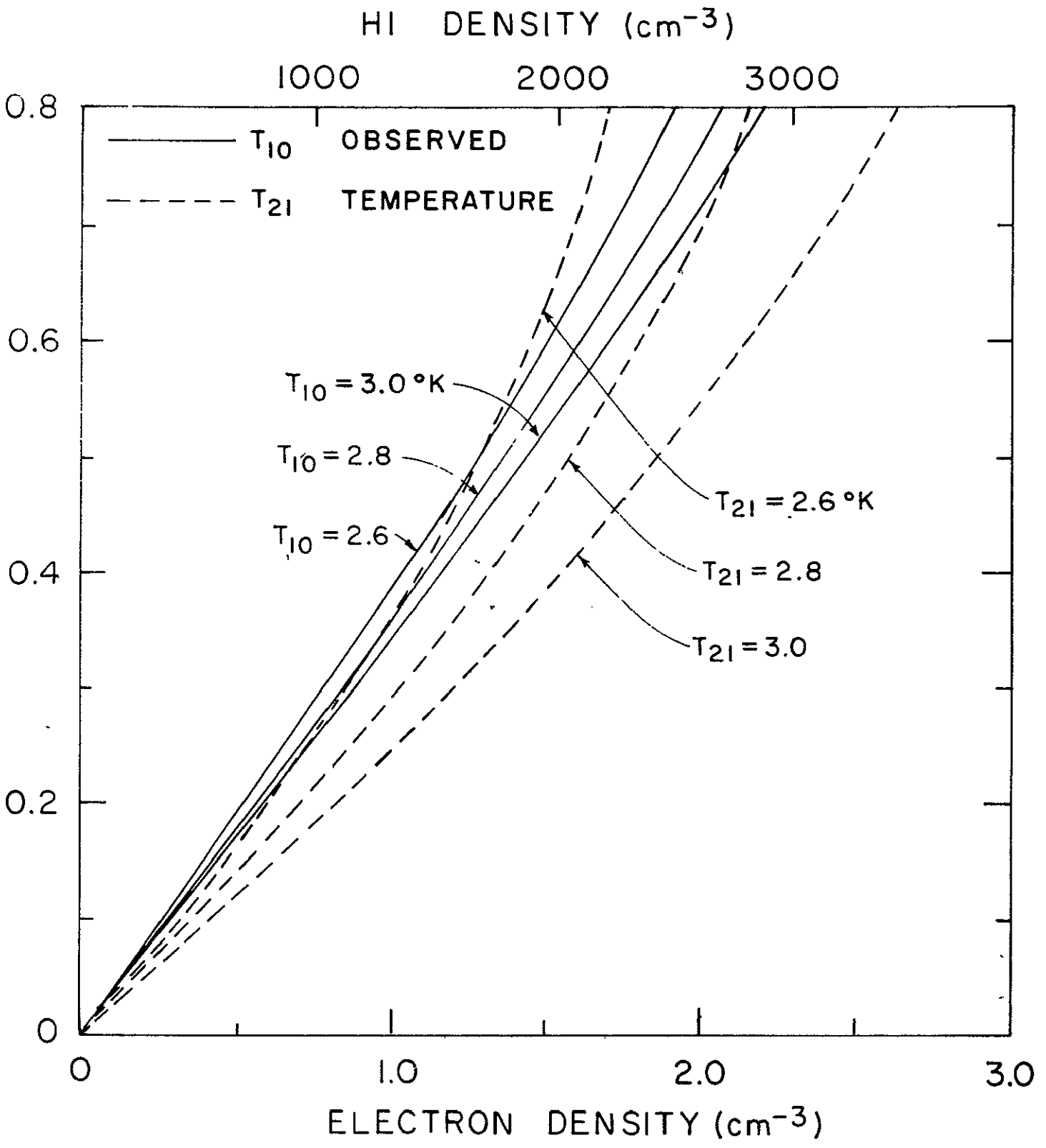
HI DENSITY (cm^{-3})
1000
2000
3000
0.8
0.6
0.4
0.2
0
T_{10} OBSERVED
T_{21} TEMPERATURE
$T_{10} = 3.0$ °K
$T_{10} = 2.8$
$T_{10} = 2.6$
$T_{21} = 2.6$ °K
$T_{21} = 2.8$
$T_{21} = 3.0$
0
1.0
2.0
3.0
ELECTRON DENSITY (cm^{-3})

Figure 18. T_{21} of CN which would be expected for excitation by a mixture of radiation and 125°K electrons or H I atoms as a function of observed T_{10} and electron or H I density. Again we assume that the H I - CN cross section obeys dipole selection rules for CN excitation.

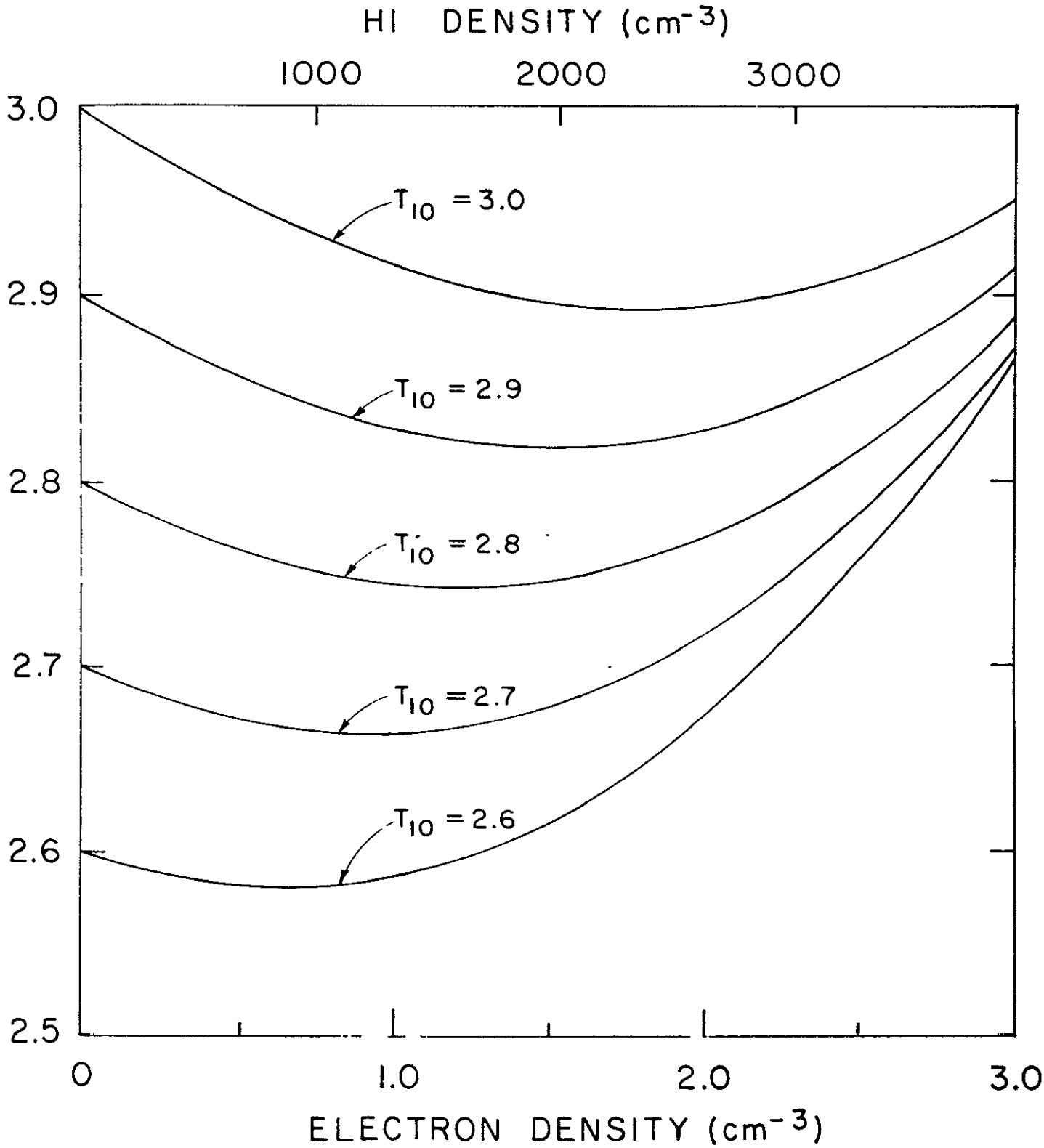
HI DENSITY (cm⁻³)
1000
2000
3000
3.0
2.9
2.8
2.7
2.6
2.5
T10 = 3.0
T10 = 2.9
T10 = 2.8
T10 = 2.7
T10 = 2.6
0
1.0
2.0
3.0
ELECTRON DENSITY (cm⁻³)

Figure 19. $J=0 \rightarrow 1$ excitation cross-section for protons or singly charged ions as a function of velocity

$$\bar{v} = \sqrt{\frac{8kT}{\pi m_p}} = 1.31 \times 10^6 \text{ cm/sec}$$

where $T = 10^4$ °K.

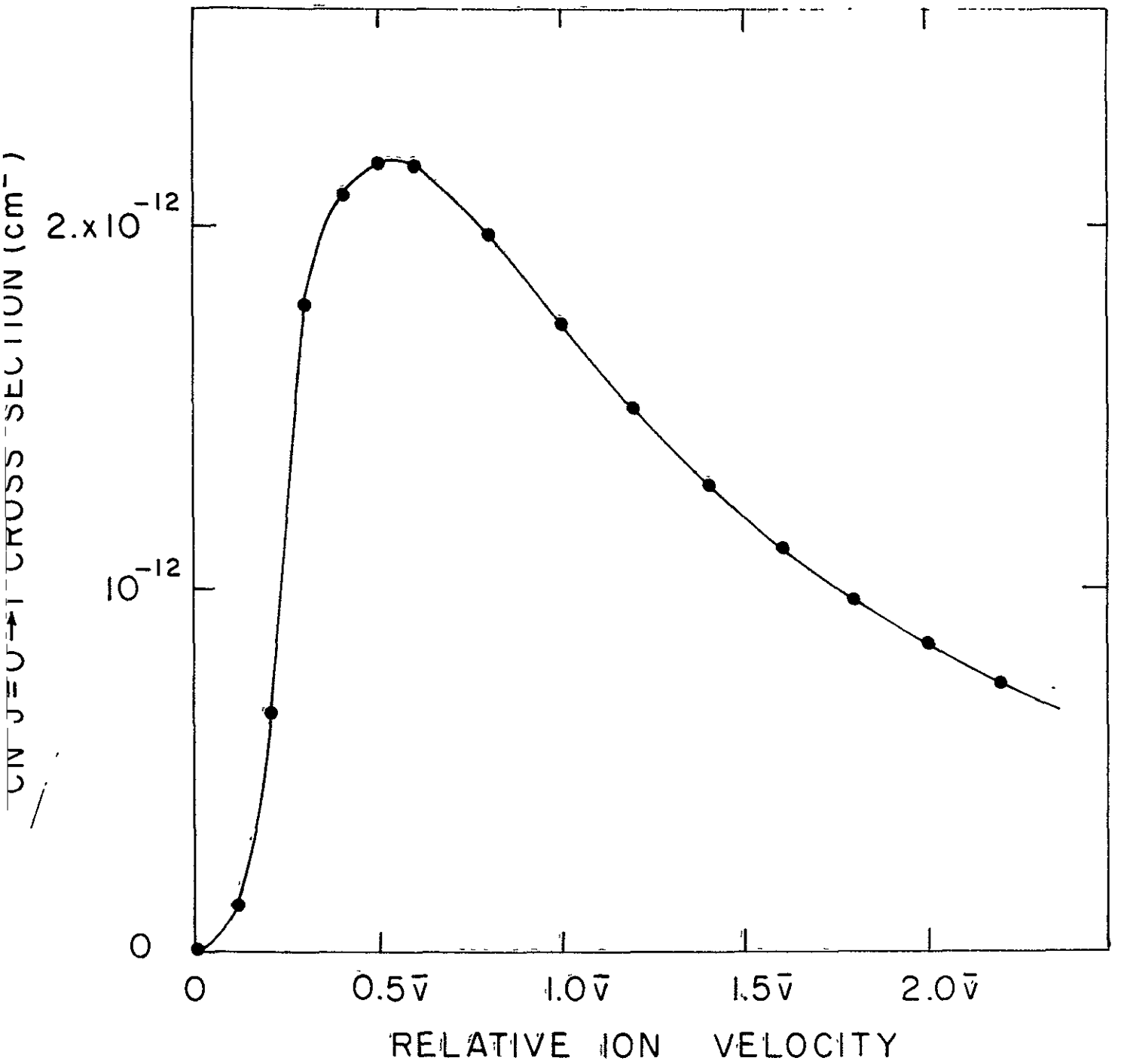
CH3+ + H2 CROSS SECTION (cm²)
2.x10⁻¹²
10⁻¹²
0
0
0.5v̄
1.0v̄
1.5v̄
2.0v̄
RELATIVE ION VELOCITY

Figure 20. Coordinate system used for treating the excitation of a polar molecule by protons.

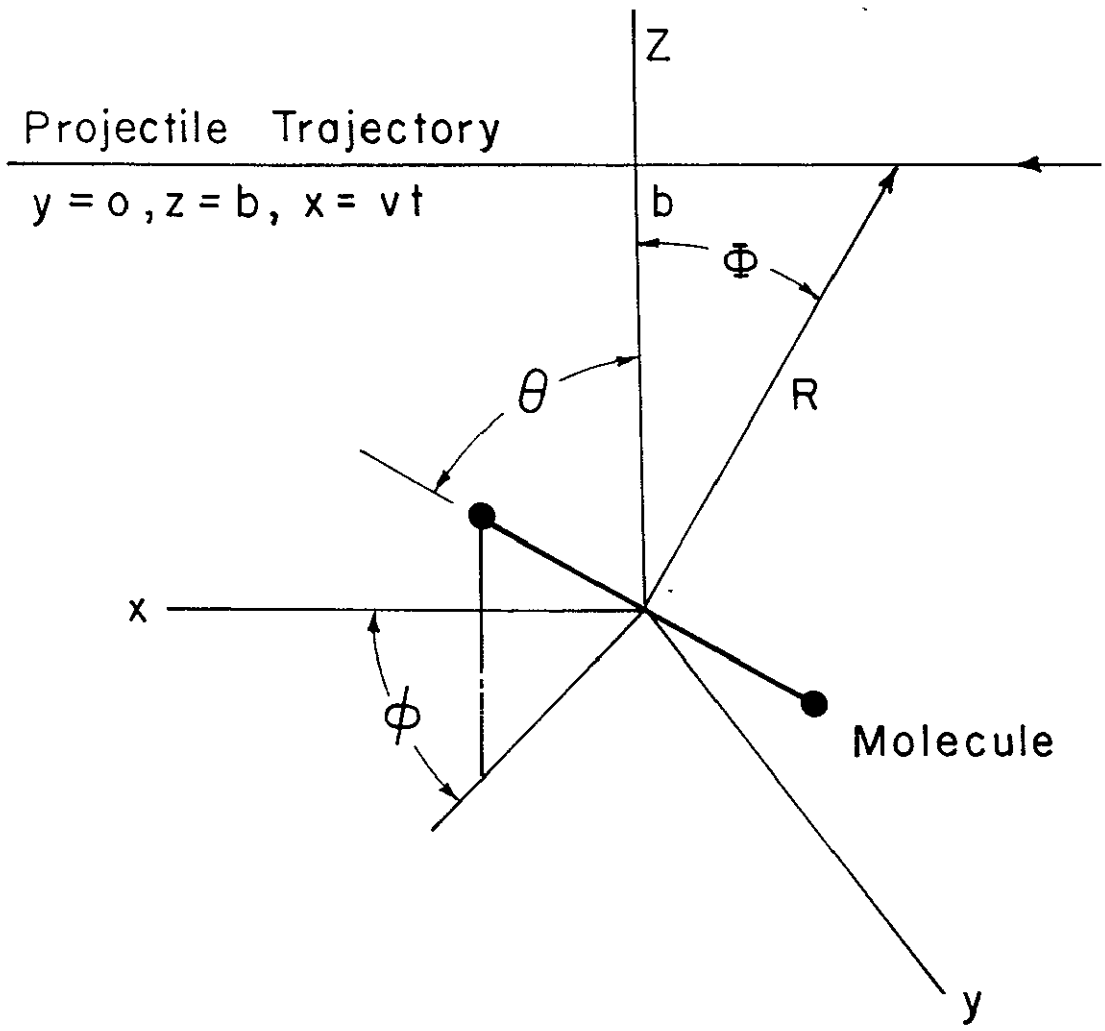
Z
Projectile Trajectory
y = o , z = b, x = v t
b
Φ
θ
R
x
ϕ
Molecule
y

Figure 21 Excitation of the $J = 1 \rightarrow 1$ and $0 \rightarrow 2$ transitions by protons as a function of impact parameter. The proton velocity is $v = 1.342\ \bar{v} = 1.75 \times 10^6$ cm/sec, where v is the most probable proton velocity at a kinetic temperature of 10^4°K. The discrete points result from the numerical integration of Schrödinger's equation.

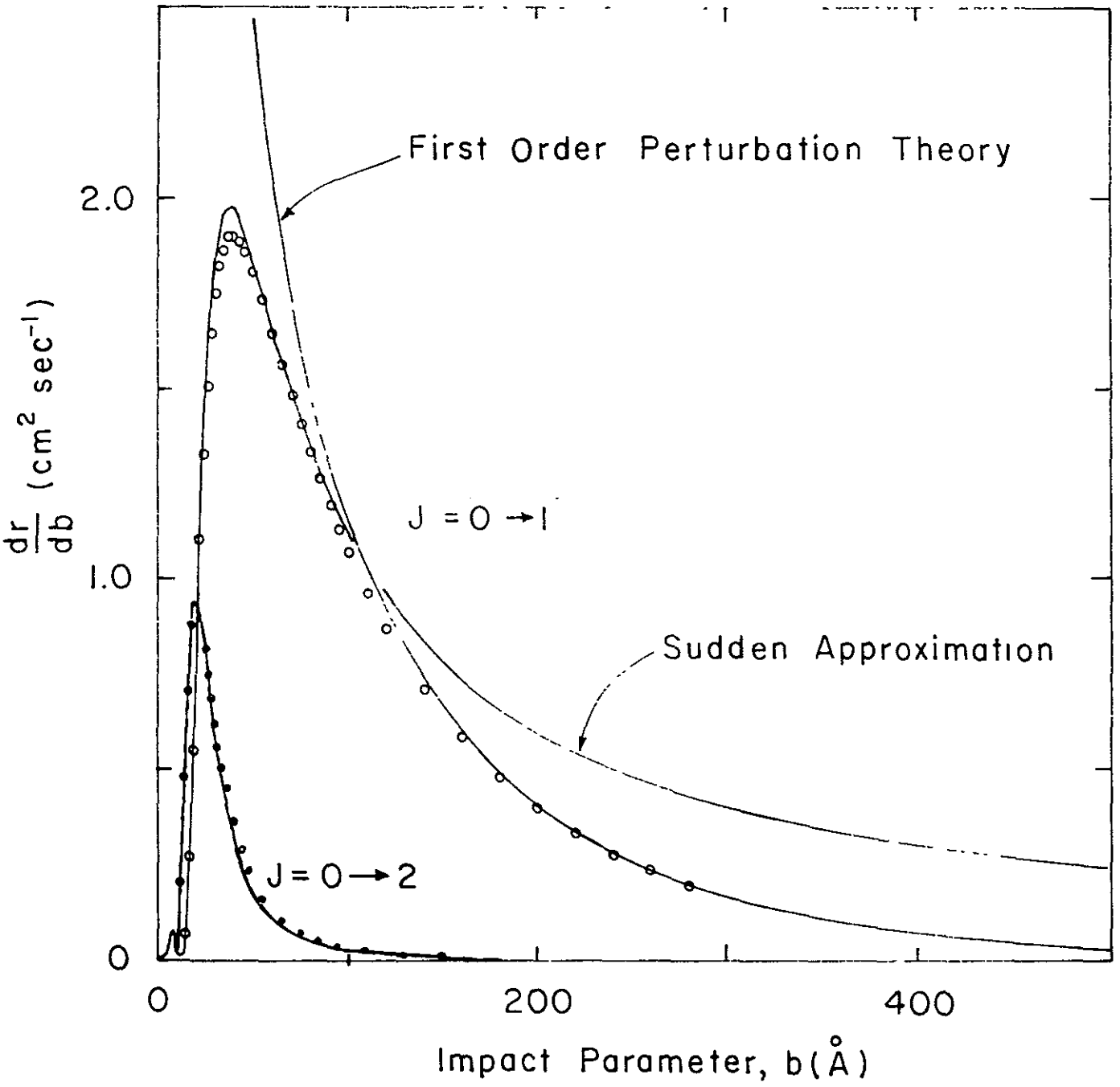
First Order Perturbation Theory
Sudden Approximation
J = 0 → 1
J = 0 → 2
2.0
1.0
0
0
200
400
dr/db (cm² sec⁻¹)
Impact Parameter, b(Å)

Figure 22. Excitation of the first-excited level of CH from the ground state by protons as a function of impact parameter. As with Figure 21, the proton velocity is 1.75×10^6 cm/sec.

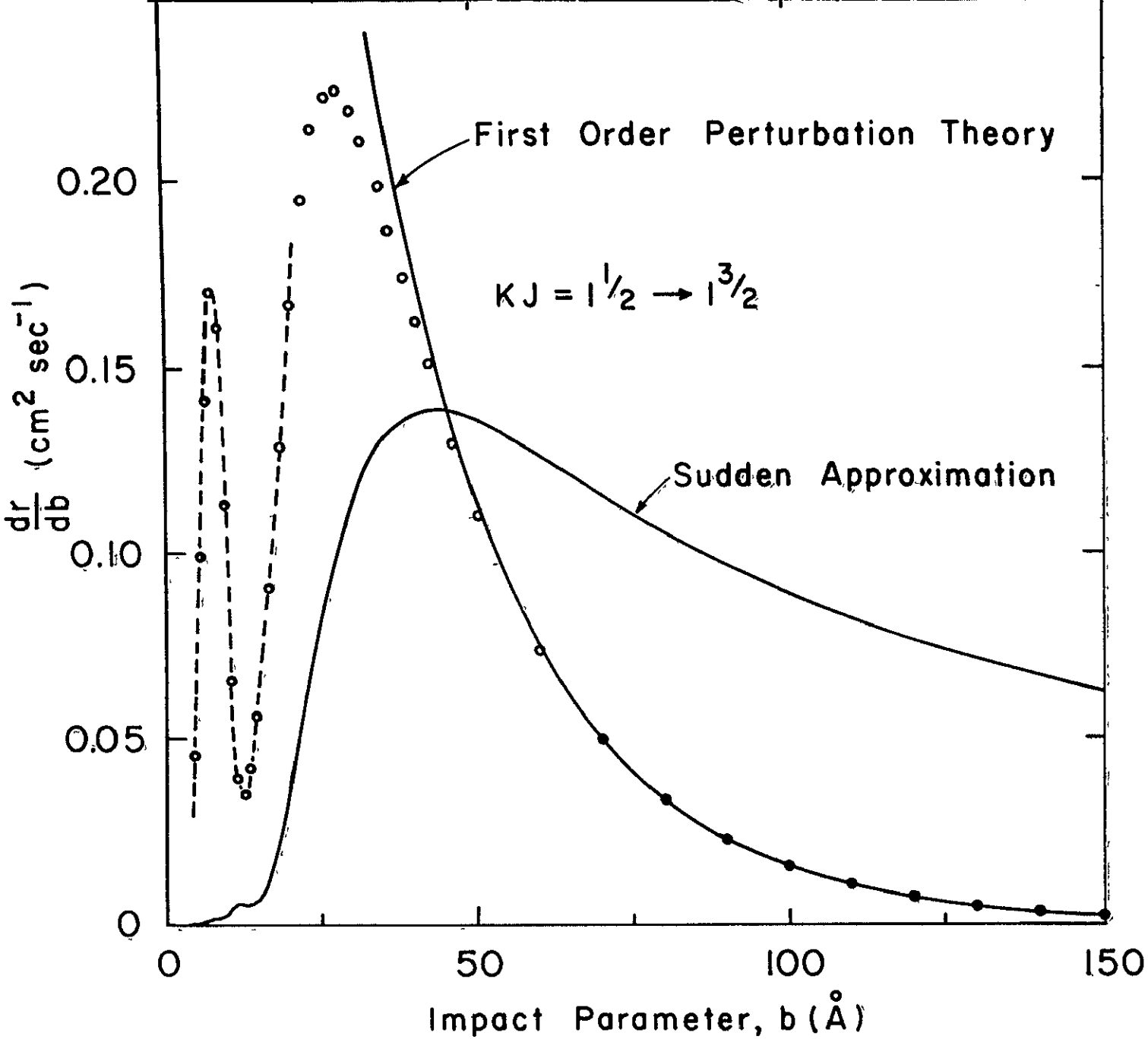
First Order Perturbation Theory
KJ = 1 1/2 → 1 3/2
Sudden Approximation
dr/db (cm² sec⁻¹)
0.20
0.15
0.10
0.05
0
0
50
100
150
Impact Parameter, b (Å)

Figure 23. Number density of protons and electrons, as a function of the HII kinetic temperature, required to produce the 3°K excitation temperature of the J = 1 CN level.

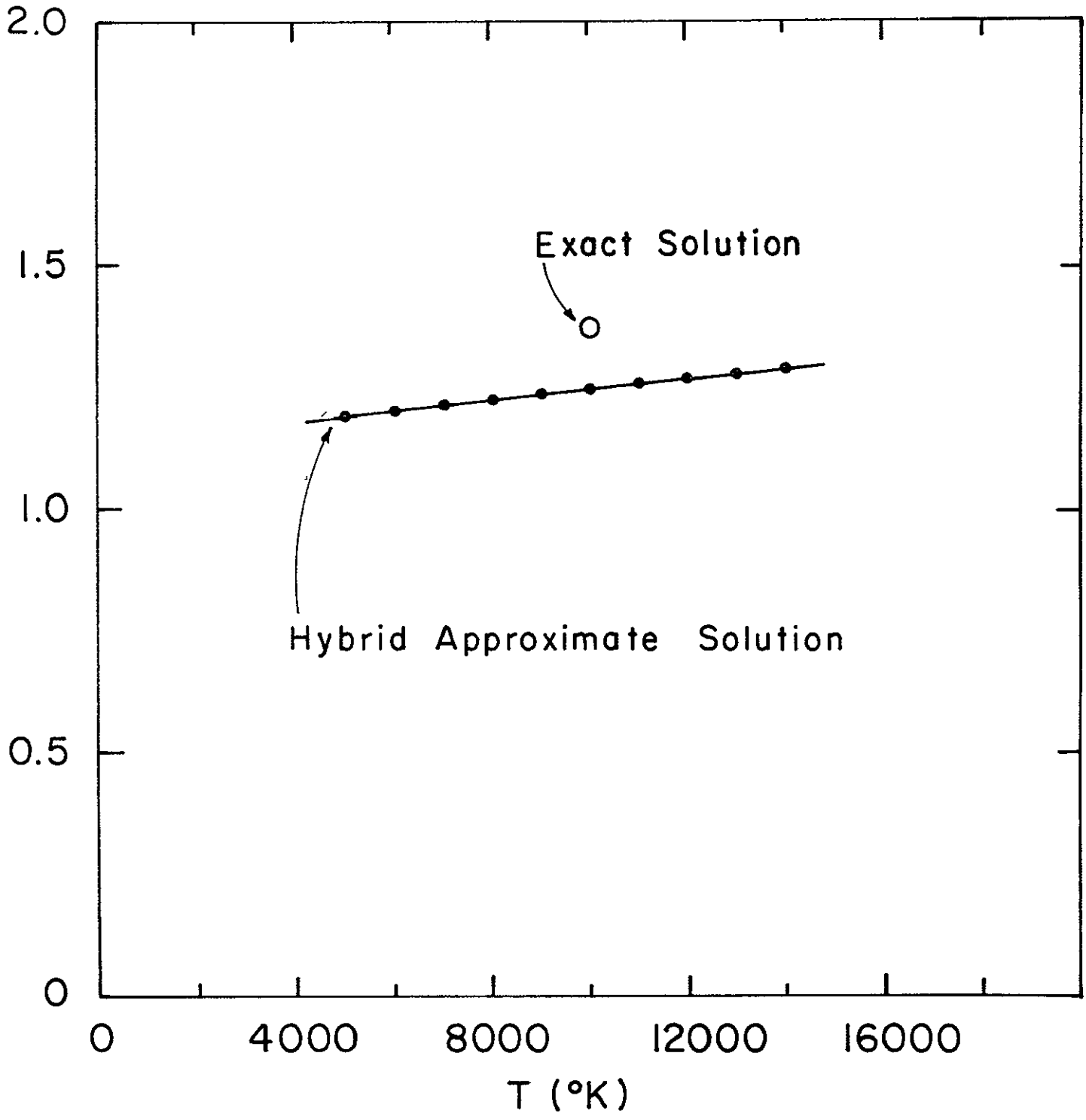
2.0
1.5
1.0
0.5
0
Exact Solution
Hybrid Approximate Solution
0
4000
8000
12000
16000
T (°K)

Figure 24. Rotation temperature of the J = 2 and 3 CN levels, as a function of the H II kinetic temperature, when the number density of charged particles is such that the rotational temperature of the J = 1 level is 3°K.

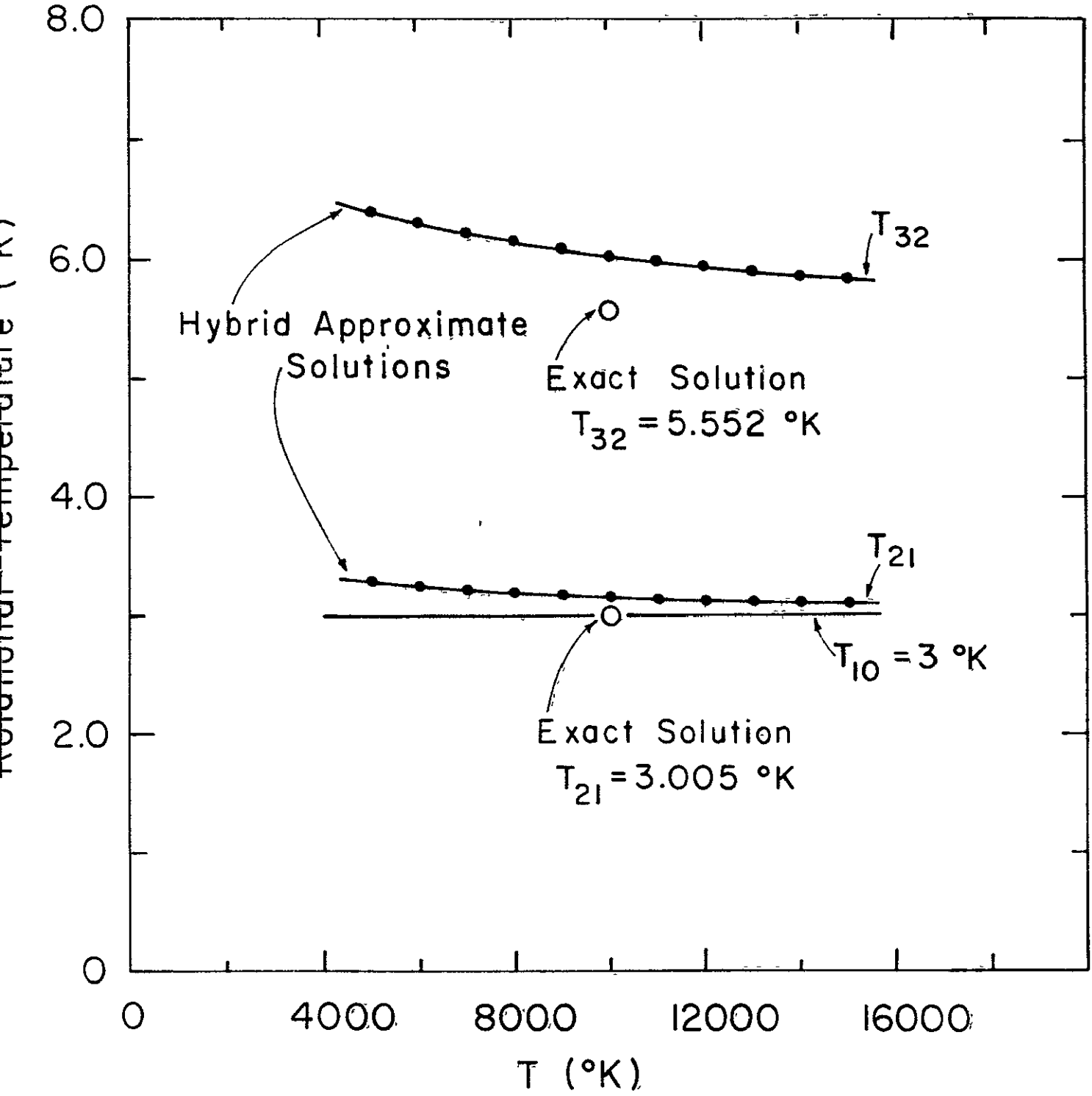
8.0
6.0
4.0
2.0
0
Rotational Temperature (°K)
0
4000
8000
12000
16000
T (°K)
T_{32}
Hybrid Approximate Solutions
Exact Solution
$T_{32} = 5.552$ °K
T_{21}
$T_{10} = 3$ °K
Exact Solution
$T_{21} = 3.005$ °K

Figure 25. Rotational temperature of the J = 1 CN level as a function of the number density of protons and electrons, for an HII temperature of 10,000°K.

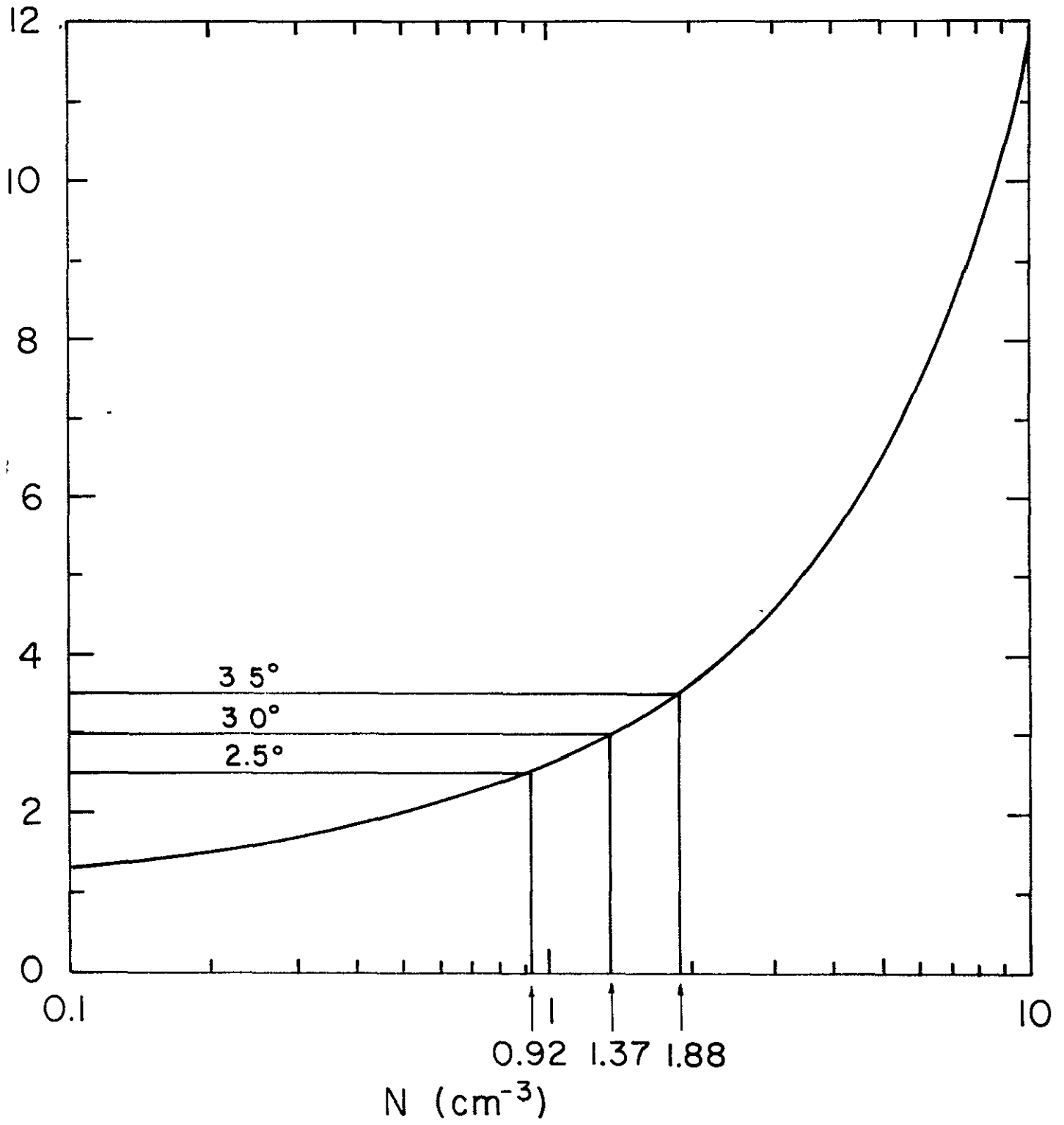
12
10
8
6
4
2
0
3 5°
3 0°
2.5°
0.1
1
10
0.92
1.37
1.88
N (cm⁻³)

Figure 26. Velocity profiles of CN and Ca II absorption in the spectrum of ζ Ophiuchi compared with H I 21cm emission in the same direction.

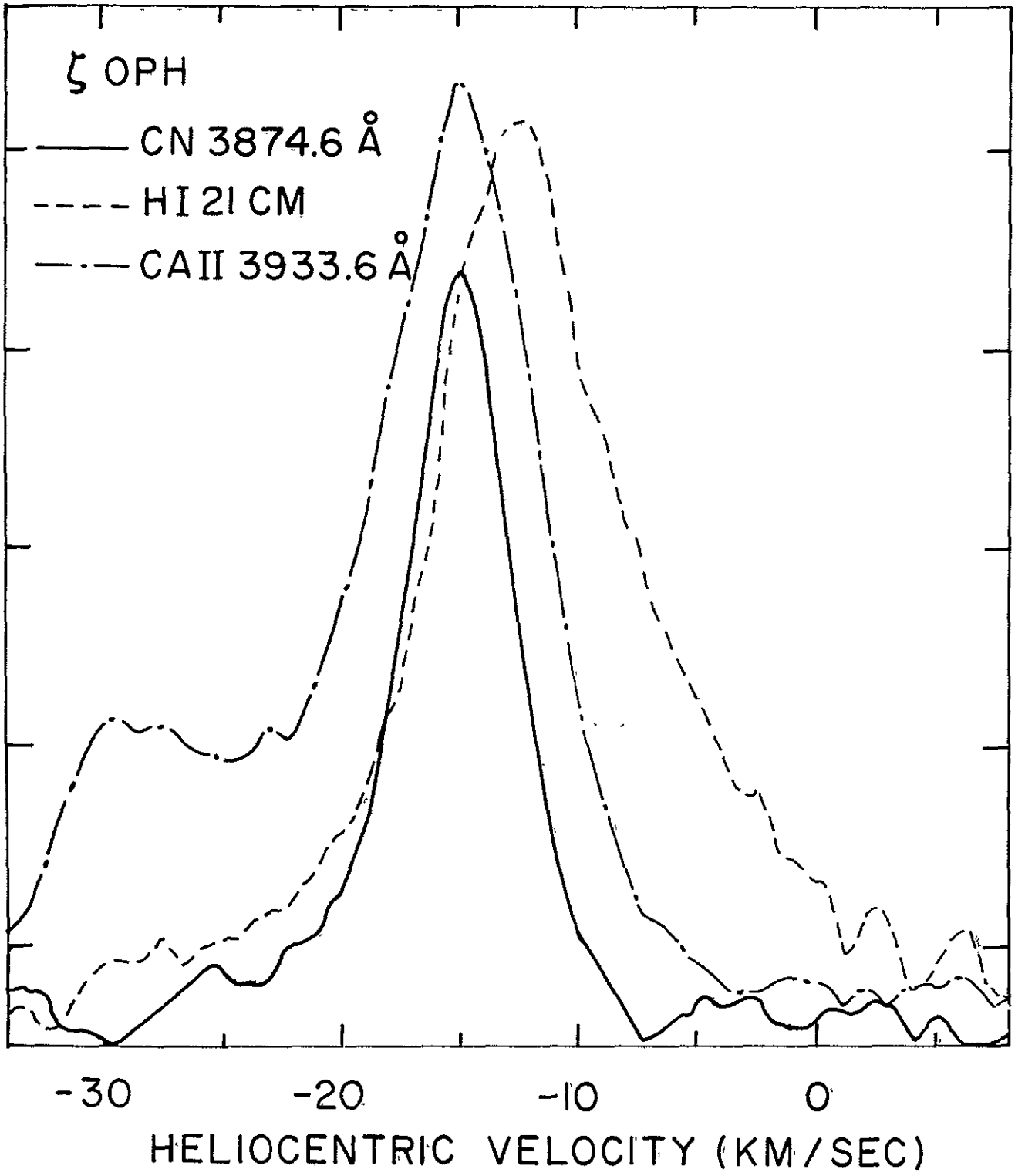
ζ OPH
CN 3874.6 Å
HI 21 CM
CAII 3933.6 Å
-30
-20
-10
0
HELIOCENTRIC VELOCITY (KM/SEC)

Figure 27. Velocity profile of CN absorption in the spectra of X Persei and ζ Persei compared with H I 21cm emission in the corresponding directions. These two stars are only separated by about one degree of arc and appear to share the same interstellar cloud.

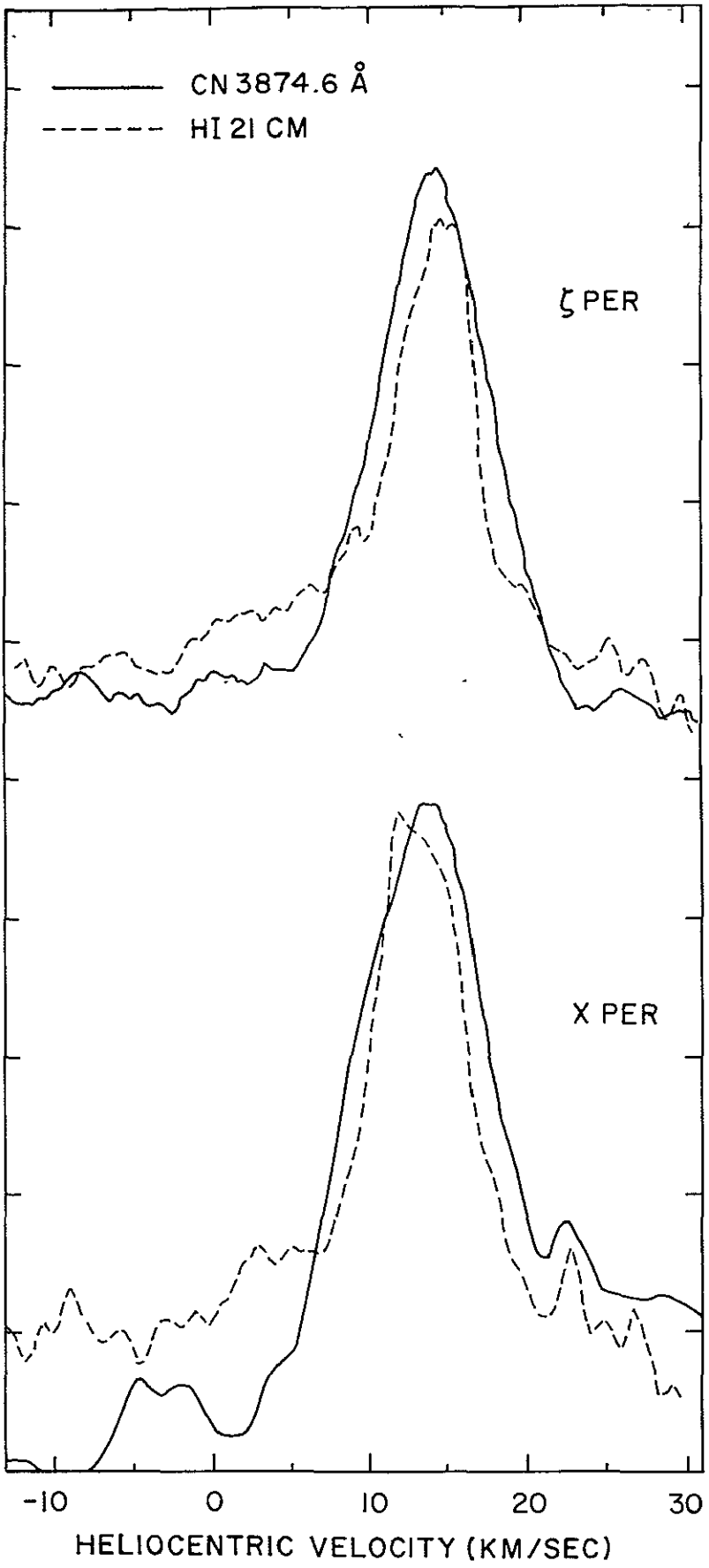
CN 3874.6 Å
HI 21 CM
ζ PER
X PER
-10
0
10
20
30
HELIOCENTRIC VELOCITY (KM/SEC)

Figure 28. Velocity profiles of CN and Ca II absorption in the spectrum of 20 Aquilae compared with H I 21cm emission in the same direction.

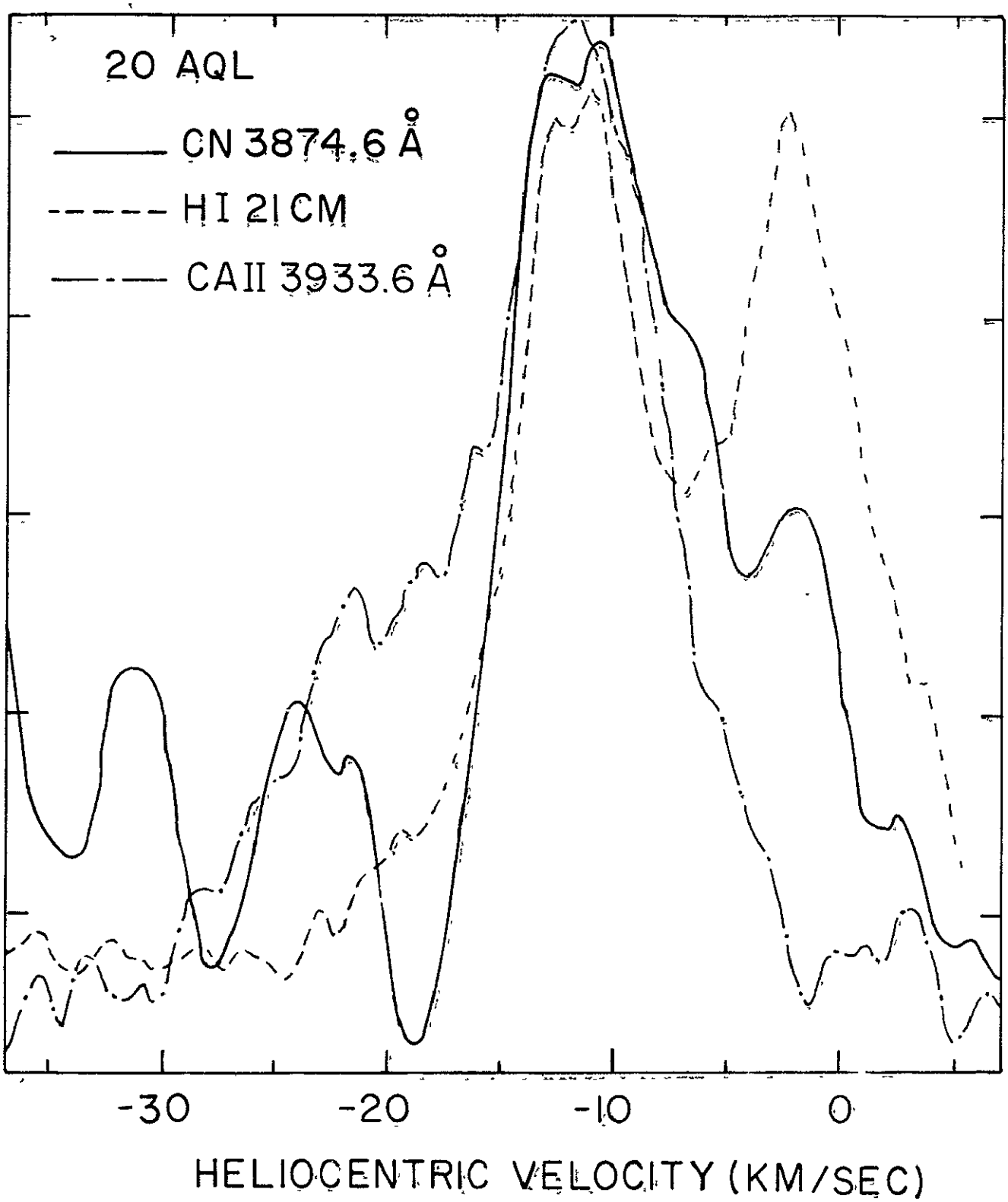
20 AQL
CN 3874.6 Å
HI 21 CM
CAII 3933.6 Å
-30
-20
-10
0
HELIOCENTRIC VELOCITY (KM/SEC)

Figure 29: Comparison of the excitation temperature T_{10}(CN) in ζ Ophiuchi and ζ Persei, with the series of direct measurements of the background radiation made by the Princeton group.

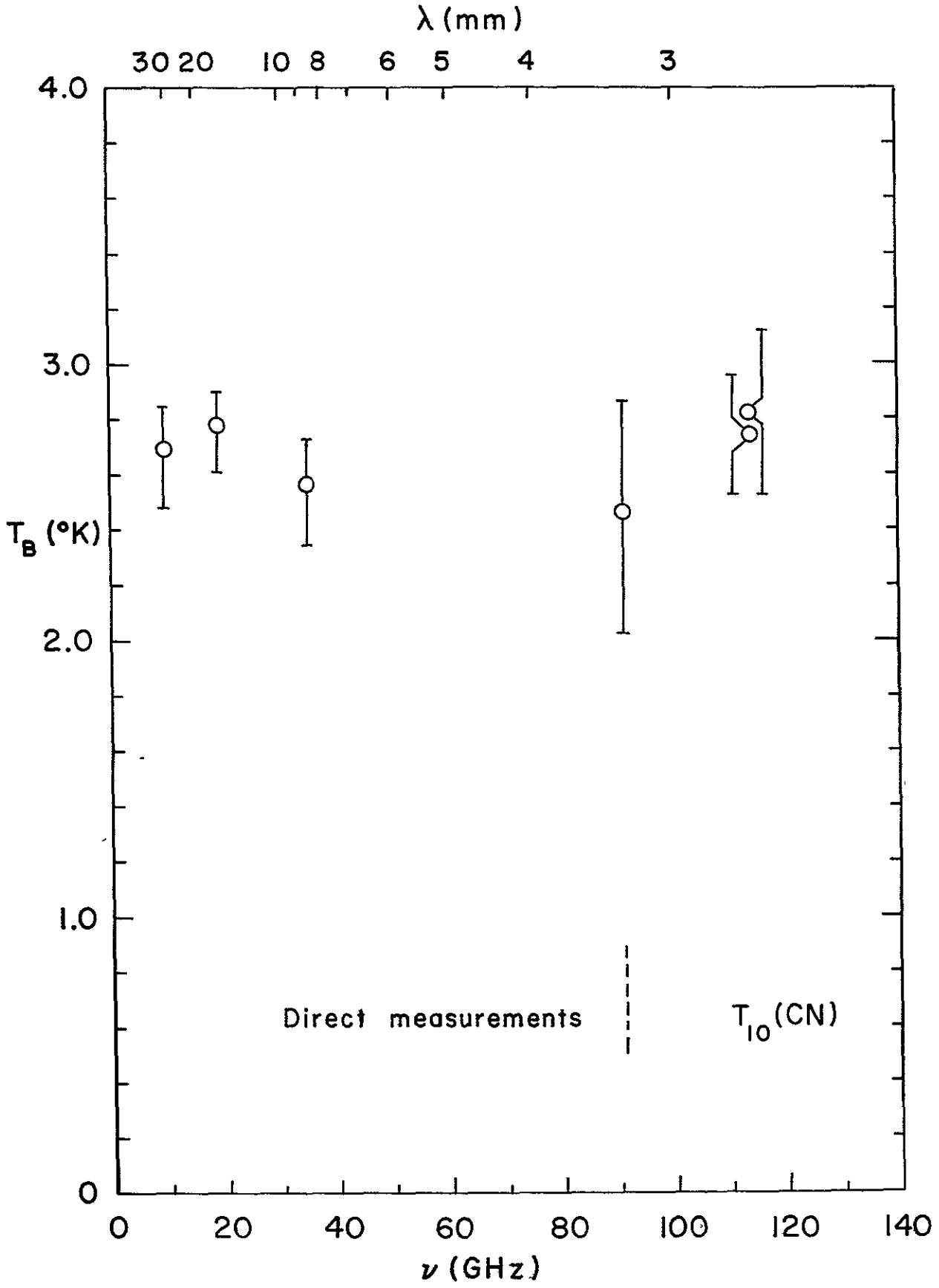
λ (mm)
30 20 10 8 6 5 4 3
4.0
3.0
2.0
1.0
0
T_B (°K)
Direct measurements
T_{10}(CN)
0 20 40 60 80 100 120 140
ν (GHz)

Figure 30. Three cases of error limit regions:

A. Region is symmetric about most probable value which is < 0; area between $\beta_m - \eta$ and $\beta_m + \eta$ equals success probability.

B. Region not symmetric about most probable value which is < 0; area between zero and $\beta_m + \eta$ equals success probability

C. Most probable value equals zero; area between zero and η equals success probability.

In all cases, total area for positive β is normalized to one.

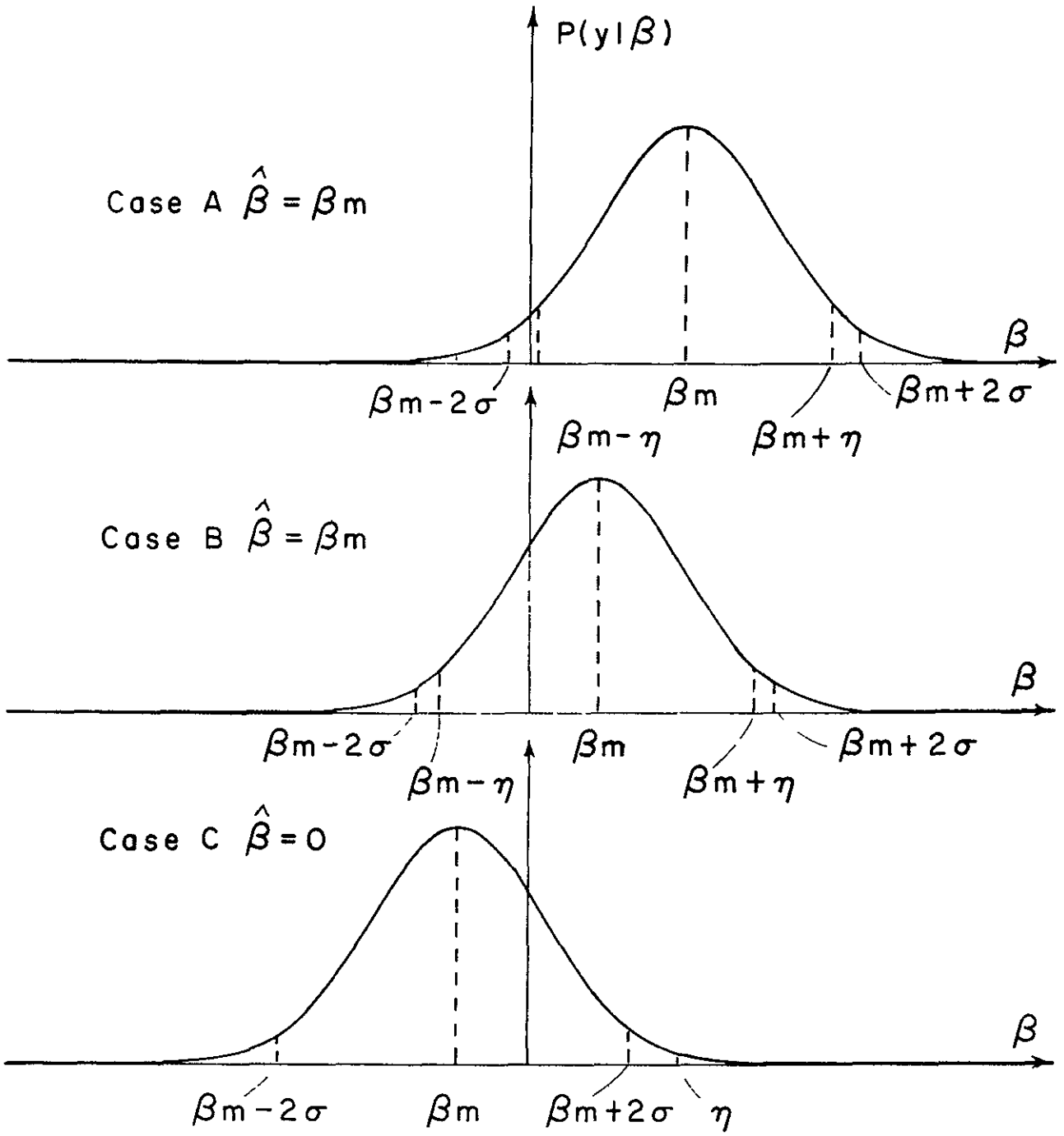
P(y|β)
Case A $\hat{\beta} = \beta m$
β
βm−2σ
βm
βm+2σ
βm−η
βm+η
Case B $\hat{\beta} = \beta m$
β
βm−2σ
βm−η
βm
βm+η
βm+2σ
Case C $\hat{\beta} = 0$
β
βm−2σ
βm
βm+2σ
η